ELECTROCHEMICAL CONTROL AND MINIMIZATION OF HYDROGEN SULFIDE FORMATION IN ANAEROBIC SYSTEMS

Natalia Sergienko

Universitat de Girona

ICRA Institut Català de Recerca de l'Aigua

Doctoral Thesis

Electrochemical control and minimization of hydrogen sulfide formation in anaerobic systems

Natalia Sergienko
2021

PhD program: Water Science and Technology

Supervisor: Prof. Jelena Radjenovic
Co-supervisor: Dr. Oriol Gutiérrez Garcia-Moreno
Co-supervisor and academic tutor: Prof. Ignasi Rodríguez Roda-Layret

Thesis submitted in fulfilment of the requirements for the degree of Doctor from the University of Girona

Acknowledgments

"Ability is nothing without opportunity."
Napoleon Bonaparte

I would like to express my gratitude to Prof. Jelena Radjenovic, who gave me an opportunity to work, learn and grow intellectually in such a warm and welcoming place as ICRA. This work would be impossible without her knowledge and guidance as well as emotional support in the difficult moments. I would also like to thank my co-supervisor, Dr. Oriol Gutiérrez, for his helpful contributions, especially during the first year of my PhD. My gratitude also extends to Prof. Ignasi Rodroguez-Roda, who is responsible for such a great working environment of TiA, full of scientific discussions, opinions and ideas.

I would like to thank all the people that I have worked with all these years. First, I want to thank the entire ICT team, Sara, Olga and Natalia, for their technical support and patience. Thanks also to Veronica, Nuria and Janina for all your help with administrative stuff and beyond. I would like to mention my Electron4Water team members, Anna, Elizabeth, Giannis, Luis, Natalia and Nick. Because of them those numerous hours spent in the lab turned into great memories. Besides that, I am very grateful to all the students that ever passed by D08: Anna, Eliza, Marc, Fede, Esther and many more, who made my experience in ICRA so fun and enjoyable.

Last but not least, I would like to thank my husband Guille who was supporting me during all these years of PhD, sharing my small victories and understanding my upsets. I would also like to specially mention his parents who became my second family here in Spain. Также, я бы хотела поблагодарить моих маму и папу. Спасибо за вашу поддержку и веру в меня, без вас у меня ничего бы не получилось.

Outline

List of publications

N. Sergienko, E. Irtem, O. Gutierrez, J. Radjenovic, Electrochemical removal of sulfide on porous carbon-based flow-through electrodes, Journal of Hazardous Materials, 375 (2019) 19-25.

N. Sergienko, J. Radjenovic, Manganese oxide-based porous electrodes for rapid and selective (electro)catalytic removal and recovery of sulfide from wastewater, Applied Catalysis B: Environmental, 267 (2020) 118608.

N. Sergienko, J. Radjenovic, (Electro)catalytic oxidation of sulfide to colloidal sulfur over manganese oxide coated electrode with TiO_2 nanotubes interlayer, Applied Catalysis B: Environmental, 296 (2021) 120383.

Patents:

N. Sergienko, J. Radjenovic, Method to prepare an electrode with a manganese oxide coated titanium oxide nanotube array interlayer, electrode obtained thereof, and uses of the electrode.

List of acronyms

ACF – activated carbon felt

BDD – boron doped diamond

CE – coulombic efficiency

COD – chemical oxygen demand

CV – cyclic voltammetry

CaOH – lime

DO – dissolved oxygen

E_{EO} – electric energy per order

EDX – energy-dispersive X-ray spectroscopy

EIS – electrochemical impedance spectroscopy

FRP – fibre-reinforced plastic

Fe(II) – ferrous iron

Fe(III) – ferric iron

GC – glassy carbon

GF – graphite felt

H_2SO_4 – sulfuric acid

HDPE – high-density polyethylene

HOMO – highest occupied molecular orbital

HRT – hydraulic retention time

HS^-/H_2S – sulfide

IC – ion chromatography

IEM – ion exchange membrane

KCl – potassium chloride

LUMO – lowest unoccupied molecular orbital

MMO – mixed metal oxide

$Mg(OH)_2$ – magnesium hydroxide

Mn_xO_y – manganese oxide

NTA – nanotubes array

$NaNO_3$ – sodium nitrate

NaOH – caustic soda

OC – open circuit

PO_4^{3-} – phosphate

PVC – polyvinyl chloride

PolyS – polysulfides

RE – reference electrode

S^0 – zero valent sulfur

$S_2O_3^{2-}$ – thiosulfate

$S_{8\ col}$ – colloidal sulfur

$S_{8\ dep}$ – electrodeposited elemental sulfur

S_8 – elemental sulfur

SEM – scanning electron microscopy

SHE – standard hydrogen electrode

SO_2 – sulfur dioxide

SO_3 – sulfur trioxide

SO_3^{2-} – sulfite

SO_4^{2-} – sulfate

SOB – sulfur oxidising bacteria

soNRB – sulfide-oxidizing nitrate-reducing bacteria

SRB – sulfate reducing bacteria

Ti – titanium

TiO_2 – titanium dioxide

XPS – X-ray photoelectron spectroscopy

XRD – X-ray diffraction spectroscopy

List of figures

List of tables

Summary

Formation of hydrogen sulfide represents a major challenge in the operation of wastewater collection systems. Hydrogen sulfide is malodourous and toxic gas, which causes corrosion of pipes, wells, and constructions, hence damaging the structural integrity of the collection systems and significantly reducing their lifetime. Control of hydrogen sulfide formation, accumulation and emission is normally handled by the dosing of chemicals to the waste stream, which leads to considerable operating costs and risks associated with the transport, storage and handling of chemicals.

Electrochemical treatment is an attractive alternative to the existing technologies for sulfide control, as it offers a robust removal of sulfide *in situ* and avoids the costs and risks related to chemical usage. Mechanisms and products of electrochemical sulfide oxidation are strongly dependent on the nature of the electrode materials employed. For example, oxidation of sulfide at mixed metal oxide (MMO) coated titanium electrodes mainly proceeds via its indirect oxidation by the electrochemically generated oxygen, resulting in sulfur, sulfate and thiosulfate as final products [1]. However, indirect oxidation is non-selective, and about ~50% of the total electrons is used for organics oxidation, thus lowering the current efficiency of the process. Sulfide is an electrochemically active species and can also be directly oxidized to elemental sulfur at low anodic potential, hence reducing the energy requirements of the treatment. Though sulfur is biologically available, its utilization of as electron acceptor in bacterial metabolism is limited mainly due to low solubility of sulfur in water. Thus, electrochemical oxidation of sulfide to sulfur should help to minimize the reformation of sulfide. However, questions remain regarding the suitability of electrochemical abatement of hydrogen sulfide for real-scale applications due to several drawbacks

such as the lack of appropriate anode materials and gradual electrode passivation with the electrodeposited sulfur. Therefore, the main goal of this thesis was to investigate the performance of electrochemical sulfide oxidation to elemental sulfur by: *i)* using carbon-based electrode materials known to have high selectivity towards S^0, *ii)* developing new anode materials capable of fast and selective sulfide oxidation to elemental sulfur at low applied potentials, and *iii)* applying different regeneration strategies for the removal of the electrodeposited S^0 and sulfur recovery.

The first study conducted in this thesis is focused on the evaluation of porous carbon anodes, graphite felt (GF) and activated carbon felt (ACF), for the electrochemical removal of sulfide. Both materials can oxidize sulfide to elemental sulfur with ~90% selectivity and in synthetic solutions and real sewage. The observed removal rate of sulfide at ACF was much higher compared to GF as it was governed by the chemisorption, while sulfide oxidation on GF relied solely on electron transfer. The sulfur formed remained deposited at the anode surface, thus achieving its complete separation from the waste stream, but at the same time passivating the anode surface and leading to a substantial deterioration in the process performance. Cathodic polarisation of GF anode used for sulfide oxidation enabled only a partial dissolution (~30% removal) of the electrodeposited sulfur, and thus could not prevent completely the anode saturation with sulfur. In the case of ACF anode, the deposited sulfur layer was resistant towards all tested regeneration strategies, demonstrating irreversibility of the sulfide chemisorption.

To address the previously encountered limitations of carbon-based anodes, the second study conducted in this thesis focused on the application of manganese oxide-coated GF electrodes for (electro)catalytic removal of sulfide. GF-Mn_xO_y electrodes showed exceptional performance in terms of sulfide oxidation, enabling its rapid oxidation and complete separation from the water in the form of the deposited elemental sulfur. The oxidation of sulfide to sulfur was characterised by

very fast kinetics because of the high catalytic activity of the Mn_xO_y coating towards sulfide. Continuous regeneration of the reacted Mn_xO_y coating (i.e., reoxidation of the reduced Mn) was achieved through the application of anode potentials of only 0.4 V vs Standard Hydrogen Electrode (/SHE), thus maintaining the performance of the system over several application cycles. Nevertheless, the passivation of the anode by the formed elemental sulfur led to a gradual decrease of the rates of sulfide oxidation. Cathodic polarisation of the used GF-Mn_xO_y enabled the dissolution of the sulfur layer, yet it also had a negative impact on the stability of the Mn_xO_y coating by causing its reductive dissolution.

Finally, the third study of this thesis investigated the performance of the manganese oxide coated titanium plate with the titanium dioxide nanotube array (Ti/TiO_2-NTA) interlayer for the (electro)catalytic oxidation of sulfide to elemental sulfur. Substitution of GF substrate with the TiO_2-NTA enables more efficient regeneration of the reacted Mn compared with the material developed in the previous study, and thus drastically enhanced its stability. The Ti/TiO_2 NTA - Mn_xO_y anode yields a thirty-fold higher normalized reaction rate compared to the Mn_xO_y-coated GF anodes (i.e., $175 \cdot 10^4$ m^3 h^{-1} m^{-2} and $6 \cdot 10^4$ m^3 h^{-1} m^{-2} for Ti/TiO_2NTA-Mn_xO_y and GF-Mn_xO_y, respectively). Moreover, enhanced electron transfer between the substrate and the catalyst decreased the energy requirements of system, from 0.44 for GF- Mn_xO_y material to 0.3 kW h m^{-3} in the case of the Ti/TiO_2-NTA-Mn_xO_y anode. More importantly, loss of performance due to electrode passivation in both synthetic electrolyte and real sewage was effectively prevented by switching from sulfur electrodeposition to the production of colloidal sulfur. Considering the small footprint, low cost, stability, high efficiency and selectivity, the electrocatalytic sulfide removal based on the Ti/TiO_2 NTA-MnO_2 can potentially evolve into an important desulfurization technology for sewage or other types of waste streams.

Resumen

La formación de sulfhídrico representa un desafío importante en la operación de los sistemas de recolección de aguas residuales urbanas. El sulfhídrico es un gas tóxico y maloliente que causa la corrosión de tuberías, pozos y construcciones, perjudicando la integridad estructural de los sistemas de recolección y reduciendo significativamente su vida útil. El control de la formación de sulfhídrico normalmente se realiza mediante la dosificación de productos químicos al agua residual, lo que genera considerables costos operativos y riesgos asociados con el transporte, almacenamiento y manejo de productos químicos.

El tratamiento electroquímico del sulfhídrico es una alternativa atractiva comparado con las tecnologías utilizadas habitualmente para el control de sulfhídrico, ya que ofrece una eliminación robusta del sulfhídrico *in situ* y evita los costes y riesgos relacionados con el uso de productos químicos. Los mecanismos y productos de la oxidación electroquímica del sulfhídrico dependen en gran medida del tipo de materiales y electrodos empleados. Por ejemplo, la oxidación de sulfhídrico en electrodos de titanio recubiertos de óxido de metal mixto (MMO) procede principalmente de su oxidación indirecta por el oxígeno generado electroquímicamente, que a su vez produce azufre, sulfato y tiosulfato como productos finales [1]. Sin embargo, esta oxidación indirecta no es selectiva, y aproximadamente el 50% del total de electrones se utiliza para la oxidación de compuestos orgánicos, lo que reduce la eficiencia actual del proceso. El sulfhídrico es una especie electroquímicamente activa que también se puede oxidar directamente a azufre elemental a bajo potencial anódico, reduciendo así los requisitos de energía necesarios. Aunque el azufre elemental puede ser utilizado por microorganismos, su uso como aceptor de electrones en el metabolismo bacteriano está limitado principalmente debido a la baja solubilidad del azufre en

agua. Por tanto, la oxidación electroquímica de sulfhídrico a azufre debería ayudar a minimizar el problema de su reducción. Sin embargo, todavía hay incógnitas sobre la idoneidad de la eliminación electroquímica de sulfhídrico a escala real debido a varios inconvenientes, como la falta de materiales de ánodo apropiados y la pasivación gradual del electrodo con el azufre electrodepositado. Por lo tanto, el objetivo principal de esta tesis es investigar el desempeño de la oxidación electroquímica de sulfhídrico a azufre elemental mediante: *i)* el uso de materiales de electrodo a base de carbono con una alta selectividad hacia producción de S^0, *ii)* el desarrollo de nuevos materiales de ánodos capaces de oxidación rápida y selectiva de sulfhídrico a azufre elemental a potenciales bajos, y *iii)* aplicación de diferentes estrategias de regeneración para la eliminación del S^0 electrodepositado y la posterior recuperación de azufre.

El primer estudio realizado en esta tesis consiste en la evaluación de ánodos de carbono poroso, fieltro de grafito (GF) y fieltro de carbón activado (ACF), para la eliminación electroquímica de sulfhídrico. Ambos materiales pueden oxidar el sulfhídrico a azufre elemental con una selectividad de ~90% tanto en soluciones sintéticas como en aguas residuales reales. La tasa de eliminación de sulfuro observada en ACF resultó mucho más alta en comparación con GF, ya que estaba gobernada por la quimisorción, mientras que la oxidación de sulfuro en GF se basó únicamente en la transferencia de electrones. El azufre formado permaneció depositado en la superficie del ánodo, logrando así su completa separación de la corriente residual, pero al mismo tiempo pasivando la superficie del ánodo y provocando un deterioro sustancial en el rendimiento del proceso. La polarización catódica del ánodo GF utilizado para la oxidación del sulfuro permitió solo una disolución parcial (~ 30% de eliminación) del azufre electrodepositado y, por lo tanto, no pudo evitar por completo la saturación del ánodo con azufre. En el caso del ánodo de ACF, la capa de

azufre depositada mostró resistencia a todas las estrategias de regeneración probadas, lo que demuestra la irreversibilidad de la quimisorción del sulfuro.

Para superar las limitaciones encontradas anteriormente respecto a los ánodos a base de carbono, el segundo estudio realizado en esta tesis se centró en la aplicación de electrodos GF recubiertos de óxido de manganeso para la eliminación (electro)catalítica de sulfhídrico. Los electrodos GF-Mn_xO_y mostraron un rendimiento excepcional en términos de oxidación de sulfuros, lo que permitió su rápida oxidación y separación completa del agua en forma de azufre elemental depositado. La oxidación de sulfhídrico a azufre se caracterizó por una cinética muy rápida debido a la alta actividad catalítica del recubrimiento de Mn_xO_y. La regeneración continua del recubrimiento de Mn_xO_y reaccionado (es decir, la re-oxidación del Mn reducido) se logró mediante la aplicación de potenciales de ánodo de solo 0.4 V vs electrodo de hidrógeno estándar (/SHE), manteniendo así el rendimiento del sistema durante varios ciclos de aplicación. Sin embargo, la pasivación del ánodo por el azufre elemental formado condujo a una disminución gradual de las velocidades de oxidación del sulfuro. La polarización catódica del GF-Mn_xO_y usado permitió la disolución de la capa de sulfhídrico, pero también tuvo un impacto negativo en la estabilidad del recubrimiento de Mn_xO_y al provocar su disolución reductora.

Finalmente, el tercer estudio de esta tesis investigó el rendimiento del titanio recubierto de óxido de manganeso con la capa intermedia de matriz de nanotubos de dióxido de titanio (Ti/TiO_2-NTA) para la (electro)oxidación catalítica de sulfhídrico a azufre elemental. La sustitución del sustrato GF por TiO_2-NTA altamente conductivo permite una regeneración más eficiente del Mn reaccionado en comparación con el material desarrollado en el estudio anterior y, por lo tanto, mejoró drásticamente su estabilidad. El ánodo Ti / TiO_2 NTA - Mn_xO_y produjo una velocidad de reacción normalizada treinta veces superior a la de los ánodos GF revestidos con Mn_xO_y (es decir,

$175 \cdot 10^4$ m^3 h^{-1} m^{-2} y $6 \cdot 104$ m^3 h^{-1} m^{-2} para Ti/TiO_2NTA-Mn_xO_y y GF- Mn_xO_y, respectivamente). Además, la transferencia de electrones mejorada entre el sustrato y el catalizador disminuyó los requisitos de energía del sistema, de 0.44 para el material GF-Mn_xO_y a 0.3 kW h m^{-3} en el caso del ánodo Ti/TiO_2-NTA-Mn_xO_y. Más importante aún, la pérdida de rendimiento debido a la pasivación del electrodo tanto en electrolito sintético como en aguas residuales reales se evitó de manera eficaz cambiando de la electrodeposición de azufre a la producción de azufre coloidal. Teniendo en cuenta el tamaño reducido, el bajo costo, la estabilidad, la alta eficiencia y la selectividad, la eliminación de sulfuro electrocatalítico basada en Ti / TiO2 NTA-MnO_2 puede evolucionar potencialmente a una importante tecnología de desulfuración para aguas residuales u otros tipos de corrientes de desechos.

Resum

La formació de sulfhídric representa un desafiament important en l'operació dels sistemes de recollida i transport d'aigües residuals urbanes. El sulfhídric és un gas tòxic i odorós inductor de corrosió en canonades, pous i construccions de ciment, perjudicant la integritat estructural dels sistemes de sanejament, reduint significativament la seva vida útil. El control de la formació de sulfhídric normalment du a terme mitjançant la dosificació contínua de productes químics (oxidants, precipitants, amb capacitat de canviar el pH) directament a l'aigua residual, cosa que genera no només importants costos d'operació si no també riscos associats amb transport, emmagatzematge i manipulació d'aquests productes químics.

El tractament electroquímic és una alternativa atractiva a les tecnologies existents per al control de sulfhídric, ja que ofereix una eliminació robusta de sulfhídric in situ i evita els costos i riscos relacionats amb l'ús de productes químics. Els mecanismes i productes de l'oxidació electroquímica del sulfhídric depenen en gran mesura de la naturalesa dels materials dels elèctrodes empleats. Per exemple, l'oxidació de sulfhídric en elèctrodes de titani recoberts d'òxid de metall mixt (MMO) procedeix principalment de la seva oxidació indirecta per l'oxigen generat electroquímicament, produint sofre, sulfat i tiosulfat com a productes finals [1]. No obstant això, aquesta oxidació indirecta no és selectiva, i aproximadament el 50% del total d'electrons s'utilitza per a l'oxidació de compostos orgànics, el que redueix l'eficiència global del procés. El sulfhídric és una espècie electroquímicament activa i també es pot oxidar directament a sofre elemental a baix potencial anòdic, reduint així els requisits d'energia de sistema. Tot i que el sofre elemental pot ser degradat biològicament, el seu ús com a acceptor d'electrons en el metabolisme bacterià està limitat principalment a causa de la baixa solubilitat del sofre en aigua. Per tant, l'oxidació electroquímica de sulfhídric a sofre hauria d'ajudar a minimitzar la problema seva reducció. No

obstant, encara queden incògnites sobre la idoneïtat de l'eliminació electroquímica de sulfhídric en aplicacions a escala real a causa de diverses limitacions, com la falta de materials anòdics apropiats i la passivació gradual de l'elèctrode degut a l'electrodeposició del sobre. Per tant, l'objectiu principal d'aquesta tesi és investigar el funcionament-rendiment de l'oxidació electroquímica de sulfhídric a sofre elemental mitjançant: i) l'ús de materials d'elèctrode a força de carboni amb una alta selectivitat cap a producció de S^0, ii) el desenvolupament de nous materials anòdics capaços de dur a terme l'oxidació ràpida i selectiva de sulfhídric a sofre elemental a potencials baixos, i iii) l'aplicació de diferents estratègies de regeneració per a la remoció de l'S0 electrodepositat i recuperació de sofre.

El primer estudi realitzat en aquesta tesi consisteix en l'avaluació de ànodes de carboni porós, feltre de grafit (GF) i feltre de carbó activat (ACF), per a l'eliminació electroquímica de sulfhídric. Tots dos materials poden oxidar sulfhídric a sofre elemental amb una selectivitat de ~90% tant en solucions sintètiques com en aigües residuals reals. La taxa d'eliminació de sulfur observada en ACF va ser molt més alta en comparació amb GF, ja que estava governada per la quimisorció, mentre que l'oxidació de sulfur en el GF es va basar únicament en la transferència d'electrons. El sofre format va romandre dipositat a la superfície de l'ànode, aconseguint així la seva completa separació del corrent d'aigua residual, però a el mateix temps passivant la superfície de l'ànode i provocant un baixada substancial del rendiment del procés. La polarització catòdica de l'ànode de GF utilitzat per a l'oxidació de sulfur va permetre només una dissolució parcial (30% d'eliminació) del sofre electrodepositat i, per tant, no va poder evitar completament la saturació de l'ànode amb sofre. En el cas de l'ànode de ACF, la capa de sofre dipositada es va mostrar resistent a totes les estratègies de regeneració provades, el que demostra la irreversibilitat de la quimisorció del sulfur.

Per adreçar les limitacions trobades anteriorment dels ànodes basats en carboni, el segon estudi realitzat en aquesta tesi es va centrar en l'aplicació d'elèctrodes GF recoberts d'òxid de manganès per a l'eliminació (electro)catalítica de sulfhídric. Els elèctrodes GF-Mn_xO_y van mostrar un rendiment excepcional en termes d'oxidació de sulfurs, cosa que va permetre la seva ràpida oxidació i separació completa de la fase líquida en forma de sofre elemental dipositat. L'oxidació de sulfhídric a sofre es va caracteritzar per una cinètica molt ràpida degut a l'alta activitat catalítica del recobriment de Mn_xO_y. La regeneració contínua del recobriment de Mn_xO_y reaccionat (és a dir, la re-oxidació de l'Mn reduït) es va aconseguir mitjançant l'aplicació de potencials d'ànode de només 0.4 V vs elèctrode d'hidrogen estàndard (/SHE), mantenint així el rendiment de sistema durant diversos cicles d'aplicació. No obstant això, la passivació de l'ànode pel sofre elemental format va conduir a una disminució gradual de les velocitats d'oxidació del sulfur. La polarització catòdica de GF-Mn_xO_y usat va permetre la dissolució de la capa de sulfhídric, però també va tenir un impacte negatiu en l'estabilitat del recobriment de Mn_xO_y provocant la seva dissolució reductora.

Finalment, el tercer estudi d'aquesta tesi es va investigar el rendiment del titani recobert d'òxid de manganès amb la capa intermèdia de matriu de nanotubs de diòxid de titani (Ti/TiO_2 NTA) per dur a terme l'(electro)oxidació catalítica de sulfhídric a sofre elemental. La substitució del substrat GF per TiO_2-NTA altament conductiu va permetre una regeneració més eficient de l'Mn reaccionat en comparació amb el material desenvolupat en l'estudi anterior i, per tant, va millorar dràsticament la seva estabilitat. L'ànode Ti/TiO_2 NTA - Mn_xO_y produeix una velocitat de reacció normalitzada trenta vegades més gran en comparació amb els ànodes GF revestits amb Mn_xO_y (és a dir, 175 · 104 m^3 h^{-1} m^{-2} i 6 · 104 m^3 h^{-1} m^{-2} per a Ti/ TiO_2 NTA-Mn_xO_y i GF- Mn_xO_y, respectivament). A més, la millor transferència d'electrons entre el substrat i el catalitzador va reduir els requisits

d'energia de sistema, de 0.44 per al material GF-Mn_xO_y a 0.3 kW h m^{-3} en el cas de l'ànode Ti / TiO_2 NTA-Mn_xO_y. Més important encara, la pèrdua de rendiment a causa de la passivació de l'elèctrode, tant en l'electròlit sintètic com en les aigües residuals reals, es va evitar de manera eficaç canviant de l'electrodeposició de sofre a la producció de sofre col·loidal. Tenint en compte la petita petjada, el baix cost, l'estabilitat, l'alta eficiència i la selectivitat, l'eliminació de sulfurs electrocatalítics basada en el Ti / TiO2 NTA-MnO_2 pot evolucionar cap a una important tecnologia de desulfuració per a aigües residuals o altres tipus de corrents de residus.

Chapter 1. Introduction

1.1. Sulfur chemistry in aqueous solutions

More than 200 years of the extensive research dedicated to chemistry of elemental sulfur revealed an impressive degree of its molecular complexity. Sulfur can exist in solid, liquid, gaseous [2] and colloidal forms [3], it is characterised by the largest number of allotropes [4] and the largest number of binary oxides [5]. Typically referred to as non-metal, sulfur has been found to become a metal under high pressure (i.e., 10 K at 930 kbar) and even a superconductor under extreme conditions (i.e., 17 K at 2600 kbar) [6, 7].

In aqueous solutions, sulfur can exist in a number of oxidation states including -2 as in sulfide (HS^- /H_2S/S^{2-}), 0 as in elemental sulfur (S^0), +2 as in thiosulfate ($S_2O_3^{2-}$), +4 as in sulfite (SO_3^{2-}) and +6 as in sulfate (SO_4^{2-}) [8]. The most common inorganic sulfur species relevant for aqueous electrochemical systems along with their oxidation numbers are listed in **Table 1.1**.

Table 1.1 Oxidation states of sulfur species commonly found in aqueous solutions.

Compound name	Formula	Oxidation number
Hydrogen sulfide	HS^-	-2
Hydrogen sulfide ion (bisulfide)	H_2S	-2
Sulfide ion	S^{2-}	-2
Polysulfide	S_n^{2-}	-2/n
Elemental sulfur	S^0	0
Thiosulfate	$S_2O_3^{2-}$	+2
Sulfite	SO_3^{2-}	+4
Sulfate	SO_4^{2-}	+6

Thermodynamic stability of sulfur can visualised with Pourbaix E_h-pH diagram [9]. The Pourbaix diagram describes the thermodynamic stability of different sulfur species in the aqueous system as a function of pH and electrochemical potential, however, it does not provide any information

regarding the reaction rate or kinetics. As can be seen from Pourbaix diagram (**Figure 1.1**), H_2S, HS^-, S^0, HSO_4^- and SO_4^{2-} are sulfur species that can exist in equilibrium in aqueous solutions. Previously mentioned S_n^{2-}, $S_2O_3^{2-}$ and SO_3^{2-} are considered to form false equilibria and therefore are excluded from the diagram. Elemental sulfur is only thermodynamically stable in aqueous solutions at acidic pH (pH < 6), while increase of pH above 6 leads to its disproportionation to H_2S, HS^- and S_n^{2-} and SO_4^{2-}. However, practice shows that the kinetics of this reaction is rather slow and it normally occurs at very high temperature or pH [9]. Unlike elemental sulfur, both sulfide and sulfate in aqueous solutions remain stable over the entire pH range.

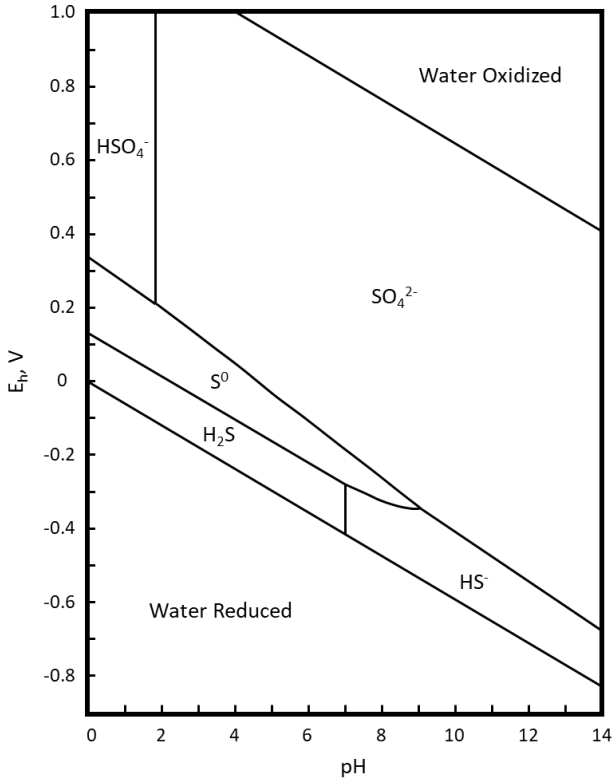

Figure 1.1 Pourbaix diagram of sulfur representing its various forms in a 0.1 M solution at 25°C and oxygen pressure of 1 bar as a function of E_h and pH, adapted from [9]. The electrochemical potential scale is expressed versus Standard Hydrogen Electrode (SHE).

1.1.1. Elemental sulfur and sulfur allotropes

The reactivity of sulfur towards S-S bond formation explains the diversity of sulfur allotropes. Allotropes of sulfur include 30 possible crystalline phases, each of them characterised by different viscosity, colour, and melting point. Depending on the bond length and angle, the molecular structure of allotropes can be cyclic or open [10]. Open allotropes rarely exist in their pure form and are normally mixed with cyclic sulfur molecules. According to the molecular symmetry, cyclic sulfur allotropes can be roughly divided into two groups [4]. Asymmetrical cyclic sulfur molecules (e.g., S_7, S_9, S_{11}, S_{13} etc.) are characterised by unequal bonds and irregular motif around the ring [11]. These molecules alternate short and long sulfur bonds, which causes ring strain and accounts for their instability [2]. On the contrary, sulfur rings, which consists of 6, 8 or 12 sulfur atoms are highly symmetrical, the bond characteristics and motifs around the ring are equal (**Figure 1.2**) [11]. Although one could expect that all these highly symmetric sulfur allotropes are more stable compared to the asymmetric ones, S_6 and S_{12} are quite unstable due to unfavourable torsion angles. As a result, under standard temperature and pressure conditions, the optimal sulfur molecule configuration is S_8 ring and all sulfur allotropes end up transformed into S_8 [10].

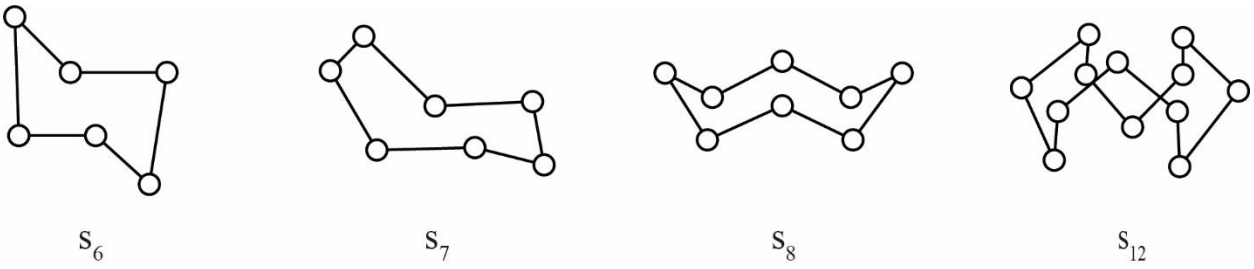

Figure 1.2 Molecular structures of the homocyclic S_6, S_7, S_8 and S_{12} molecules [4].

Sulfur molecule, which forms a cyclic crown S_8 ring, is also called orthorhombic sulfur (α-sulfur). α-S8 orthorhombic sulfur is soft, odourless, bright yellow solid, with very low solubility in water (i.e., 5 µg L^{-1} at 20 °C). It melts at 115.21°C, boils at 444.6°C and can be easily sublimed [4]. After thermal treatment, α-S8 cyclic sulfur can be transformed to β- or γ-S8 cyclic sulfur. These sulfur molecules have similar geometry, though, the bond length, bond angles and torsion angles are affected by the difference in crystal structures. However, this transformation is reversible and as soon as sulfur is cooled down below certain temperature (i.e., 96 °C), the crystal structure will be converted back to the initial α-sulfur phase [12].

1.1.2. Colloidal sulfur

As mentioned above, sulfur is almost insoluble in water [4]. However, when sulfur particles are small enough, sulfur can be suspended in a colloidal solution [13]. Colloidal particles have the size that ranges from 1 to 100 nm and consist either of α-S8 orthorhombic sulfur (hydrophobic sulfur colloids) or of a combination of chain and ring sulfur molecules with hydrophilic terminal groups like sulfonate or functionalised organic group (hydrophilic sulfur colloids) [3, 14, 15]. Both hydrophobic and hydrophilic particles are characterised by the negative surface charges. The balance between electrostatic repulsion forces and Van der Waals attraction forces stabilizes the suspension [14-16]. Hydrophobic sulfur particles are actually amphipathic, meaning that they are composed of liquid rather than crystalline sulfur [3]. Liquid sulfur is thermodynamically unstable, therefore, it eventually crystalizes into minute crystals of α-S8, which coagulates into particles of up to 50 µm and precipitates [3, 15].

Unlike hydrophobic colloidal sulfur solution, that can only reach concentration of 0.1 g L^{-1}, hydrophilic colloidal suspensions can be much more concentrated (e.g., 600 g L^{-1} of sulfur) [17].

Even though certain stabilization of the hydrophilic suspension is achieved due to hydrophilic terminal groups, unstable sulfur chains and various cyclic sulfur allotropes eventually transform into α-S8 and settle like hydrophobic sulfur [15].

1.1.3. Hydrogen sulfide

Covalent hydride of sulfur also called hydrogen sulfide (H_2S) is a gas with characteristic smell of a rotten egg, stable under conditions of standard temperature and pressure [18]. Hydrogen sulfide can be dissolved in aqueous solutions (80 mM at 37°C, 100 mM at 25°C, 122 mM at 20°C), and its solubility greatly depends on the temperature, partial pressure, and nature of the solution [19-21]. For example, increasing temperature and salinity significantly lowers the solubility of sulfide [22]. During the solvation process, H_2S does not form hydrogen bonds with water molecules, and instead behaves rather like a hydrophobic solute [23]. After its dissolution, hydrogen sulfide can easily volatilize from the surface considering its high Henry´s constant (i.e., 3.99) [18]. Thus, hydrogen sulfide exists in a dynamic equilibrium between gas and liquid phases (**Figure 1.3**):

$$H_2S_{(g)} \leftrightarrow H_2S_{(aq)} \leftrightarrow HS^- + H^+ \leftrightarrow S^{2-} + 2H^+ \qquad \text{(Eq. 1.1)}$$

Solvated hydrogen sulfide is a weak acid, which dissociates into proton and hydrogen sulfide (HS^-) , its conjugate base [24]. HS^- dissociates further yielding S^{2-} and an additional proton. H_2S ionization in aqueous solution at given pH can be calculated according to the Henderson-Hasselbalch equation, knowing that its pK_a value is 6.98 ± 0.01 at 25 °C [20, 25]. For example, H_2S dissolution at pH 8, yields approximately 10 % of H_2S and 90% of HS^-. Given that the pK_a value for the ionization of HS^- is very high ($pK_a(HS^-)$=17 – 19 at 25°C), S^{2-} presence in the solution is negligible [26, 27]. A recent study claimed that S^{2-} simply does not exist as the authors could not detect its formation even under very favourable conditions [28].

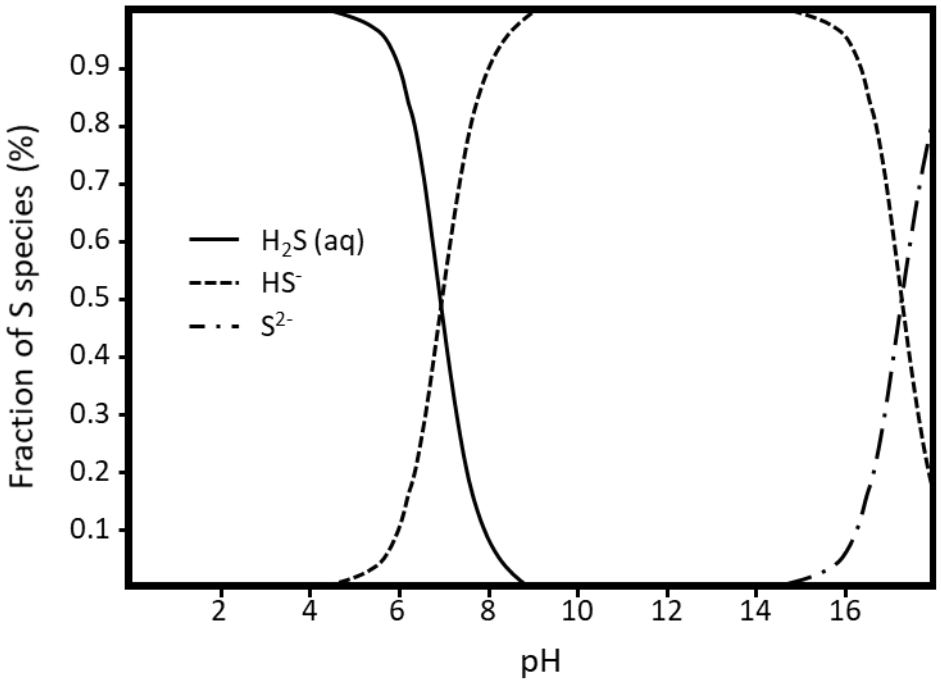

Figure 1.3 Sulfide solubility chart showing the relative fraction of each sulfide species at different pH, adapted from [29].

According to the Le Chatelier's principle for an open system, the equilibrium in aqueous hydrogen sulfide speciation will constantly shift leftwards, favouring the formation and volatilization of $H_2S_{(g)}$. The equilibria shift must be considered especially when working at acidic pH or in non-buffered solutions, as it causes major sulfide loss and solution alkalinisation [30, 31].

H_2S is a highly reactive species. Sulfur in H_2S has an oxidation state of -2, the possible lowest for sulfur. It can react with various oxidizing agents such as oxygen, hydrogen peroxide, chlorine, and ozone [25, 32-35]. Sulfide is also characterised as nucleophile and can react via nucleophilic substitution with a wide range of electrophiles, including metal salts [36-38].

1.1.4. Polysulfides

Polysulfides contain unbranched chains comprised of one divalent sulfur atom and up to eight zero-valent sulfur atoms [39-41]. The presence and the chain length of polysulfide species is determined by the pH of the solution. Polysulfides cannot exist in acidic environments, as these conditions are favourable for the formation of cyclic sulfur molecules (e.g α-S_8). As pH is increased to a more basic range, sulfur ring will open to form a water soluble polysulfide chain [42]. At mildly alkaline pH, polysulfides with chain lengths of S_4^{2-}, S_5^{2-}, S_6^{2-} are dominant in the solution, while shorter chained ones including S_2^{2-} and S_3^{2-} can only be observed at very high pH (i.e., pH>11) [40].

Polysulfides are a key intermediate that is typically involved in many processes of sulfur transformation. For example, sulfide can perform a nucleophilic attack on elemental sulfur, yielding polysulfides with different chain lengths [41, 42]:

$$HS^- + (n-1)/8\ S_8 \rightarrow S_x^{2-} + H^+ \qquad \text{(Eq. 1.2)}$$

1.1.5. Sulfur oxyanions

Sulfate (SO_4^{2-}) is the most abundant sulfur oxyanion in Earth's water bodies. The anion of sulfate is tetrahedral, which consists of central sulfur atom surrounded by the four oxygen atoms (**Figure 1.4**) [43]. The arrangement of sulfate results in the shortening of the S-O bonds, which accounts for the high stability of the anion [44]. In addition, shortening of the bonds kinetically inhibits the reduction of this oxyanion at ambient temperatures, though SO_4^{2-} is the most oxidized sulfur species [45]. Sulfate reduction can be achieved by the microbial metabolic activity since sulfate capturing by adenosine triphosphate yields adenylyl sulfate, where S-O bond is elongated due to

the attachment of the phosphate group. Bond elongation is followed by reduction of sulfate to sulfide carried out by adenosine phosphosulfate (APS) reductase enzyme [46].

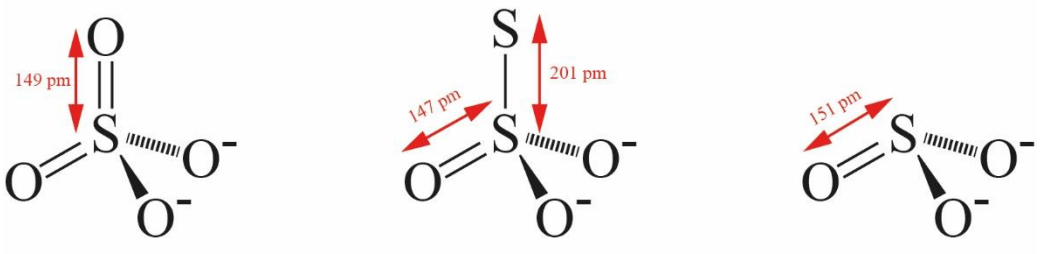

Figure 1.4 Ionic structures of sulfate (SO_4^{2-}), thiosulfate ($S_2O_3^{2-}$) and sulfite (SO_3^{2-}).

The structure of thiosulfate ($S_2O_3^{2-}$) resembles that of sulfate, with sulfur atom replacing one oxygen. Such ionic structure and charge distribution imply that $S_2O_3^{2-}$ is readily involved in redox reactions in which the each sulfur atoms react differently. Since S-S bond is less stable compared to the S-O, the outer sulfur of thiosulfate can be easily reduced to sulfide, while the inner sulfur stays bonded to oxygen [47].

At acidic pH thiosulfate decomposes, yielding bisulfite and zero-valent sulfur [48]:

$$S_2O_3^{2-} + H^+ \rightarrow S^0 + HSO_3^- \qquad \text{(Eq. 1.3)}$$

Bisulfite can also be produced by the dissolution of $SO_{2(g)}$ in water [49]:

$$SO_2 + H_2O \rightarrow HSO_3^- + H^+ \qquad \text{(Eq. 1.4)}$$

At neutral pH, typical for natural waters, bisulfite dissociates yielding sulfite:

$$HSO_3^- \rightarrow SO_3^{2-} + H^{+\,-} \qquad \text{(Eq. 1.5)}$$

Under aerobic conditions, sulfite rapidly reacts with the dissolved oxygen, producing sulfate [50]:

$$SO_3^{2-} + 0.5O_2 \rightarrow SO_4^{2-} \quad \text{(Eq. 1.6)}$$

1.2. Global sulfur cycle

Sulfur is one of the most abundant elements on earth [10]. The wide range of possible sulfur valence states results in a balanced cycle achieved through closely interconnected geochemical and biological processes. These processes of sulfur transformations and recycling occur through lithosphere, hydrosphere, atmosphere and biosphere. Moreover, sulfur cycle closely interacts with the cycles of many other elements (e.g., oxygen, carbon, iron and nitrogen), which further increases its impact on the global ecosystem [51-54].

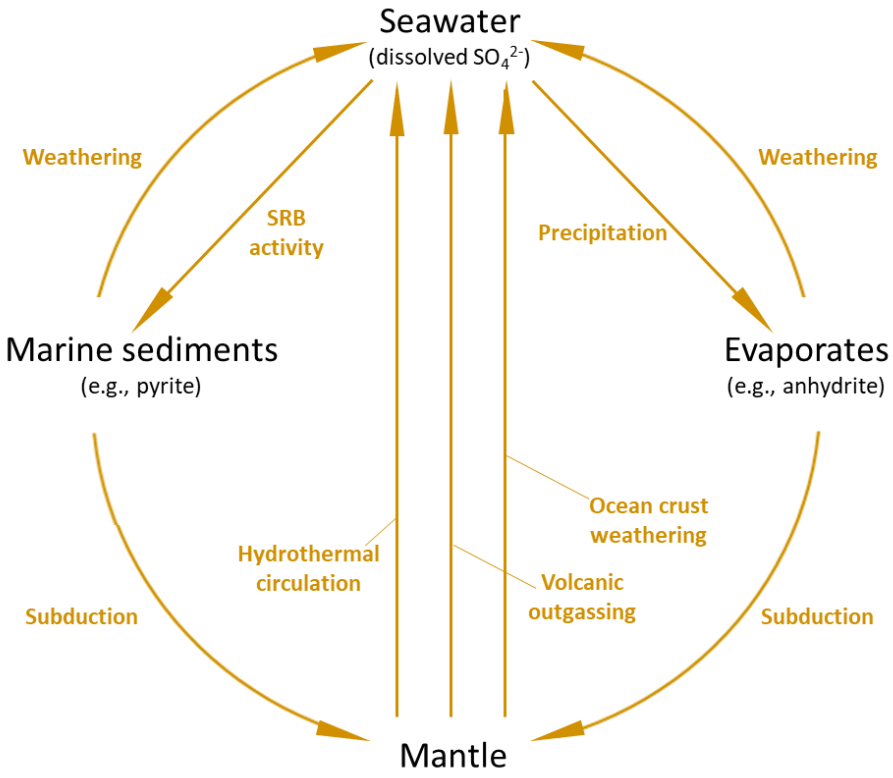

Figure 1.5 Simplified sulfur cycle from geochemical prospective, adapted from [55].

The main global sulfur reservoirs include: sulfate dissolved in the world's oceans, sulfate in the ancient evaporate deposits and sulfide typically in the form of pyrite FeS_2 in the marine sediments [55-57]. The sulfur reservoirs are continuously replenished by juvenile sulfur or gaseous sulfur (SO_2 and H_2S) as a result of the volcanic activity, and eventually end up rained out to the oceans [58]. Another source of sulfur reservoirs augmentation is wearing of the ingenious rocks such as pyrite and gypsum, which transfers the sulfur to the oceans [56]. The global sulfur cycle is comprised of essential processes, which recycle sulfur between these reservoirs (**Figure 1.5**).

The most important flux of sulfur takes place in the world's oceans. The process is mainly driven by the bacterial sulfur reduction, which typically occurs in the anaerobic environments within the marine sediments. Sulfate reducing bacteria (SRB) perform anaerobic respiration using sulfate as a terminal electron acceptor, and reducing it to sulfide [59]. Sedimentary organic matter normally serves as an electron donor, although some SRB species can utilize H_2 for this purpose [60].

$$SO_4^{2-} + 2CH_2O \rightarrow H_2S + 2HCO^{3-} \qquad \text{(Eq. 1.7)}$$

The major fraction of biologically produced sulfide reaches aerobic environment and gets re-oxidized back with dissolved oxygen or becomes oxidized within the anaerobic sediment through interaction with Fe(III) or Mn(IV) [61]. Besides that, sulfide can react with dissolved Fe^{2+} or Fe(II) in the sediments to form sedimentary pyrite and organosulfur complexes with the sedimentary organic matter [62]. Another minor sulfur sink is the formation of sulfate evaporate deposit, when sulfate is incorporated into the marine carbonate rocks. The sedimentary rocks, including pyrite or sulfate evaporates, can be either exposed to weathering environment and converted back to sulfate, or lost to the mantle through the process of subduction [55].

Sulfur species found in natural environments can be utilized as electron donor or acceptor in various microbial metabolisms. The balance between oxidative and reductive processes gives rise to biologic sulfur cycle, where sulfur is continuously recycled between sulfate and reduced forms such as sulfide or sulfur containing amino acids [55, 57, 59, 63]. The cycle embraces an eight-electron change between sulfate and sulfide and occurs through the formation of intermediates such as elemental sulfur, thiosulfate, and sulfite (**Figure 1.6**).

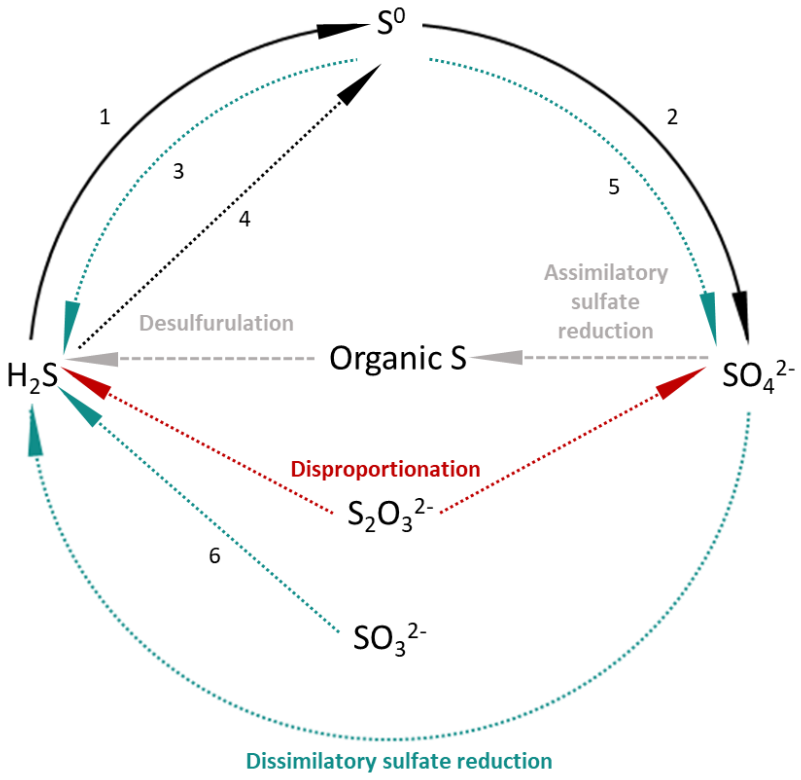

Figure 1.6 Simplified biological sulfur cycle adapted from [64]. Solid lines represent aerobic reactions, dotted lines represent anaerobic reactions, and dashed lines indicate processes that can be both aerobic and anaerobic. **1** and **2**: Aerobic colourless sulfur bacteria, **3**: Sulfur reducing bacteria, **4** and **5**: Anaerobic purple sulfur bacteria and green sulfur bacteria, **6**: Sulfite-reducing bacteria.

Previously mentioned sulfate reducing microorganisms include SRB and sulfate reducing archaea [65]. The metabolism of SRB can be dissimilatory, which is catabolic and aimed at energy gain, or assimilatory, when sulfate is reduced for anabolic needs [66]. Dissimilatory pathway is a large scale process which consumes significant quantities of sulfate and expels resulting sulfide in the environment [67]. On the contrary, assimilatory sulfate reduction requires only small amounts of sulfate , that is utilized for amino-acids production [68].

In the absence of other terminal electron acceptors (e.g., sulfate, sulfite, thiosulfate, nitrate or nitrite), SRB are able to utilize colloidal sulfur as a respiratory substrate [65, 69, 70]. Elemental sulfur is relatively bioavailable and, unlike sulfate, it does not require additional step of energy-dependent activation prior to the reduction [64]. However, the utilization of elemental sulfur as electron acceptor is limited mainly due to the low solubility of sulfur in water (0.16 μmol l^{-1}at 25 ^{o}C) [13, 71]. Interestingly, colloidal sulfur can inhibit SRB growth in the presence of sulfate probably due to shift of the potential of redox couple to unfavourable positive values [13, 70].

Sulfide can be oxidized to sulfate by the sulfur oxidising bacteria (SOB). Based on the preferred energy source, SOB can be divided into photolithotrophs, which obtain energy from light, and chemolithotrophs, whose main energy source is sulfide oxidation [72, 73]. Although most sulfur oxidizers require oxygen as terminal electron acceptor (e.g., colorless sulfur bacteria), some phototrophic SOBs are able to grow in the anaerobic conditions using nitrate or nitrite (e.g., purple sulfur bacteria and green sulfur bacteria) [74, 75]. Diversity of SOBs entails a variety of possible sulfide oxidation products, including elemental sulfur, thiosulfate and sulfate [55, 72].

Thiosulfate can be microbially disproportionated into sulfide and sulfate. Many of these bacteria are also capable of sulfate reduction, though obligate disproportionators can also be found [76, 77].

1.3. Anthropogenic impact on sulfur cycle

Even though sulfur contamination of water bodies is becoming increasingly prominent due to the industrialization and urbanization, this problem is often overlooked because sulfur is seen as a natural component of the ecosystem [55]. Meanwhile, in the recent decade, average sulfate concentration in the polluted rivers increased from less than 0.1 mM to 0.2 mM [78]. Even though sulfate ingestion at moderate concentrations is not associated with any adverse human health effect, its excessive presence in the drinking water (i.e.,>5 mM) may cause different gastroenterological implications for consumers [79]. Increased sulfate load can interfere with the ecosystem balance by creating stressful conditions for the living organisms. In extreme cases, sulfate pollution can lead to death of aquatic invertebrates [80, 81]. Sulfate contamination also has an impact on the carbonate wearing, erosion and global carbon cycle [82, 83].

However, the most harmful environmental impact of sulfate contamination is indirect, which occurs when sulfate is reduced to hydrogen sulfide in an anaerobic environment [81]. It represents a serious threat for various aquatic organisms through several mechanisms such as mitochondrial depolarisation, decreased haemoglobin oxygen affinity and inhibition of up to 20 enzymes involved in the aerobic respiration, including cytochrome *c* oxidase [84-87]. Sulfide can also increase the availability of nutrients through the reaction with iron phosphates present in the marine and freshwater sediments [88, 89]. This interaction results in the formation of iron sulfide,

with subsequent release of phosphate, which can lead to the intensification of eutrophication in the water bodies [78].

Exposure to hydrogen sulfide is acutely toxic for humans. Hydrogen sulfide poisoning typically occurs in the places of its accumulation like industrial settings or sewer systems [90, 91]. At concentrations as low as 1 – 2 mg L^{-1}, hydrogen sulfide can already be recognised by the nauseous "rotten egg" odour. At 10 mg L^{-1}, hydrogen sulfide causes irritation of the respiratory tract and breathing difficulties even at short exposure time. Increased exposure, both in terms of time and concentration, affects nervous, respiratory and cardiovascular systems [92]. Besides that, hydrogen sulfide at concentrations above 150 mg L^{-1} leads to olfactory fatigue [93]. The inability to detect hydrogen sulfide is life threatening, given that at high concentrations (i.e., >500 mg L^{-1}) it can cause death or loss of consciousness, sometimes accompanied with irreversible neurotoxic processes [94]. Intake of sulfide containing drinking water is also potentially hazardous, however, it never occurs in practice because sulfide at concentration high enough to be threatening for human health makes the water unpalatable. For example, at concentration as low as 0.1 mg L^{-1}, sulfide presence can already be detected by most people [95].

To prevent and control the problems caused by sulfate pollution, it is intrinsic to identify the sources of contamination. Agriculture often requires the extensive use of pesticides, many of which contain substantial amounts sulfur. The runoff from agricultural land significantly increases the sulfur load in the nearby water bodies [96]. Sulfur from chemical pesticides can also infiltrate underneath the areas of agricultural activity, which increases sulfate concentrations in the shallow groundwater systems [97]. Sulfate pollution caused by the numerous industrial processes is even more severe. For example, petroleum refining and mining, pulp and paper production, tannery

operations and fermentation discharge effluents where sulfate concentration can reach several thousands of mg L^{-1} [98-101].

Urban water cycle also interferes with the sulfur balance by producing sulfate containing waste streams. Sulfate is naturally present in water, however, its concentration in waste streams is further increased through utilization of alum-based flocculants used for the potable water purification and human waste discharge [102, 103]. Moreover, certain strategies aimed at the optimization of water use such as substitution of freshwater with seawater for cooling or toilet flushing can further increase the sulfate content in the urban wastewater. For example, this approach has been practiced for more than 50 years in Hong Kong, leading to massive production of saline effluent with higher sulfate content compared to average sewage, i.e., 550 mg L^{-1}, vs 15 mg L^{-1} of sulfate typically present in the sewage [104, 105].

Sulfur containing waste is also being heavily discharged into the atmosphere, mostly in the form of sulfur dioxide (SO_2). Even though natural processes such as major forest fires or volcanic eruptions can result in the release of substantial amount of SO_2 into atmosphere, these events occur only sporadically, while emissions caused by the anthropogenic activity are continuous and long-term [106, 107]. As a result, 76% of the total atmospheric SO_2 originates from the anthropogenic sources, predominantly from the combustion of fuels including coal, natural gas, biogas and oil [108, 109]. Under high temperature, organic sulfur, metal sulfides or hydrogen sulfide contained in these fuels are oxidized to sulfur dioxide or, to a lesser extent (i.e., 1 – 10%), to sulfur trioxide (SO_3) [110, 111]. In addition, industrial processes like treatment of sulfide ores of non-ferrous metals, oil refining and sulfuric acid production also contribute to the global anthropogenic SO_2 emissions [112]. Sulfur dioxide is highly toxic to humans and may lead to adverse health effects [113]. In turn, sulfuric acid, the product of SO_2 oxidation, is the major cause of acid rains which

cause serious damage to vegetation, corrosion and acidification of soil and water bodies [114]. Moreover, the tendency of sulfuric acid to nucleate leads to the formation of ultrafine aerosols, which contribute to the global warming either directly or through enhancing cloud formation [106, 115-117]. These fine acidic sulfate aerosols also represent a major public health hazard as inhalation of acidic species is highly damaging for lungs [118, 119]. Besides that, the presence of sulfuric acid aerosols in the atmosphere significantly reduces the visibility [119, 120]. Even though sulfur dioxide emissions were reduced in the past 40 years primarily due to the introduction of desulfurization technologies and substitution of coal with cleaner fuel alternatives, sulfur compounds remain a major air pollutant, especially in the developing countries [121].

1.4. Sulfide-induced corrosion in sewers

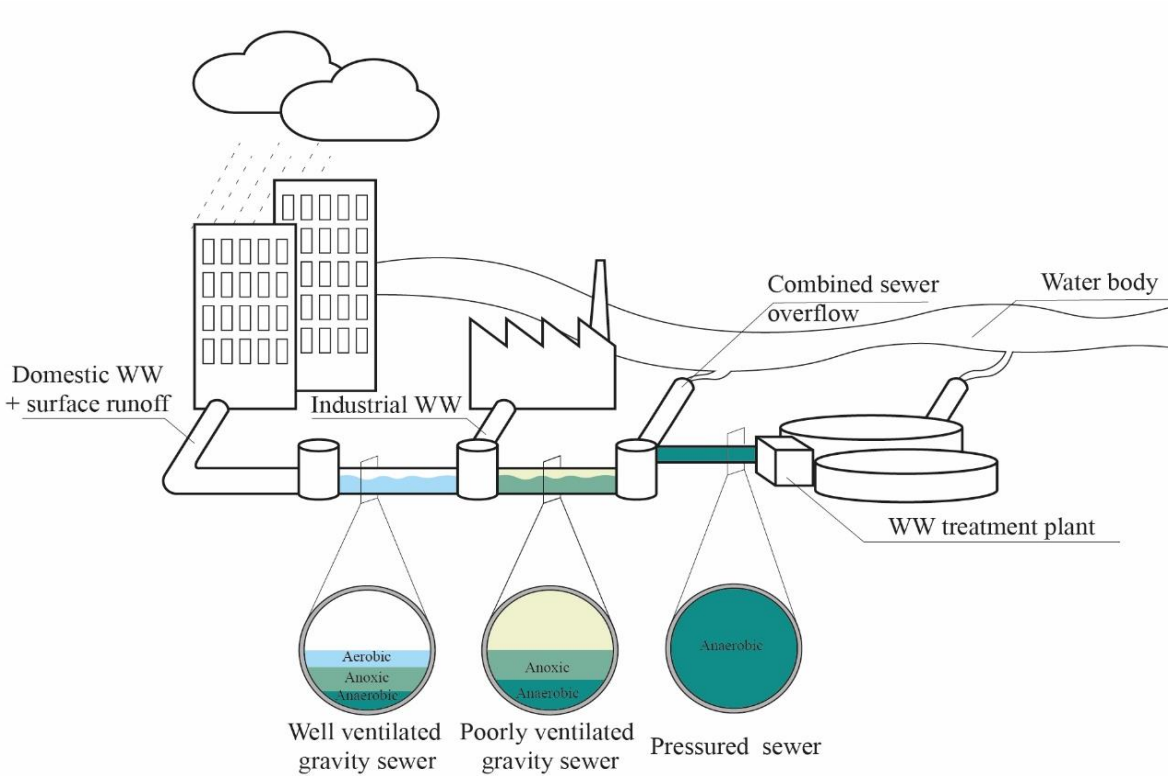

Figure 1.7 Schematic diagram of gravity and pressure sewers.

Wastewater streams typically end up discharged into the sewer networks. While serving its main purpose of wastewater collection and transportation, sewer system also acts as a "bioreactor", transforming wastewater components under anaerobic, anoxic or aerobic conditions (**Figure 1.7**). Dissolved oxygen in transported wastewater is quickly depleted in the process of microbial organic matter degradation [122]. As a result, anaerobic conditions are typically prevalent in the aqueous phases of both gravity and pressurised sewers, except for those that are characterised by the high flow-through velocity and forced re-aeration of the gaseous phase [123, 124]. The absence of oxygen favours the SRB anaerobic respiration, resulting in sulfate reduction to sulfide [65].

Biologically produced sulfur cannot be oxidized under anaerobic conditions. Instead, it is released as hydrogen sulfide into the gaseous phase of manholes, gravity sewers and pumping stations (**Figure 1.8**) [125]. The build-up and the release of sulfide is particularly substantial under favourable conditions for SRB growth and activity. Since the metabolism of SRB requires both sulfate and biodegradable organic matter, the optimal ratio between them leads to abundant hydrogen sulfide formation [126, 127]. Another crucial factor for the biological activity of SRB is the flow rate of the waste stream. In gravitational sewers, slow flow through rate favours SRB activity by enhancing sedimentation and promoting anaerobic conditions in the formed sediment [128]. On the contrary, low velocities in the pressurised sewers may supress sulfide generation as organic matter and sulfate essential for its production become quickly depleted [125]. An increase of velocity up to a point that still allows formation of biofilm with sufficient thickness significantly increases potential for the sulfide formation [129]. Temperature above 15^{o}C not only stimulates SRB activity, but also enhances the emission of hydrogen sulfide into the air phase of sewer networks [130, 131]. Besides that, the emission of hydrogen sulfide into the gaseous phase can be promoted by high turbulence of the flow or the decrease of the steam pH [132].

After its release into the gaseous phase, sulfide can be absorbed into the liquid film covering moist concrete pipe surface [133-135]. Hydrogen sulfide absorption process, together with the concrete carbonation, reduces the pH of the pipe surface from pH 13 to pH 9 [133, 135-138]. Neutral pH makes the concrete surface suitable for the neutrophilic SOB colonization. Neutrophilic SOB can oxidize hydrogen sulfide diffused into the liquid film into various sulfur species including S^0, $S_2O_3^{2-}$ and SO_4^{2-} [139-141]. Sulfuric acid, the main product of the SOB activity, reacts with the concrete surface and further lowers its pH. When pH is decreased until pH 4 – 5, acidophilic SOB gradually take over the surface, while neutrophiles become inhibited [134]. Acidophilic SOB can perform direct oxidation of hydrogen sulfide into sulphuric acid. Moreover, acidophilic SOB is more versatile in terms of the electron donor, for example, they can also utilize $S_2O_3^{2-}$ and S^0 deposited at the sewer walls as a result of the hydrogen sulfide oxidation with oxygen [138, 139, 142-144]. Interestingly, sulfuric acid production in sewers is not a strictly biological process. For example, at very high hydrogen sulfide concentration (e.g 100 mg L^{-1}), hydrogen sulfide can be oxidized to sulfate chemically [145]. Under these conditions, acidophilic SOB activity can be initiated immediately, avoiding the first step of pH reduction [146].

Hardened concrete typically used for sewer construction is alkaline, therefore it is prone to degradation under acidic environments [147]. The reaction between sulfuric acid and alkaline components of the concrete results in the formation of gypsum, which can further react with the aluminate phase producing etteringite [138, 148-150] (**Figure 1.8**):

$$H_2SO_4 + CaCO_3 \rightarrow H_2O + CO_2 + CaSO_4 \qquad \text{(Eq. 1.8)}$$

$$3CaSO_4 + 3CaO{\cdot}Al_2O_3{\cdot}6H_2O + 26\ H_2O \rightarrow 3CaO{\cdot}Al_2O_3{\cdot}3CaSO_4{\cdot}32\ H_2O \qquad \text{(Eq. 1.9)}$$

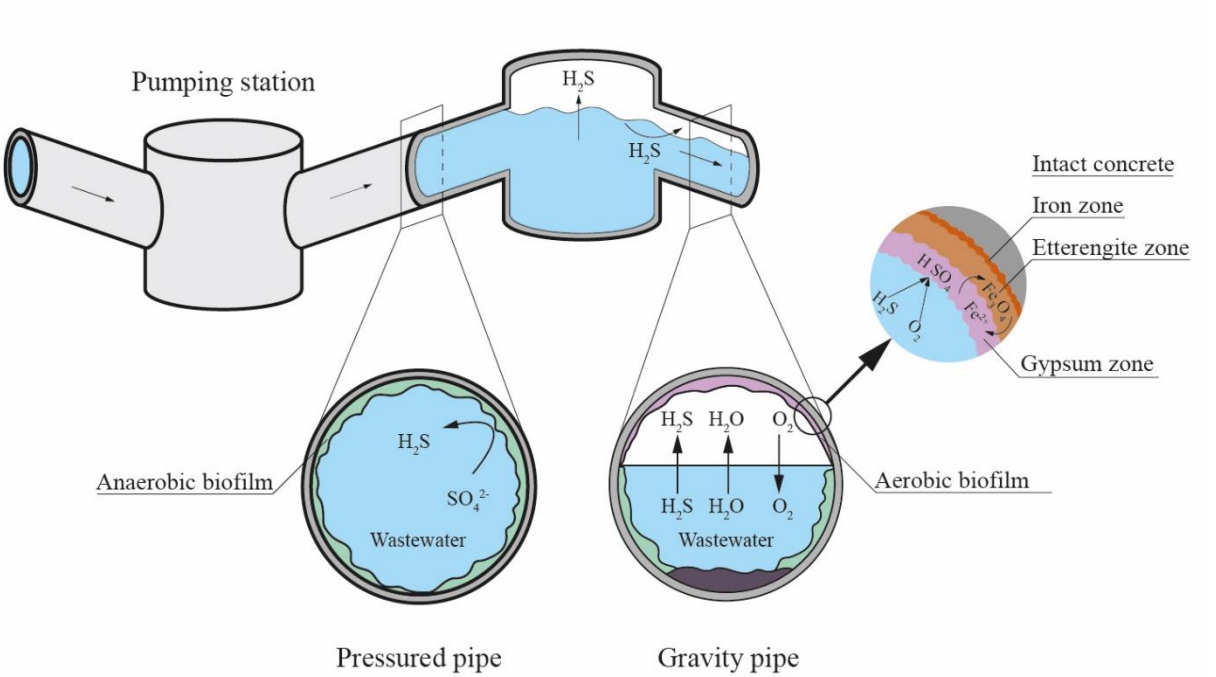

Figure 1.8 Schematic diagram of sewer system, summarizing the major processes that lead to release of hydrogen sulfide, acid formation in the aerobic biofilms and the onset of sewer corrosion.

Formation of these corrosion products leads to a significant concrete mass loss. The observed concrete loss is typically the highest at the sewer crown and the pipe walls around the water surface level [139]. The reported concrete corrosion rates vary greatly, probably because the process of corrosion can be affected by many factors. However, the average rates range between 2 – 3 mm per year, reaching 10 mm per year in the extreme cases [147]. Both gypsum and etteringite have a larger volume compared to the pristine concrete, therefore their formation is associated with the internal cracking and pitting of the material [148, 149]. Thus, the corrosion process allows deeper penetration of the moisture, acid and bacteria into the concrete structure, accelerating the process of corrosion [150]. In the case of the steel reinforced concrete pipes, the gradual destruction of the protective concrete layer leads to a direct exposure of steel rebar to the corrosive environment of

the sewer. Rust, the main product of steel corrosion, fills the pores of the steel-concrete interface and further increases the expansive stress on the surrounding concrete layer (**Figure 1.8**) [148, 151, 152]. Sulfide induced corrosion can be avoided by substituting the concrete with the corrosion-resistant materials, for example vitrified clay, PVC, FRP or HDPE. In this case, instead of reacting with the moist concrete surface, hydrogen sulfide will accumulate in the sewer atmosphere, reaching threateningly high concentrations of up to 800 mg L^{-1} [153, 154].

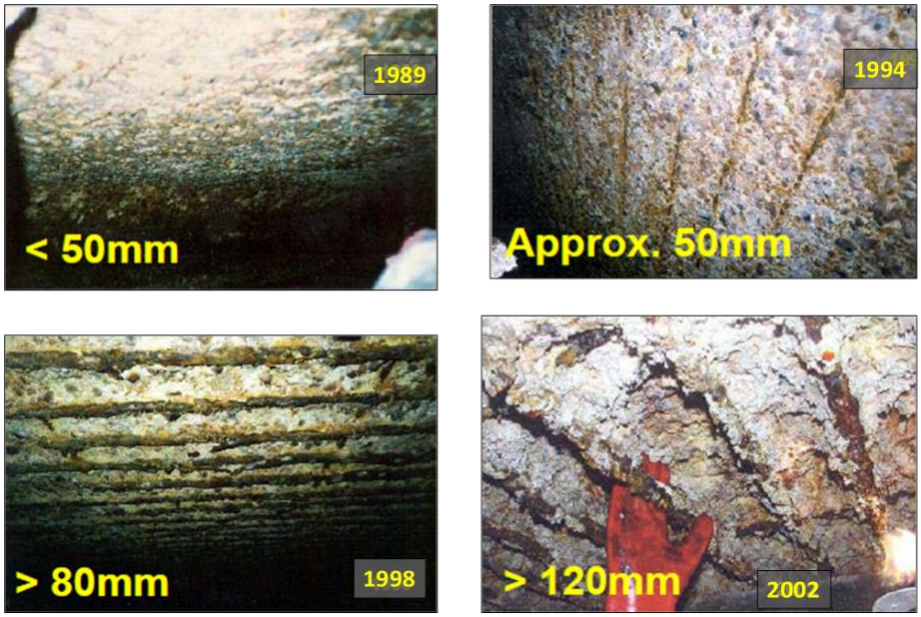

Figure 1.9 Rapid sulfide induced corrosion, which occurred in a large gravity sewer pipe (10 km length) in Sydney over 13 years. Personal communication with Oriol Gutierrez.

1.5. Chemical sulfide control in the sewer systems

Sulfide control and removal in the sewer systems can be achieved through various strategies. For example, sulfide-related problems can be avoided at the stage of the sewer system design through the optimization of the waste stream hydraulics, introduction of the appropriate ventilation of the pipe headspace or utilization of the corrosion-resistant pipe materials [146, 149, 154-156].

Unfortunately, it is not always economically viable to change or upgrade wastewater collection systems, even though most of them are prone to sulfide accumulation. The common solution that can be easily fitted to the already existing sewers is the addition of various chemicals to the waste stream [157]. Chemical sulfide control methods include: *i)* prevention of anaerobic conditions in the sewer system by increasing redox potential of the wastewater through the injection of air, oxygen or nitrate [124, 157-161], *ii)* increasing the pH of the waste stream through the addition of caustic (NaOH), lime (CaOH) or magnesium hydroxide ($Mg(OH)_2$) [124, 158, 162, 163], *iii)* inhibition of the SRB activity achieved by the dosing of biocides [164-167], and *iv)* precipitation of sulfide with iron salts [168-170]. Chemical sulfide control is a simple and straightforward approach which can immediately prevent sulfide accumulation in sewers, however it requires constant or intermittent dosing of chemicals to maintain a sufficient degree of desulfurization. The constant need for chemical supply demands pumping system and appropriate storage facilities, which significantly increase the capital investments into the sewer network. Moreover, it entails substantial operational costs related to the chemical supply, power, maintenance etc [171]. Another drawback of the chemical sulfide control is related to serious environmental and occupational risks associated with the transportation, handling, and storage of chemicals [172]. Due to these limitations, chemical desulfurization approach is mainly suitable as a technique applied locally or in small-scale sewer networks.

1.5.1. Increase of wastewater redox potential

1.5.1.1. Oxygen/air dosing

Air or oxygen injection is a simple and non-toxic method for hydrogen sulfide control in the sewer systems. Previously, several studies claimed that air or sulfide [173-175]. Application of this

approach to sewer systems, however, demonstrated several serious drawbacks. First, oxygen transfer in sewage is limited due to the low oxygen solubility. Limited transfer can be slightly improved by substituting air with pure oxygen, which generally yields slightly higher dissolved oxygen (DO) concentrations upon injection, i.e., 5-7 mg L^{-1} vs 3-5 mg L^{-1} when injecting air [156]. Even though the oxygen solubility is higher in the pressurised sewers (i.e., 45-50 mg L^{-1} of DO) due to the increased pressure, its concentration is still not sufficient to ensure the aerobic conditions over long pipelines or during infrequent pump operations [128, 156].

Another limitation is associated with the ability of SRB to withstand the high levels of DO (i.e., up to 1.5 mM) through several defence strategies [176]. For example, some SRB can generate superoxide dismutase and catalase enzymes to detoxify the reactive oxygen species like peroxides and superoxides [177-179]. Moreover, several SRB not only survive the aerobic conditions, but also utilize the oxygen directly as a terminal electron acceptor due to the presence of the membrane terminal oxygen reductases [180, 181]. Another efficient response of the SRB to the oxidative stress is aerotaxis or coexistence with aerobic communities, where their activity can remain unhindered [176, 177]. Therefore, even though the aerobic conditions limits SRB growth, chemiosmotic energy conservation of the bacteria can be maintained even in the presence of oxygen [178, 180]. If aerobic conditions are not ensured or DO is depleted, which happens quite often considering the limited oxygen transfer in sewage, SRB will thrive again leading to a rapid recovery of hydrogen sulfide yields to the initial levels [182].

Injection of oxygen can potentially prevent the hydrogen sulfide release into the gaseous sewer space by oxidizing it back to sulfate [25]. However, the kinetics of sulfide oxidation with oxygen are quite slow [183]. For example, according to Buisman et al. sulfide oxidation with oxygen is 75 times slower than the biological sulfide oxidation [184]. Moreover, this approach only offers

temporary solution since sulfate is quickly converted back sulfide when subjected to the anaerobic conditions at some point of the pipeline [182].

From the first sight, this method seems attractive in terms of costs. Indeed, oxygen and air are very accessible and cheap reagents. Nevertheless, in order to ensure efficient sulfide control, oxygen needs to be introduced at various points of the pipeline, which significantly complicates the maintenance and increases operating costs [128].

1.5.1.2. Nitrate dosing

Amendment of the wastewater with nitrate to achieve the elimination of malodours and sulfide in sewer systems has been practiced for more than 80 years [185]. Suppression of hydrogen sulfide production at elevated nitrate concentration is achieved through two main mechanisms. First, elevated nitrate concentration promotes the activity of the sulfide-oxidizing nitrate-reducing microbial community (soNRB), which combines the oxidation of sulfide and reduction of nitrate, forming polysulfides, elemental sulfur, sulfate, nitrite and nitrogen, depending on the nitrate to sulfide ratio [160, 186]. Another mechanism which lowers the sulfide production is the competition between the nitrate reducing bacteria and the SRB [159, 187].

The nitrate concentration is the key parameter, which determines the efficiency and the end products of the process. Excess of nitrate in the stream can lead to its incomplete reduction and formation of nitrite, which is undesirable as its presence at low pH is associated with the corrosion of iron pipes and rebar of the reinforced concrete pipes. On the other hand, insufficient nitrate dosing cannot ensure strictly anaerobic conditions over the entire pipeline and sulfide accumulation is resumed as soon as the nitrate is depleted [159].

Even though the nitrate solubility in water is higher than that of oxygen, the preservation of anaerobic conditions through the entire pipe significantly increases the costs related to the chemical dosing and, therefore, limits the application of the discussed approach in practice [187]. In order to minimize the addition of nitrate and lower the cost of the treatment, several studies suggested that nitrate dosing should only be performed at the point close to the end of the sewer [163]. In this manner, hydrogen sulfide, built up in the anaerobic areas of the sewer, will be rapidly oxidized when passing through the aerobic section [159]. Moreover, nitrate dosing located exclusively upstream enhances the sulfide production capacity of the downstream biofilm, leading to an increased sulfide production rates when nitrate is depleted [187].

1.5.2. pH elevation

Increase in pH achieved by the addition of chemicals is a sulfide control approach widely used by the wastewater industry. This method implies a drastic increase of the sewage pH to pH>9 for a short period of time. When the pH is increased, hydrogen sulfide release is supressed since these conditions keep the dissolved sulfide species in the form of HS^- and prevent its volatilization into the gaseous space of the sewer [124]. Besides that, basic pH has a biocidal effect on the SRB community, achieved through the inactivation of a large fraction of the bacterial cells in the sewer biofilm [188]. The SRB inhibition is temporary and hydrogen sulfide production starts already after the first day and recovers to its initial level 5 – 7 days after the treatment [163]. Therefore, to ensure the efficiency of the pH shock approach, the pumping event should occur with sufficient frequency [156]. Alternatively, pH shock can be coupled with other methods to enhance its inhibitory effect on the microbial biofilm. For example, periodic shock loading can be coupled with the oxygen injection. As a result, thinning of the biofilm layer caused by the pH stress allows oxygen penetration into the deeper layers. The combination of these methods causes a more drastic

damage of the SRB biofilm, leading to a prolonged biofilm recovery periods between the dosing events [158].

Sewage pH can be increased with the alkalis based on the caustic soda (NaOH), lime (CaOH) or magnesium hydroxide ($Mg(OH)_2$). Magnesium hydroxide is a non-hazardous compound, which is the safest and the easiest in terms of the storage and handling [162]. The maximum pH which can be achieved through magnesium hydroxide dosing is lower compared to the other compounds (i.e., pH 9 vs pH 12.5 – 13 for NaOH), which helps to prevent the potential disturbance of the downstream biological wastewater treatment [156]. Another advantage of the magnesium hydroxide is related to its self-buffering characteristics, which enables it to slow down re-acidification through loading of the sewer with the unreacted alkalinity [162]. However, magnesium hydroxide is not always the most optimal choice. For instance, caustic soda is preferred for application in small sewer systems with low flow rates and high area to volume ratios, since a very small amount per volume of wastewater is sufficient to achieve the hydrogen sulfide control [157, 189].

1.5.3. Biocides

Another strategy to prevent the sulfide accumulation in the sewer systems involves the usage of biocides, chemicals capable of suppressing the bacterial activity and minimizing the growth of the biofilm. Biocides can be approximately divided into oxidizing and non-oxidizing types. Oxidizing biocides penetrate through the cell membrane causing irreversible cell damage to the bacteria. For example, common oxidizing antimicrobial agents include chlorine, chloramines and chlorinating compounds, also widely used for the wastewater and water disinfection. Even though the chlorine-containing biocides are capable of suppressing the SRB activity, full inhibition of the SRBs cannot

be achieved, as its inhibitory effect is limited to the upper layer of the biofilm [164, 190]. In addition to the mild inhibitory effect, application of such biocides is associated with the undesirable drawbacks, including the corrosion of metals and production of the disinfection by-products, some of which are potentially carcinogenic [191]. Recently, several studies proposed ferrate as environmentally benign alternative to chlorine for water disinfection [192, 193]. Ferrate dosing demonstrated a strong biocidal effect on the SRBs even with a very short contact time (i.e., 15 min) [166]. Furthermore, ferrate showed impressive results in the prevention of biofilm formation, which is highly beneficial for the SRB growth control [194]. Ferrate can also act as an oxidizing agent, transforming sulfide into sulfate and elemental sulfur. The ensuing iron (III) oxides is non-toxic, moreover, it can potentially serve as a coagulant for the removal of other contaminants [195, 196].

Ozone is another example of a powerful oxidizing biocide, capable of the SRB inhibition. In addition to the direct deactivation of SRBs, ozone can promote unfavourable aerobic conditions for its activity, while oxidizing the already formed sulfide [197]. However, ozonation can increase the overall toxicity of the treated wastewater through the formation of mutagenic and carcinogenic byproducts [198]. The concern regarding ozone corrosive potential towards wastewater infrastructure itself is still ongoing [199].

Free nitrous acid, formed through the addition of nitrite and acid to the waste stream, is characterised by a strong inhibitory effect on the SRB activity [167, 200, 201]. Even though nitrite itself decreases the biological sulfide production, its effect is toxic rather than inhibitory, meaning that the SRB activity is quickly recovered as soon as nitrite is absent [161]. On the contrary, nitrite in its protonated form significantly decreases the SRB population, resulting in the long-lasting suppression of the hydrogen sulfide production. However, such SRB inactivation typically requires

relatively long exposure times (e.g., 6 – 24 h) [201]. Moreover, the presence of nitrite can stimulate a microbial-induced corrosion of the stainless steel [202].

Non-oxidizing biocides damage the cell membrane and interfere in the biological processes. For example, they can affect reproduction, interfere with the respiration process or destroy the cell walls. Non-oxidizing antimicrobial agents include molybdate, formaldehyde, paraformaldehyde, glutaraldehyde and isothiozolone. Exposure to the non-oxidizing biocides can completely inhibit the SRB biofilm activity [165, 203-205]. Even though these biocides are widely used for the prevention of oil souring, they are generally avoided in the wastewater treatment due to their general toxicity and low biodegradability, which can deteriorate the performance of the downstream wastewater treatment [166, 197].

1.5.4. Precipitation with iron salts

Sulfide removal through chemical precipitation is a widespread approach applied for the prevention of hydrogen sulfide accumulation in the sewer systems [206]. This method involves the addition of iron salts of chloride, sulfate or nitrate to the waste stream, which leads to the formation of insoluble metal sulfides [207]. The reaction pathway is determined by the form of the iron, which can be ferrous (i.e., Fe(II)) or ferric (i.e., Fe(III)) [169]. Fe(II) can react with the sulfide directly, forming a highly insoluble iron sulfide precipitate (FeS) [207]. The reaction between Fe(II) and sulfide is not instantaneous, therefore, sufficient contact time must be ensured for efficient sulfide management [168]. On the other hand, the reaction between Fe(III) and sulfide starts with the reduction of Fe(III) to Fe(II), coupled with the sulfide oxidation to elemental sulfur. In turn, the resulting Fe(II) forms iron sulfide precipitate [208]. Even though the sulfide reaction with Fe(III) requires one additional step, the kinetics of this reaction is faster compared to the

direct precipitation of sulfide with Fe(II) [169]. However, Fe(III) is available for the direct interaction with other ions typically present in sewage (e.g., OH^-, PO_4^{3-}), which can decrease the overall efficiency of the treatment [170]. Several studies reported the biocidal effects of Fe(III) on the SRB biofilm, however, the concentration of Fe(III) required for the microbial suppression is too high to be applied in practice due to the economical limitations [209, 210].

Sulfide precipitation with iron salts is associated with several serious drawbacks and limitations. For example, it causes stream acidification, which leads to a decreased efficiency of sulfide precipitation, as well as reduction of the wastewater redox potential and increase in the concentration of chlorides, sulfate or nitrate [172]. The formed iron sulfide tends to precipitate along the pipeline, which can cause clogging [211]. The remaining iron sulfide particles end up being discharged with the sewage to wastewater treatment plants, where the presence of iron sulfide may disturb the biological treatment processes [212].

1.6. Electrochemical sulfide control

1.6.1. Electrochemical systems and their thermodynamics

Electrochemistry, the study of the mutual transformation between electrical and chemical energy, can be applied to a variety of fields including remediation and resolution of environmental nuisances [213]. Every electrochemical system is comprised of two electrodes connected via external conductive circuit and separated by an electrolyte that supports ionic movement [214]. Depending on the correlation between the electrode potential and the electron orbital energy of the ionic species, heterogeneous transfer of electrons to or from electrode can occur. When the energy of electrons in the electrode is lower than that of the energy of the highest occupied molecular

orbital (HOMO) of the adjacent ions in the electrolyte, electrons can be donated to the electrode, resulting in the oxidation the ionic species (**Figure 1.10 a**) [215, 216]. The flow of electrons from the ionic species into the electrode is also called anodic current, and the electrode at which it occurs is called the anode [214, 217]. If the energy of the electrons in the electrode material is higher than that of the energy of the lowest unoccupied molecular orbital (LUMO) of the adjacent ions, then electrons can be donated to the electrode, leading to the reduction of the ionic species (**Figure 1.10 b**) [215, 216]. The electrode where such reaction occurs is called the cathode [214, 217]. Even though the reactions of oxidation and reduction are spatially separated, they are coupled to each other by the necessity to balance the overall cell reaction [214, 218]. Hence, the electrons produced at the anode, are conducted through the external circuit and consumed at the cathode.

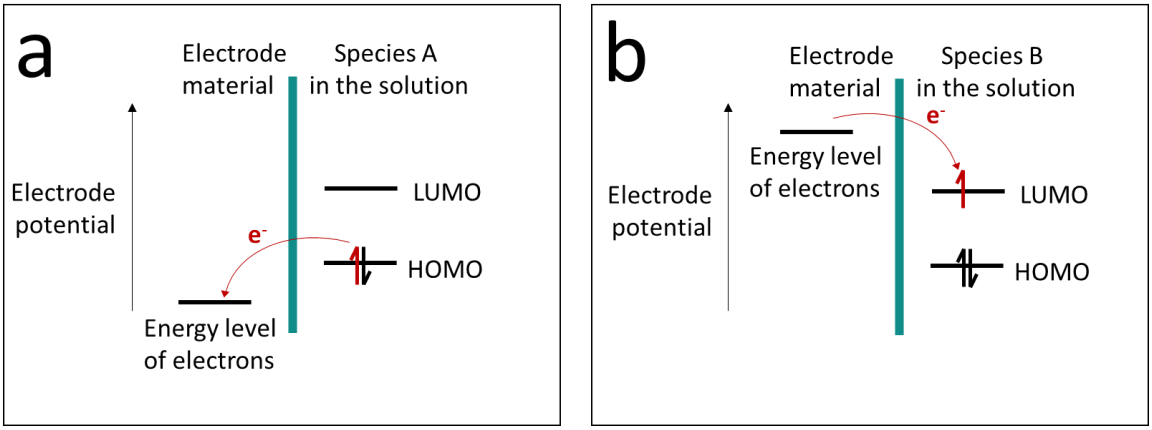

Figure 1.10 Energy diagrams schematically illustrating electrochemical a) oxidation and b) reduction reactions.

Thermodynamically favourable cell reaction occurs spontaneously producing flow of electrons or ions. Such electrochemical reactions are called galvanic (**Figure 1.11 a**) [214, 217]. Unlike spontaneous processes, the occurrence of certain reactions requires energy input. Electrochemical reactions that consume energy are referred to as electrolytic (**Figure 1.11 b**) [214, 217]. The type

of the cell determines the polarity of the electrodes. For a galvanic reaction, reduction occurs at a higher potential than oxidation, therefore, the cathode in the galvanic cells is positively charged. For an electrolytic cell, the opposite is true and the positively charged electrode is the anode [216].

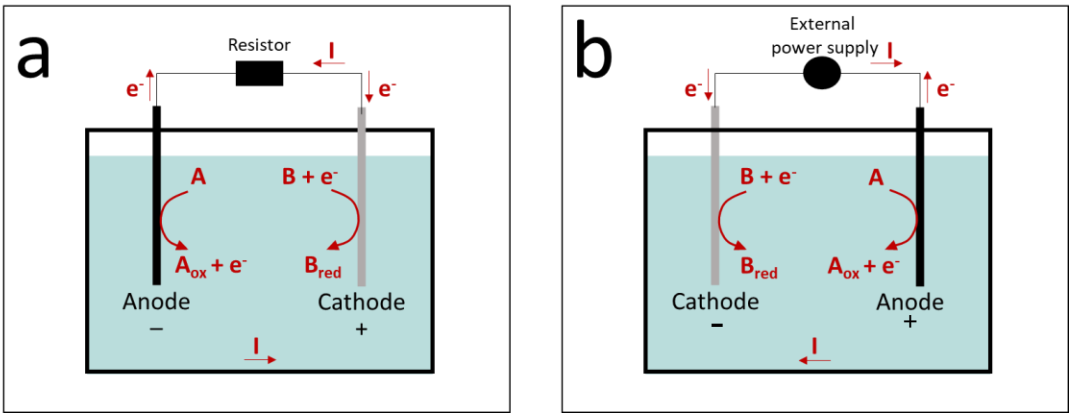

Figure 1.11 Schematic diagram of simplified a) galvanic and b) electrolytic cells.

The tendency of a cell reaction to occur spontaneously can be deduced from the change in Gibbs free energy for the cathodic and anodic reactions [219]:

$$\Delta G = (\sum_i s_i m_i)_{anode} - (\sum_i s_i m_i)_{cathode} \qquad \text{(Eq. 1.10)}$$

where ΔG is the Gibbs free energy expressed in Joule (J), m_i the chemical potential of species i, and s_i the stoichiometric coefficient of species i. Galvanic processes are characterised by the negative Gibbs free energy (ΔG<0), while the Gibbs free energy of the electrolytic processes is positive (ΔG>0) [214, 217, 219].

The Gibbs free energy can also be used to express the equilibrium potential of an electrochemical reaction [214, 220]:

$$E^0 = -\frac{\Delta G}{nF} \qquad \text{(Eq. 1.11)}$$

where n is the number of electrons transferred per mole of product, F is the Faraday constant (96485.3 C mol^{-1}) which is a measure for the charge per mole of electrons and E^0 (V) is the standard electrode potential or equilibrium potential. The standard redox potential (E^0) corresponds to a

determined standard state of 0.1 MPa, 25◦C, activity (i.e., concentration) of ideal solution of 1 M, and equilibrium potential of any other state. In **Table 1.2** the standard redox potentials for several reactions involving transformation of sulfur species are presented [221].

Table 1.2 Standard redox potentials (E^0) for half reactions involving sulfur species.

Redox reaction	**E^0, V**
$HS^- \rightarrow S(s) + 2e^- + H^+$	-0.476
$HS^- + OH^- \rightarrow S(s) + 2e^- + H_2O$	-0.213
$2HS^- + 3H_2O \rightarrow S_2O_3^{2-} + 8e^- + 8H^+$	0.200
$S(s) + 4H_2O \rightarrow SO_4^{2-} + 6e^- + 8H^+$	0.357

Under conditions distinct from standard, the equilibrium potentials are calculated by the Nernst equation [214, 217, 220]:

$$E = E^0 - \frac{RT}{nF} ln\left(\frac{c_R}{c_O}\right) \quad \text{(Eq. 1.12)}$$

where R is the universal gas constant (8.3144 J mol^{-1} K^{-1}), T the absolute temperature (K), c_R is the concentration of the species of the product or reduced side and c_O the concentration of the reactant or oxidized species.

In addition to the anode and the cathode, an electrochemical cell can also include a third electrode called reference electrode [214, 222]. The reference electrode is comprised of several phases, which maintain constant composition, thus providing a stable potential by which the potential of anode and cathode can be monitored. The reference electrodes commonly used in the environmental electrochemistry include the standard hydrogen electrode (SHE), the silver/silver chloride (Ag/AgCl) and the Standard Calomel Electrode (SCE) [213]. The correlation of potential scales of these electrodes can be seen from **Figure 1.12**.

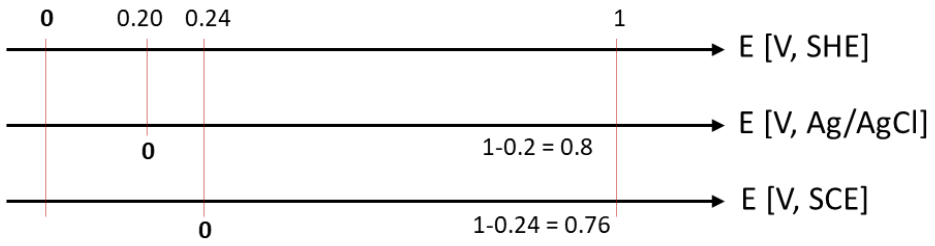

Figure 1.12 The correlation of the potential scales of reference electrodes at 25°C.

1.6.2. Kinetics and rates of electrochemical reactions

As was previously mentioned, electrochemical reactions occur via the heterogeneous electron transfer, meaning that the reaction occurs solely at the electrode-solution interface. Therefore, the reaction rate depends on the area of the electrode or the area of the phase boundary where the reaction occurs:

$$Rate\ [mol\ sec^{-1}\ cm^{-2}] = \frac{i}{nFA} = \frac{j}{nF} \qquad \text{(Eq. 1.13)}$$

where i is the current (A), A is the electrode surface (cm^2) and j is current density ($A \cdot cm^{-2}$). Thus, in order to compare redox processes that occur at electrodes of different size, the rate of reaction must be normalized to the area of the electrode [219, 223].

The simplest electrochemical redox reaction (i.e., $O + ne^- \leftrightarrow R$) can be considered as a set of equilibria involved in the migration of the reactant to the electrode, the heterogeneous electron transfer at the electrode, and the diffusion of the product away from the electrode surface into the bulk of the electrolyte (**Figure 1.13**). The rate of such reaction depends on four major factors: (i) mass transfer to the electrode surface, (ii) kinetics of electron transfer, (iii) preceding and following

reactions, (iv) surface reactions (adsorption) [214, 218-220]. The overall rate of the reaction is limited by the slowest process.

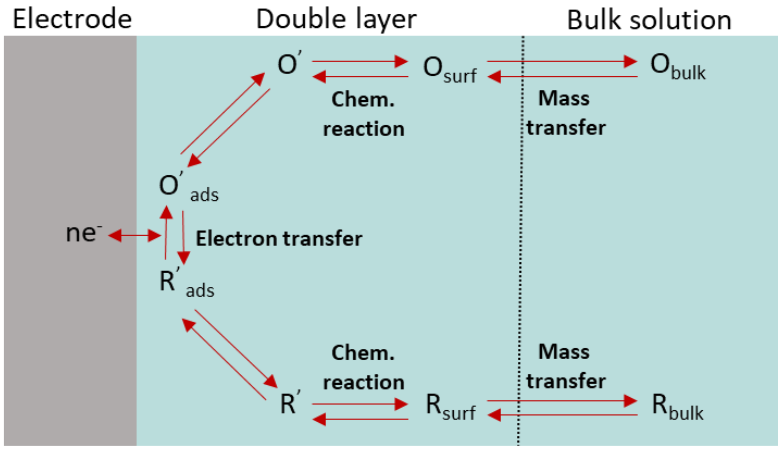

Figure 1.13 Processes involved in an electrode reaction. Adapted from [219].

The first step of electrochemical reaction involves the mass transfer of the species (i.e., O) from the bulk solution to the electrode vicinity. This step can be accomplished in three different ways or their combination: (i) migration - movement of the charged or polarized species in an electric field, (ii) diffusion - movement of the species against the concentration gradient, and (iii) convection - movement of the species as a result of stirring or density gradients [214, 218-220]. The process of mass transfer is described by the Nernst-Planck equation [214, 217, 220, 224]:

$$J_J(x) = -D\frac{\partial C_j(x)}{\partial x} - \frac{z_j F}{RT} D_j C_j \frac{\partial \phi(x)}{\partial x} + C_j v(x) \qquad \text{(Eq. 1.14)}$$

where $J_J(x)$ (mol cm^{-2} sec^{-1}) is a one-dimensional flux for species j at distance x (cm) from the electrode; D_j (cm^2 sec^{-1}), z_j, and C_j (mol cm^{-3}) are the diffusion coefficient, the charge, and the concentration of the species j, respectively; $v(x)$ (cm sec^{-1}) is the rate with which a volume element moves in solution; $C_j(x)$is the concentration gradient; and $\frac{\partial \phi(x)}{\partial x}$ is the potential gradient along the x-axis. The first term of the Nernst-Planck equation describes the diffusion, the second term accounts for the migration of the species in the solution, and the last term represents the

convection of the solution. One of the main goals of the electrochemical cell engineering is aimed towards the maximization of the mass transport of the electroactive species to the electrode surface in order to achieve robust electrochemical reaction [213].

When the mass transfer is sufficiently fast, the electron transfer may become the limiting step of the redox reaction. Butler-Volmer equation can be used to predict the current in the electrochemical systems where mass transfer limitation is eliminated, i.e., reaction is limited by the charge transfer only [214, 217, 220, 225]:

$$i = i_0\left[e^{-\alpha f\eta} - e^{(1-\alpha f\eta)}\right] \quad \text{(Eq. 1.15)}$$

where i_0 is the exchange current (A), f is the transfer coefficient, α is a dimensionless parameterwith values between 0 and 1, and η is the overpotential (V). Overpotential can be defined as the difference between an electrode potential and the equilibrium potential required for a non-spontaneous reaction to occur [214]. Therefore, the best electrode material is the one that demonstrates the lowest overpotential for the selected reaction [213].

For chemically irreversible electrocatalytic reactions one term (anodic or cathodic) is much bigger than the other and the Butler-Volmer equation can be simplified to Tafel equation [214, 217, 220, 226]:

$$\eta = \frac{RT}{\alpha F} ln i_0 - \frac{RT}{\alpha F} log i \quad \text{(Eq. 1.16)}$$

The pathways of certain electrochemical reactions can involve a chemical reaction preceding the reaction at the electrode surface (**Figure 1.13**) [219]. These reactions typically have a dramatic effect on the faradaic current and can become rate-limiting if electron transfer is sufficiently fast. In addition to the reactions preceding the electron transfer, the reactions that affect the electrode surface can influence the overall reaction rate. These reactions include adsorption, desorption and

crystallization [219]. These processes change electrolyte-electrode interface, thus influencing the electrochemical behavior of the electrode.

1.6.3. The voltage loses of an electrochemical cell

The potential losses of an electrochemical cell are comprised of several components such as (i) activation losses, (ii) ohmic losses and (iii) mass transfer losses [214, 227, 228]. Hence cell potential can be described according to the following equation:

$$E_{cell} = ([E_{anode} - E_{cathode}])_{theoretical} - \eta_{anode} - \eta_{cathode} - IR_{\Omega} \qquad \text{(Eq. 1.17)}$$

where $([E_{anode} - E_{cathode}])_{theoretical}$ corresponds to the theoretical cell potential, η_{anode} and $\eta_{cathode}$ are the anode and cathode overpotential, respectively and IR_{Ω} is the ohmic resistance of the system. Overpotential losses that occur as the result of mass transfer and charge transfer limitations are discussed above. The Ohmic resistance to the flow of electrons through the electrically conductive components of the cell and to the flow of ions through the electrolyte leads to substantial decrease of voltage, which can be determined with Ohm's law [214]:

$$\Delta E_{ohm} = iR_{ohm} \qquad \text{(Eq. 1.18)}$$

The ohmic resistance can be decreased by (i) minimization of the distance between the anode and the cathode, (ii) addition of salts to increase the electrolyte conductivity and (iii) utilization of low resistance membranes or its complete elimination when possible [213].

1.6.4. Electrode material

The kinetics of an electrochemical reaction is controlled by the properties of the electrode–electrolyte interface and the availability of the reactant at the vicinity of the electrode surface [214]. Hence physical, chemical, and electronic properties of the electrode material are of immense

importance in the electrochemical cell design. The material characteristics that influence the electron-transfer kinetics include: (i) type of electrode material, (ii) surface cleanliness, (iii) surface microstructure, (iv) surface chemistry, and (v) electronic properties [219]. In wastewater treatment mainly anode material is of interest since most of the pollutant degradation and removal processes occur because of the oxidation. An overview of the anode materials commonly used for electrochemical wastewater remediation along with their overpotential for oxygen evolution is presented in **Table 1.3**.

Table 1.3 On-set potential for oxygen evolution at commonly used anode materials versus SHE adapted from [229, 230].

Electrode material	Standard potential for O_2 evolution (E^0), V	Conditions
Ti/Pt	1.3	0.5 M H_2SO_4
Ti/IrO_2	1.5	0.5 M H_2SO_4
Ti/RuO_2	1.6	0.5 M H_2SO_4
Ti/PbO_2	1.9	0.05 M H_2SO_4
Ti/SnO_2	1.9	0.05 M H_2SO_4
Ebonex	2.7-3.0	3.7 M H_2SO_4
BDD	2.7	0.5 M H_2SO_4

1.6.5. State of the art of electrochemical sulfide removal

Considering the increasing pressure to incorporate principles of sustainability in the wastewater treatment, traditional sulfide control needs to be reconsidered and improved in terms of reducing the operational costs and enabling resource recovery. Recently, electrochemical sulfide removal attracted significant attention due to several important advantages it offers [1, 99, 231-233]. First, this approach does not require the addition of chemicals, hence it avoids risks and costs associated with the dosing, transportation and storage of chemicals [171]. Furthermore, electrochemical

treatment units have a small footprint and can be powered by solar photovoltaic panels, making them very well-suited for the decentralized treatment of waste streams [234]. Electrochemical oxidation is a versatile technique, which efficiency is determined by several factors including electrode material, electrode potential, reactor configuration and wastewater composition [214, 235, 236]. Optimization of the operating parameters can maximize the performance of the system, leading to a robust sulfide removal [237, 238] .

Sulfide is electrochemically active species and can be directly oxidized at the electrode surface [233, 239]. Direct sulfide oxidation can lead to production of S^0, $S_2O_3^{2-}$, SO_3^{2-} or SO_4^{2-}, depending on the experimental conditions. Oxidation of sulfide to sulfur is typically preferred as it occurs at very low anode potentials, which helps to reduce the energy consumption and avoid undesirable side reactions [240]. Moreover, oxidation of sulfide to elemental sulfur enables the physical separation of sulfide from the stream, thus minimizing the problems of sulfide reformation or formation of secondary waste streams [241]. This approach is especially effective when applied for treatment of streams with high sulfide content (e.g., wastewater effluent from tanneries, paper mills, oil refineries or geothermal brines), which lowers the mass transfer limitations and increases the sulfide removal rates [231, 233, 238]. Given that the elemental sulfur is characterized by the high electrical resistance (1017 Ω cm^{-1}) [171], its deposition at the anode surface leads to the gradual passivation of the electrode and eventually halts the process [221, 241, 242]. Moreover, in the presence of organics, electrodeposited sulfur can further accelerate the performance deterioration through the stimulation of the SOB biofilm growth at the anode surface [243]. Hence, full-scale implementation of such electrochemical units demands an effective sulfur recovery strategy. Proposed chemical regeneration strategies include utilization of the organic solvents (e.g.,

toluene, benzene) capable of partial sulfur extraction (e.g., 40-80%) or addition of the surfactants for the prevention of sulfur layer formation [244, 245]. Yet, chemical approach is unlikely to be applied in practice as it is associated with high costs and environmental risks [171]. Several studies claimed that complete sulfur dissolution can be achieved *in situ* through: *i)* temporary increase of anodic potential, which can further oxidize electrodeposited sulfur to the dissolved sulfur species, or *ii)* polarity switching, which can reduce the anodically produced sulfur back to sulfide [241, 246].

Selection of an electrode material is crucial for the direct electrochemical oxidation processes. Appropriate anode material must promote selective and efficient sulfide oxidation, while being low-cost, available, and long-lasting. Several studies demonstrated that direct sulfide oxidation can be performed on dimensionally stable $Ti/IrO_2–Ta_2O_5$ or Ti/IrO_2 electrodes at the current efficiency above 50% [247, 248]. Application of such anode was associated with several problems, including parasitic reaction of chloride oxidation, reduced selectivity upon long-term application and gradual sulfur poisoning of the catalytic layer of the titanium electrode surface [247]. Boron doped diamond (BDD) anode was capable of near quantitative direct oxidation of sulfide to sulfate at high current efficiency (e.g., 90%), while maintaining the electrode surface intact [237, 249]. However, BDD is also characterized by the high affinity towards chloride oxidation to hypochlorite, which eventually leads to the formation of toxic byproducts [234]. Moreover, application of BDD on bigger scale is impeded by its high cost and complex synthesis procedure [234, 250]. Ebonex, a cost-effective alternative to BDD, was also capable of sulfide oxidation to sulfate [251, 252]. Unlike BDD, Ebonex anode demonstrated somewhat lower selectivity towards sulfide oxidation and current efficiency (e.g., 50%) due to the parasitic reaction of water oxidation [252]. Ateya et al. investigated the performance of carbon-based anodes (e.g., graphite discs) for

electrochemical sulfide removal [242]. The obtained results showed that sulfide can be selectively oxidized to elemental sulfur at the anode potential as low as 0.25 V/SHE, thus avoiding the parasitic reaction of oxygen evolution and chloride oxidation [221, 233, 242]. The coulombic efficiency (CE) of sulfide oxidation on carbon-based electrodes (e.g. carbon fiber and graphite granules) reported by Dutta et al (CE 80%) is comparable to the performance of the BDD anodes (CE 90%) [99]. The excellent activity of the carbon-based electrodes together with their low cost and high surface area make them the most suitable material for the direct electrochemical sulfide oxidation though their continuous use remains limited by the need for regeneration of the anode surface and removal of the deposited sulfur [253].

The electrochemical sulfide oxidation can be achieved via indirect mechanisms. In this case, sulfide does not exchange electrons with the anode directly. Instead, non-toxic electroactive species, produced at the anode, act as intermediaries delivering the electrons to the bulk of the electrolyte where sulfide oxidation occurs [254, 255]. The most common oxidant is oxygen, although the indirect sulfide oxidation can also be achieved with the electrochemically produced chlorine, Ag^{2+} or Ce^{4+}. Indirect electrooxidation is not limited by the mass transfer, hence the removal efficiency is not affected by the sulfide concentration [229]. The final products of indirect sulfide oxidation include various dissolved sulfur species (i.e., thiosulfate, sulfate and polysulfides), which are likely to be reduced back to sulfide along the pipeline as a result of bacterial activity. Interestingly, several studies also report electrodeposition of sulfur which occurs alongside with production of dissolved sulfur species, however, the mechanism of elemental sulfur formation remains unclear [256, 257]. Indirect sulfide oxidation is often performed using mixed metal oxide anodes (MMOs), e.g., Ti/RuO_2, Ti/IrO_2, Ti/TaO_2-IrO_2, Ti/PtO_2- IrO_2, Ti/PbO_2, Ti/SnO_2 and others [231, 232, 238, 257]. Unlike carbon-based electrodes, which require current

collectors or bipolar plates, MMO are conductive enough to be applied directly [171]. Moreover, mesh-shaped MMO effectively avoid the problem of blockage and ragging, which often occurs on carbon-based electrodes applied for the treatment of unfiltered sewage [231]. Nevertheless, this approach is characterized by several important disadvantages when compared to the direct sulfide oxidation. First, formation of oxidant species occurs at high anode potentials (i.e., > 1.2 V/SHE), which increases the energy demand of the treatment [99]. Second, the process is non-selective, which significantly reduces the coulombic efficiency (e.g., 60%) and may lead to the production of the undesired byproducts [229, 234]. Moreover, the efficiency of sulfide control with oxygen is limited due to the low oxygen solubility [182, 258]. Finally, indirect sulfide oxidation requires a two-compartment cell configuration, with an ion exchange membrane (IEM). IEM significantly increase the capital as well as operating costs of the treatment as they increase the internal resistance of the cell, are prone to fouling and loss of water due to the electro-osmosis [99, 259].

As was mentioned in the previous chapter, sulfide can be effectively precipitated with the ferrous iron, forming an insoluble metal sulfide precipitate [207]. Ferrous ion can be produced *in situ* electrochemically, thus, avoiding the need for the continuous addition of iron salt and increase of stream salinity [172]. Hydrogen bubbles produced at the cathode can facilitate the separation of the precipitate by floating of the formed particles to the surface [260]. Other important advantages of the electrocoagulation include the simplicity of the reactor configuration (i.e., can be performed without IEM) and the ease of operation [255]. Electrocoagulation is a non-selective technique, which is capable of precipitation of the suspended solids, organics, and oil typically present in the wastewater streams [260, 261]. Hence the high sulfide removal efficiency can only be achieved at high energy input [171]. The biggest drawback of the electrocoagulation is continuous

production of the iron-containing sludge, which requires the transportation, handling, and proper disposal of toxic sludge [261].

Even though electrochemical sulfide control is a highly attractive approach for sulfide control in sewer systems, its real scale application is still limited due to the lack of low-cost, efficient and selective electrode material resistant to passivation with elemental sulfur.

1.7. Catalytic removal of sulfide with manganese oxides

Manganese is an element with a unique and complex chemistry. For instance, it has the highest possible oxidation state, Mn(VII) among the first-row transition metals. Moreover, it has the highest number of oxidation states, from Mn(II) to Mn(VII), as it has five unpaired electrons [262]. The lowest possible oxidation state, Mn(II), is in its most stable form in the acidic and neutral environment, while Mn(VII) present in the aqueous solutions in the form of permanganate (MnO_4^-), is an extremely strong oxidizing agent [263]. Mn(IV), which aqueous form can only exist in the highly acidic environments (e.g., concentrated HCl solutions), is actually the most stable form of Mn in the solid state, as its oxide MnO_2 [264]. Similarly to Mn(IV), Mn(III) remains stable only at very low pH (pH~0), while at neutral pH it precipitates in a stable solid Mn_2O_3 form [265]. The ability to switch easily between these oxidation states enables Mn to participate in the numerous redox reactions, including charge rearrangements between two or more Mn ions. For example, Mn(III) under acidic conditions undergoes charge disproportionation, yielding Mn(II) and Mn(IV) [265, 266].

In addition to the oxidation state diversity, Mn also exhibits a remarkable crystallographic variety of solid oxide forms, spanning more than 30 crystal phases [267]. The basic building unit for the majority of the manganese oxide (Mn_xO_y) atomic structures is the MnO_6 octahedron [268]. These

octahedra can be organized by sharing the edges or/and corners into a large variety of configurations, most of which fall into one of two major groups: *i)* chain or tunnel structure, and *ii)* layer structures [267]. The Mn_xO_y diversity and stability over a broad pH range make it a suitable material for various applications [269]. For example, the spinel λ-MnO_2 phase is widely applied as cathode material in the lithium-ion batteries [270, 271], ramsdellite-MnO_2 is used in alkaline batteries [272, 273] and Mn(III) containing phases, such as hausmannite Mn_3O_4 and bixbyite Mn_2O_3, are well-known catalysts for water splitting [274, 275]. The versatility and redox activity of manganese together with its earth abundance, low-cost and relatively low toxicity makes it a perfect catalyst for environmental applications [276, 277]. Indeed, Mn_xO_y was successfully used for removal of various contaminants including refractory organics, such as aniline [278], formaldehyde [279, 280], phenol [281-283] with its derivatives [284-286] and low molecular weight organic acids [287, 288] as well as some volatile organic contaminants [289, 290]

Given the activity of the Mn_xO_y, they play an important role in various biogeochemical cycles, including sulfur cycle [61]. Manganese oxide, ubiquitously present in the marine surface sediments, is the major oxidizing agent driving sulfide oxidation [291]. The reaction between manganese oxides and sulfide occurs rapidly, its rate significantly exceeds sulfide precipitation with iron [168, 291, 292]. The final product of this reaction is mainly determined by the local pH, with sulfate as the dominant product at low pH, and elemental sulfur as the main product (80%) at pH 8 [293, 294].

Several studies attempted to exploit the affinity of the Mn_xO_y towards sulfide oxidation. For instance, manganese-based adsorbents can effectively remove hydrogen sulfide from flue gas, biogas or ambient air [295-297]. However, sulfide oxidation with manganese oxides was barely

applied for wastewater treatment. Several studies proposed sulfide control method based on homogeneous catalysis achieved through the dosing of potassium permanganate [298, 299]. Even though fast sulfide removal rates were initially achieved, the performance of this processes was gradually deteriorated as Mn becomes depleted due to its interaction with sulfide [300]. Besides that, direct addition of permanganate to waste stream is not desirable since it can affect water quality [301].

Chapter 2. Objectives

The main objective of the present doctoral thesis was to develop an electrochemical system capable of rapid and selective oxidation of sulfide to elemental sulfur and to propose a strategy for the mitigation of electrode passivation.

To achieve this goal, following sub-objectives were pursued:

1) To investigate the electrochemical removal of sulfide using porous, carbon-based electrodes with a large specific surface area:

- To study the kinetics and underlying mechanisms of the direct sulfide oxidation at graphite felt (GF) or activated carbon felt (ACF) electrodes.

- To investigate the efficiency of the electrochemical sulfide removal from real sewage using flow-through cells equipped with the ACF and GF anodes.

- To evaluate different regeneration strategies of the sulfur-loaded ACF and GF electrodes, including *i)* further oxidation of S^0 to soluble species (e.g., $S_2O_3^2$, SO_3^{2-}, SO_4^{2-}) via anodic polarization, *ii)* reduction of S^0 back to sulfide via cathodic polarization, and *iii)* cathodic polarization of the used electrode in the presence of HS^-, to enhance the chemical dissolution of S^0 and formation of soluble polysulfides.

2) To develop a new Mn_xO_y-coated GF electrode and investigate its performance in the electrocatalytic sulfide oxidation:

- To evaluate the catalytic activity of the GF-Mn_xO_y anode towards sulfide oxidation and to enhance it by fine-tuning the coating synthesis procedure.

- To determine the role of the applied anode potential in the electrocatalytic sulfide oxidation at the GF-Mn_xO_y electrodes.

- To investigate the performance of the GF-Mn_xO_y electrodes for sulfide removal from real sewage.

-To investigate the performance of the cathodic sulfur recovery and to determine its impact on the subsequent sulfide removal and stability of the Mn_xO_y coating.

3) To develop a new Mn_xO_y-coated TiO_2 NTA electrode and investigate its performance in the electrocatalytic sulfide oxidation:

- To determine the impact of the TiO_2 NTA interlayer on the activity and stability of the Mn_xO_y coating.

- To study the impact of the operating parameters (i.e., applied potential, pH, sulfide concentration) on the sulfide removal kinetics and formed reaction products.

- To investigate the performance of the Ti/TiO_2 NTA-Mn_xO_y anode for sulfide removal from real sewage.

Chapter 3. Material and methods

3.1. Electrochemical characterisation of the electrode materials and reactions

Electrochemical activity of the carbon-based materials and the onset potentials for anodic and cathodic transformation of the adsorbed sulfur were determined by performing cyclic voltammetry (CV) at glassy carbon (GC) electrode in 10 mM KH_2PO_4/K_2HPO_4 at pH 8, and in 2.8 mM HS^- at pH 8. Voltammetric studies could not be performed at the GF and ACF electrode because of the large surface area and porosity in the latter case, which yields high capacitive current and makes it difficult to detect any Faradaic reactions even at low scan rates of 5 mV s^{-1}.

The optimal potential for the Mn_xO_y electrodeposition on the TiO_2 NTA electrodes was determined by performing linear sweep voltammetry from 0.2 V/SHE to 2.8 V/SHE in the electrolyte containing 0.1 M $MnSO_4$ and 0.05 M H_2SO_4. All electrode potentials in this manuscript are expressed vs SHE.

Electrochemical impedance spectroscopy (EIS) was employed to compare the charge transfer properties of bare Ti and TiO_2 NTA. The measurement was performed in 0.1 M $MnSO_4$ and 0.05 M H_2SO_4 containing electrolyte at 1.7 V/SHE, which was also employed for Mn_xO_y coating synthesis. The obtained data was fitted in the Nyquist plot.

3.2. Surface characterization of the electrode materials

The surface composition of the carbon-based electrodes (i.e., ACF and GF) utilized in the Chapter 4.1. was determined using The X-ray photoelectron spectroscopy (XPS). The analysis was performed using an X-ray photoelectron spectrometer (PHOIBOS 150, Specs, Germany). The data was analyzed using the CasaXPS package, the spectra were smoothed, and non-linear background was subtracted. All XPS spectra were calibrated using the C 1s peak at 284.6 eV. The surface composition of the samples was calculated with C1s, O1s and S2p peaks and the appropriate

sensitivity factors. Nitrogen adsorption isotherms for the ACF were obtained using the ASAP 2010 (Micromeritics, USA) analyzer at -196°C. Before the experiment, the samples were degassed at 120°C to a constant vacuum level (10 – 5 Torr) for about 24 hours. The isotherms were used to calculate the specific surface area, micropore volume and total pore volume. Surface area of GF could not be measured due to fibrous nature of the material.

XPS was also employed for the determination of the chemical state analysis of the Mn_xO_y coating (PHOIBOS 150, Specs, Germany). Mn 3s doublet peak separation values were then used to determine the valence state of Mn in the sample. The crystal structure of the Mn_xO_y coating was determined by an X-ray powder diffractometer (X'Pert MPD, PANalytical, Netherlands) with Cu as Kα radiation source. The X-ray diffraction (XRD) patterns of the samples were recorded between 10 and 80º (2h) at a scan step size of 0.02º, and a time per step of 353 s. The surface morphology and elemental composition of the materials was examined using scanning electron microscopy (SEM) and energy-dispersive X-ray spectroscopy (EDX) (The Magellan 400L, FEI, US).

The electroactive surface area of the Ti/TiO_2 NTA-Mn_xO_y electrodes was estimated by measuring the double layer capacitance observed during the cyclic voltammetry (CV) measurement in the 0.1 M $NaNO_3$. Voltametric scans were performed over a potential window between 0.4 – 1 V/SHE and at scan rates between 30 and 2 mV s^{-1}. Values for C_{dl} were determined by the linear regression of the current versus the scan rate, according to the following equation:

$$\frac{I_a - I_c}{2} = C_{dl}\nu \qquad \text{(Eq. 3.1)}$$

where I_a and I_c are the anodic and the cathodic currents observed in the forward and reversed scans (mA), respectively, and ν is the applied scan rate (mV s^{-1}). The electroactive surface area was then

determined by dividing the capacitance by 60 mF cm^{-2}, which is considered as a standard value for the metal oxide based systems [223].

3.3. Sulfide removal experiments

The general information regarding the condition of the experiments carried out in this study can be found in **Table 3.1**.

Table 3.1 Summary of the conducted electrochemical and electrocatalytic sulfide removal experiments

Working electrode	Counter electrode	Reference electrode	V, L	Mode	E_{WE}*, V	Supporting electrolyte	HS^-, mM	pH
ACF/GF	Ti/Pt-IrO_2	3.5 M Ag/AgCl	1	Non-divided, flow-through	0.4-0.9	None or real sewage	2.7	8
GF-Mn_xO_y	Pt	3.5 M Ag/AgCl	0.25	Divided, batch	0.4	2.6 mM $NaNO_3$ or real sewage	2.7	8
Ti/TiO_2 NTA-Mn_xO_y	Ti	3.5 M Ag/AgCl	0.1	Non-divided, batch	0.4-0.8	2.9 mM $NaNO_3$ or real sewage	0.9-3.2	8-12

* The potential of the working electrode is expressed vs SHE

More detailed description of the performed experiments is provided in the beginning of each chapter.

3.4. Chemical analysis

The concentration of the dissolved sulfur species (i.e., HS^-, $S_2O_3^{2-}$, SO_3^{2-}, SO_4^{2-}) was determined by ion chromatography (IC), using a Dionex IC5000 (Dionex, USA). Prior to the IC analyses, 2 mL samples were preserved by adding 0.5 mL of sulfide antioxidant buffer (SAOB) [302].

Samples were kept refrigerated and shielded from light for not more than three days. Although several attempts were made to determine the concentration of the formed polysulfides, none of the methods reported in literature was found to be reliable. For example, previous study applied oxidation of all dissolved sulfur species to sulfate with H_2O_2 at high pH as a technique to determine the formed polysulfides [303]. However, in our study the main product of such reaction was colloidal sulfur, which cannot be determined with ion chromatography [304]. Therefore, the presence of the polysulfides could only be indicated by the gradual appearance of the characteristic yellow color, and also higher concentrations of the soluble sulfur species, end products of further polysulfide oxidation [305]. In the experiments where the electrolyte solution stayed colourless throughout the experiment, the difference between the total sulfide added and the dissolved sulfur species measured was assumed to be the electrodeposited elemental sulfur. The molar ratio of the resulting elemental sulfur to sulfide added in the beginning of the experiment was considered as sulfur yield. The experiments were performed in duplicates and the measured sulfide concentrations were normalized against the initial values and then fitted with a first-order kinetic relationship. The reaction rate was calculated from the slope ($-k$) of the sulfide concentration and time curve (log–linear scale).

Chemical oxygen demand (COD) and free chlorine were measured using the LCK test cuvette method (HACH, US) when experiments were performed in real sewage. The concentration of the total dissolved manganese and other metals in the supporting electrolyte and sewage was measured by means of inductively coupled plasma-optical emission spectrometry (ICP-OES) (Agilent 5100, Agilent Technologies, US), to evaluate the stability of the Mn_xO_y coating.

3.5. Figures of merit of the electrochemical treatment

Energy consumption was expressed as electric energy per order (E_{EO}), Wh L^{-1}, needed to reduce the concentration of the sulfide by one order of magnitude in a unit volume of the treated solution, was calculated according to the following formula [306]:

$$E_{EO} = \frac{U\ I\ t}{V\ log\frac{C_i^0}{C_i^f}} \quad \text{(Eq. 3.1)}$$

where U represents cell voltage (V), I is the applied current (A),V is volume of the treated solution (L), t - reaction time (h) required to achieve the corresponding order of magnitude of removal, C_i^0 and C_i^f are the initial and final concentration of sulfide, where the used values were the lowest C_i^f and t needed for one order of magnitude removal in the cases when the oxidation was complete (>90% removal).

The amount of charge involved in the reaction was estimated by calculating current efficiency (CE) for anodic reactions (%) [307]:

$$CE = \frac{n_i\ F\ (C_i^t - C_i^0)\ V}{I\ t}\ 100 \quad \text{(Eq. 3.2)}$$

where n_i is the number of electrons required to form one mole of species i, F is Faraday constant (96485 C mol^{-1}).

Chapter 4. Electrochemical removal of sulfide on porous carbon-based flow-through electrodes

4.1. Background

This chapter investigates the performance of the anodically polarized ACF and GF in terms of sulfide adsorption and electrochemical sulfide oxidation, in clean water of low conductivity and in municipal sewage. The efficiency of the three different regeneration strategies of the sulfur-loaded ACF and GF electrodes is evaluated. Finally, the impact of the regeneration startegy of the ACF and GF anode on the subsequent electrooxidation rates of sulfide in the next working cycle is discussed.

4.2. Material and methods

The one-compartment flow-through electrochemical cell (interior dimensions 80x80x60 mm) was equipped with the ACF (Eurocarb, UK) or GF (Final Materials, France) as anodes, both with the dimensions of 80x80x10 mm, tightly encased inside a stainless steel mesh collector. However, stainless steel could not be used as a counter electrode since cathodic polarisation of stainless steel can lead to leaching of metal ions into the electrolyte, which could potentially result in FeS formation [308]. Mesh Ti/Pt-IrO_2 electrode with dimensions of 80x80x2 mm served as the counter electrode (cathode), whereas 3.5 M Ag/AgCl supplied by BASi (West Lafayette, IN, USA) was used as the reference electrode and placed in the proximity of the working electrode (i.e., ACF and GF anode). The distance between the anode and cathode was 10 mm, which was necessary on order to accommodate the reference electrode in the existing set-up. Chronoamperometric experiments were conducted at constant anodic potential of 0.4, 0.7 and 0.9 V/SHE using an Autolab potentiostat/galvanostat 302N (Metrohm, Switzerland). The ohmic drop was minimized by placing the reference electrode in the vicinity of the anode. In addition, the experiments were

conducted in the open circuit (OC), i.e., without applying the current, to investigate the chemisorption of sulfide on the ACF and GF. Freshly prepared, deoxygenated HS^- solution (2.7 mM, pH 8, 0.6 mS cm^{-1}) was circulated in the batch mode at a flow rate of 155 mL min^{-1} during up to 6 h of electrolysis and OC experiments. Although the typical wastewater conductivity is in the range 0.9-9 mS cm^{-1} [309], there was no supporting electrolyte added to the Na_2S solution to enable the evaluation of ACF and GF performance for sulfide removal and oxidation without the interferences of the counter- and co-ions. In the experiments with real wastewater, raw sewage was collected form an upstream sewer system, filtered and deoxygenated under a gentle nitrogen stream and amended with the same initial concentration of HS^- solution (i.e., 2.7 mM). The composition of the used sewage was: 0.03 ± 0.02 mM HS^-, 0.01 mM $S_2O_3^{2-}$, 0.16 ± 0.01 mM SO_4^{2-}, 529.0 ± 40.0 mg COD L^{-1} of total COD and 277.7 ± 9.8 mg COD L^{-1} of soluble COD.

Given that the experiments could not be performed in gas-tight reactors due to the possible formation of oxygen and hydrogen at the anode and cathode, respectively, a gentle flow of nitrogen was applied to the external recirculation tank to displace any air that may enter the system and prevent accidental oxidation of sulfide. To prevent the loss of sulfide due to H_2S volatilization, all experiments were performed at constant pH 8 ± 0.1 using a pH controller (Endress+Hauser, Switzerland). To regenerate the sulfur-loaded ACF and GF, three different approaches were tested: *i)* anodic polarization at +1.7 V/SHE, *ii)* cathodic polarization at -1.3 V/SHE, and *iii)* cathodic polarization at -1.3 V/SHE and in the presence of sulfide (2.7 mM), to enhance the chemical dissolution of S^0 to polysulfides [25]. The regeneration experiments were conducted during up to 6 h of electrolysis using the same flow-through reactor as described above, and sulfur-loaded ACF and GF. Sulfur loading of the ACF and GF electrodes was performed at constant anode potential

of + 0.9 V/SHE in a 9 mM HS^- solution at pH 8. Given that both anodic and cathodic recovery was performed at higher absolute values of electrode potentials, inert $NaNO_3$ (10 mM, pH 8) was added to the Na_2S solution to increase its conductivity to about 1.3 mS cm^{-1}, which is still in the lower range of the typical conductivity of wastewater (i.e., 0.9 – 9 mS cm^{-1}) [309]. The regeneration efficiency was calculated as the ratio of the dissolved sulfur species measured after the regeneration and the content of sulfur species that was pre-loaded at the carbon surface.

Electrochemical and surface characterisation of the electrode materials as well as chemical analysis are discussed in Chapter 3.

4.3. Results and discussion

4.3.1. Voltametric study of the electrochemical activity of sulfide at carbon electrodes

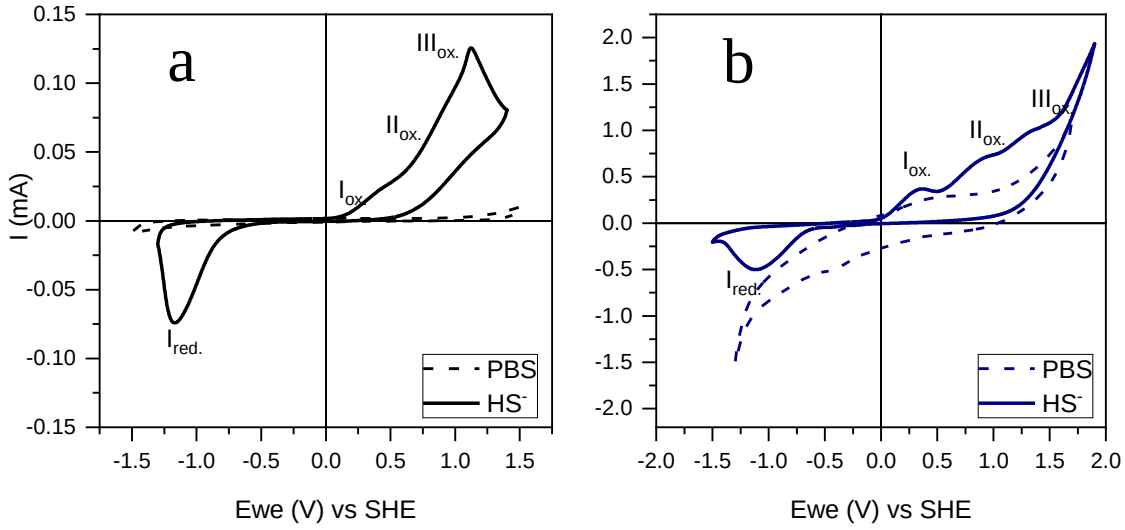

Figure 4.1 CV experiments performed at a) glassy carbon electrode (GC) in 10 mM PBS at pH 8 (---), and in 2.8 mM HS^- at pH 8 (—), and b) GF electrode in 10 mM PBS at pH 8 (---), and in 2.8 mM HS^- at pH 8 (—).

CV was carried out using a GC electrode to understand the electrochemical behaviour of sulfide at carbon-based electrode, evaluate the reversibility of the sulfide electrolysis and determine the electrode potentials applied in the anodic and cathodic regeneration strategies. The presence of HS^- yielded significantly higher anodic and cathodic currents compared with the background current recorded for phosphate buffer solution, implying the high electrocatalytic activity of the GC electrode for sulfide oxidation. Several anodic peaks were observed at potentials E_{Iox}= + 0.4 V/SHE, E_{IIox}= + 0.84 V/SHE and E_{IIIox}= + 1.1 V at the GC electrode (**Figure 4.1 a**).

It was assumed that the first E_{Iox} and the second oxidation peak E_{IIox} represented sulfide oxidation to elemental sulfur [233, 310, 311]. E_{Iox} was ascribed to the following reaction:

$$HS^- + OH^- \rightarrow S^0 + H_2O + 2e^- \quad (E^0 = -0.68V) \qquad \text{(Eq. 4.1)}$$

while E_{IIox} represented:

$$HS^- \rightarrow S^0 + H^+ + 2e^- \quad (E^0 = -0.27V) \qquad \text{(Eq. 4.2)}$$

Finally, the third oxidation peak E_{IIIox} recorded at +1.1 V/SHE was attributed to the oxidation of sulfide to sulfate [233, 311]:

$$HS^- + 9\ OH^- \rightarrow SO_4^{2-} + H_2O + 2e^- \quad (E^0 = 0.469\ V) \qquad \text{(Eq. 4.3)}$$

During the reverse scan, the formed oxidized species were reduced back to sulfide or polysulfides as it was demonstrated by the peak at E_{Ired}= -1.1 V/SHE [253]:

$$S^0 + 2\ e^- + H^+ \rightarrow HS^- \qquad \text{(Eq. 4.4)}$$

Similar peaks were observed when GF was used as an electrode (**Figure 4.1 b**). The observed oxidation peaks occurred at potential higher than theoretical at both GC and GF, which could attributed to several factors. For instance, Wang et al. demonstrated that electrooxidation pathway of sulfide is highly sensitive to pH, which leads to substantial shifts in oxidative peak positions once pH of the electrolyte is changed [310]. Moreover, a study of Thompson et al. reports

significant variation of sulfide oxidation potentials at different electrode materials, ranging from +0.36 V, +0.45 V, +0.76 V, up to +1.30V vs SCE for Pt, glassy carbon, Au and BDD, respectively [312]. Finally, other parameters such as scan rate, temperature and electrolyte composition can also influence position of the peaks [214].

Based on the recorded CVs, potentials of -1.3 and +1.7 V/SHE were selected for the cathodic and anodic recovery of the sulfur-loaded electrodes, respectively.

4.3.2. Influence of the applied anode potential on sulfide removal at GF and ACF electrodes

In the OC experiments conducted at the GF electrode without applying the potential, sulfide was partially removed (i.e., 56% removal after 6 h of recirculation) with the observed rate constant of 0.14 h^{-1} (**Figure 4.2 a**). Sulfide dissolution at pH 8 yields approximately 10 % of H_2S and 90% of HS^-, meaning that up to 10% of the sulfide present in the beginning of the experiment might be lost due to volatilization. In order to rule out volatilization of sulfide, OC experiments were also performed at pH 12 when H_2S is completely dissociated into HS^-. The effect of the electrolyte pH on sulfide removal kinetics was insignificant, therefore volatilization of sulfide can be considered negligible. Adsorption of sulfide to the GF was also excluded as the XPS analyses of the GF after the OC experiments could not detect the presence of any sulfur species. Analysis of the dissolved sulfur species during the OC experiment revealed an increase in $S_2O_3^{2-}$ and SO_4^{2-} concentrations, indicating the oxidation of HS^- via chain reactions with oxygen (**Figure 4.2 a**) [25]. Sulfide oxidation with oxygen also yielded polysulfide as was indicated by the characteristic yellow colour of the electrolyte, however, their concentration could not be determined due to the lack of reliable and robust methods for quantification of polyS. Although both the electrolyte and the reactor were purged with nitrogen to remove the DO prior to the experiments, some oxygen remains weakly physisorbed inside the GF [313]. This was also confirmed by the rapid increase followed by the

gradual decrease of the DO concentration during the OC experiment, meaning that oxygen was first released and then slowly consumed over time (**Figure 4.3).**

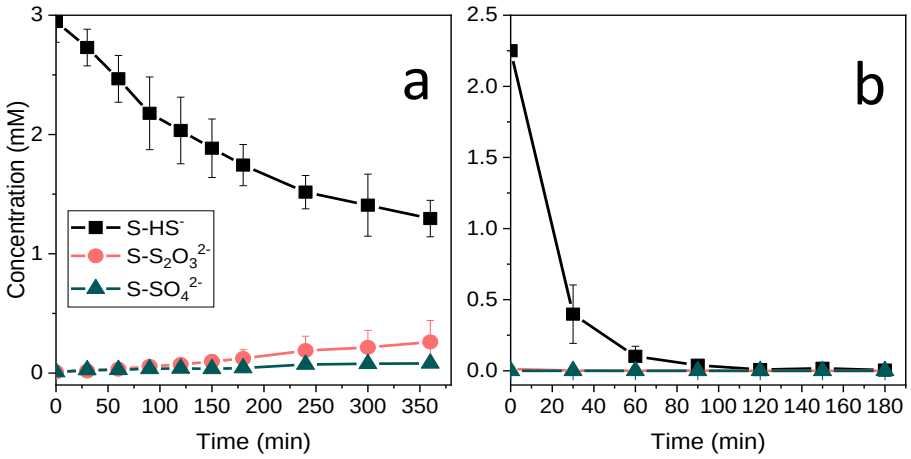

Figure 4.2 Concentration of dissolved sulfur species measured in the OC experiments using: a) GF, and b) ACF electrode.

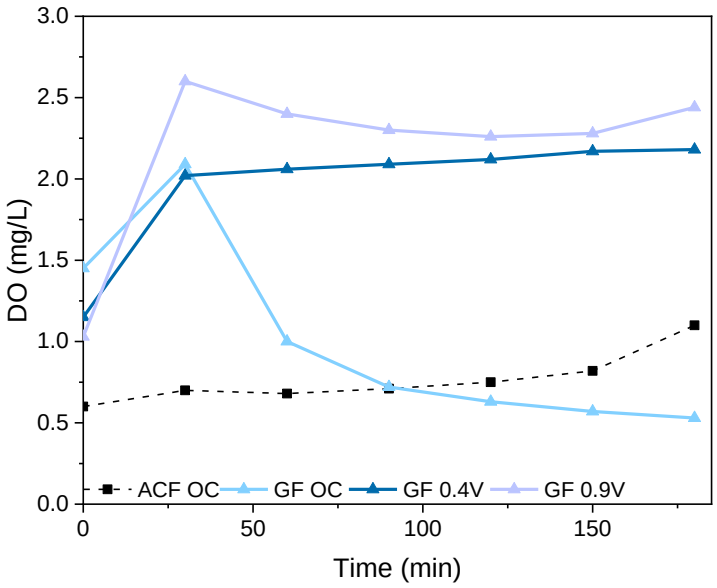

Figure 4.3 DO concentration measured in the OC and the electrooxidation experiments using GF and ACF electrode.

Application of the anode potential of 0.4 – 0.9 V/SHE at the GF electrode lead to sulfide oxidation to elemental sulfur, with minor quantities of thiosulfate (<4% of total sulfur) and sulfate (<2% of total sulfur) (**Figure 4.4 a**). The current efficiency of the reaction was estimated at 90%. Selective oxidation of HS^- to S^0 was also confirmed by the XPS analysis, where the S2p spectra had six peaks in total: two major peaks at 163.9 and 165 eV attributed to elemental sulfur and four minor peaks consistent with the oxidized sulfur in the form of S-O and sulfates [314, 315] (**Figure 4.6 d**). Electrochemical oxidation of sulfide on graphite electrodes is mainly controlled by the charge transfer across the interface, while diffusion of sulfide ion plays a minor role [233]. Indeed, the dependence between the sulfide oxidation rates and the applied potential was found to be linear (**Figure 4.5 a**). Similar results in terms of the dependence of the sulfide removal rates on the applied potential or current, and sulfur being the final product of electrooxidation were also reported in previous studies [316-318].

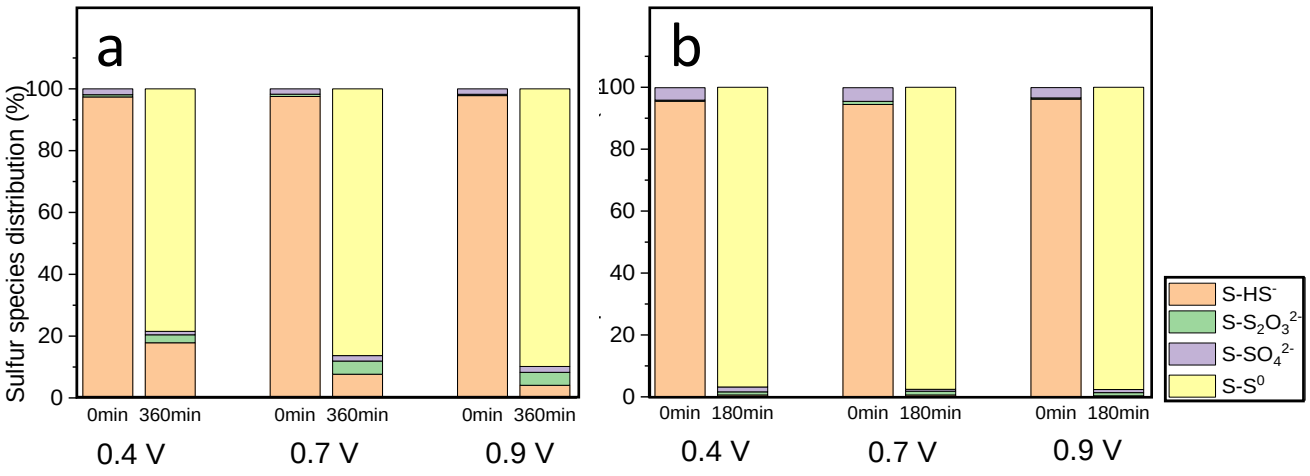

Figure 4.4 Sulfur species distribution before and after the electrochemical sulfide oxidation at: a) GF, and b) ACF electrode.

In the case of ACF, a sharp decrease in sulfide concentration was observed in the first 30 min of the OC experiments **(Figure 4.1 b)**. Given that there was no sulfur oxyanions (i.e., $S_2O_3^2$, SO_3^{2-}, and SO_4^{2-}) detected, and DO was present at very low concentration of 0.5 mg L^{-1} **(Figure 4.3)**, oxidation of sulfide initiated by oxygen was excluded. The XPS analyses confirmed that the loss of sulfide was due to the chemisorption of HS^- at the ACF surface **(Figure 4.6 a)**. The S2p spectra of the ACF used in the OC experiment can be fitted into two major peaks at 163.9 and 165 eV, typical of elemental sulfur. Strong chemisorption of sulfide at the ACF was also reported by Ayranchi and Conway [319]. Indeed, the tendency of sulfide ion to undergo specific adsorption on the activated carbon is well known [319]. Typically, the reaction starts with the substitution reaction between the sulfide ion and C(O) functional group, which results in the formation of C-S bonds. C-S gets further polymerized by the sulfide ion, creating polysulfides, which remain adsorbed at the surface. Polymerization of the polysulfide continues until a stable chain or cyclic sulfur molecules such as S_8 are formed [320, 321]. The reaction pathway can be influenced by many factors, including the presence of oxygen functional groups, as well as the ACF surface chemistry, hydrophobicity and porosity [322-324].

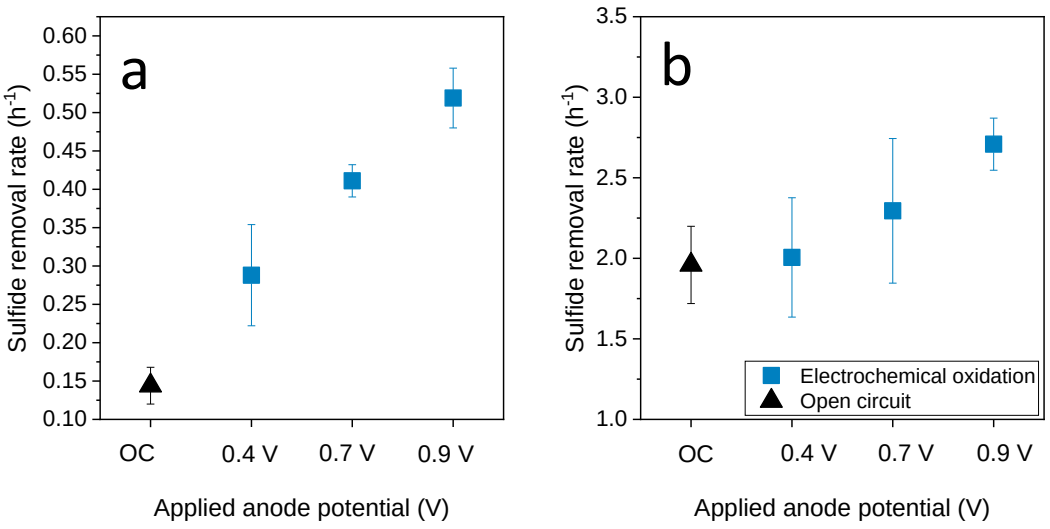

Figure 4.5 First-order sulfide removal constant (h^{-1}) in the OC experiments, and in the chronoamperometric experiments at 0.4 - 0.9 V/SHE anode potentials at: a) GF, and b) ACF electrode.

Application of 0.4 V/SHE to the ACF electrode did not significantly increase the observed removal rate of sulfide (2.0 h^{-1}) compared with the OC experiment (1.9 h^{-1}) **(Figure 4.5)**. Further increase in the anode potential to 0.7 and 0.9 V/SHE yielded somewhat higher sulfide removal rates of 2.2 and 2.7 h^{-1}, respectively. This was likely a consequence of the increased contribution of sulfide electrolysis to its overall removal, as well as the surface modification of the ACF and the generation of new oxygen-containing functional groups that improved the wettability of the felt and acted as active sites for the chemisorption of sulfide [325]. The IC analyses could not detect any sulfur oxyanions being formed in the electrolysis experiments, indicating the elemental sulfur (S^0) as the only product of sulfide removal at the ACF electrode **(Figure 4.4 b).** The fitting of the S2p spectrum demonstrated the presence of only elemental sulfur (i.e., peaks at 163.9 and 165 eV) and some minor peaks typical of the oxidized sulfur in the form of S-O and sulfate **(Figure 4.6 b).** The non-Faradaic mechanism of sulfide oxidation at ACF described above was also confirmed by current efficiency above 100% (i.e., 410%) and decreased energy consumption compared to GF

when 0.7 V/SHE was applied (i.e., 0.03 kW h m^{-3} and 0.28 kW h m^{-3} for ACF and GF, respectively).

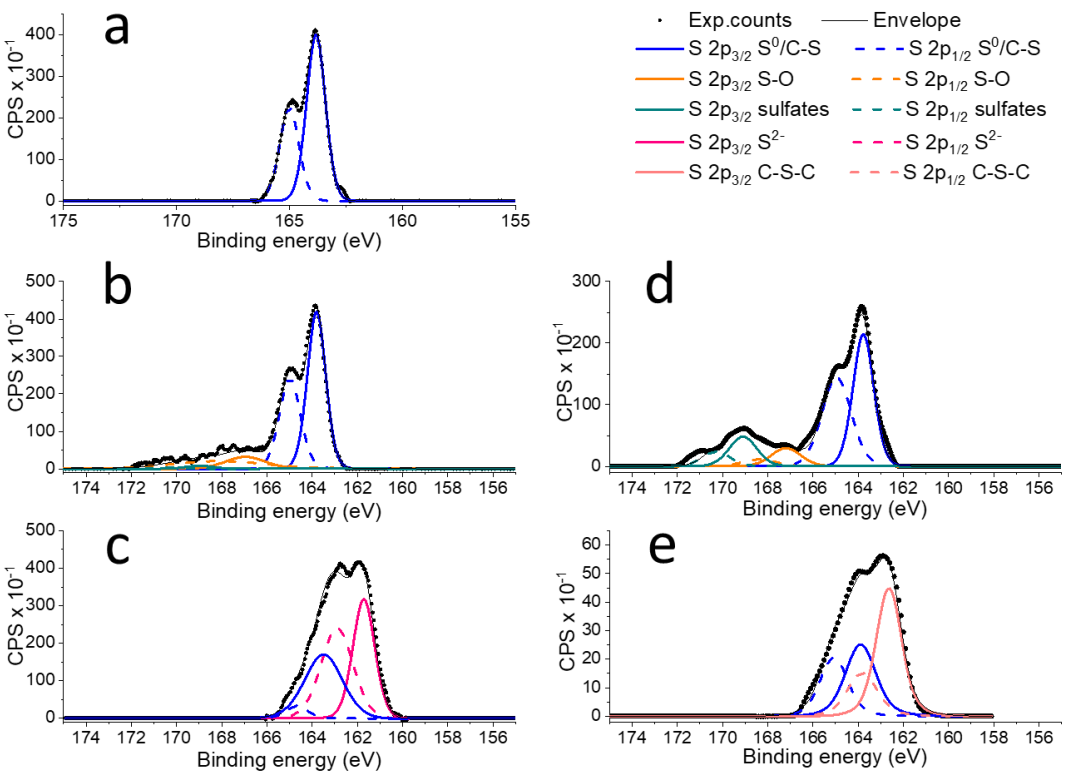

Figure 4.6 High resolution S2p XPS spectra of the: a) ACF after the OC experiment, b) ACF after the electrooxidation of HS-, c) ACF after the electrooxidation of HS- followed by the cathodic recovery, d) GF after the electrochemical oxidation of HS-, and e) GF after electrooxidation of HS- followed by the cathodic recovery.

4.3.3. Hydrogen sulfide removal from sewage

Electrooxidation of sulfide at the GF and ACF electrodes was also conducted in raw sewage sampled from the upstream sewer system at + 0.9 V/SHE (**Figure 4.7**). The observed sulfide removal rates were 3.8 h^{-1} and 0.6 h^{-1} at the ACF and GF electrode, respectively, slightly higher compared with the low conductivity HS^- solution (i.e., 2.7 h^{-1} and 0.52 h^{-1}, respectively). This was attributed to the higher conductivity of the sewage compared to the conductivity of the synthetic

feed (i.e., 0.6 mS cm^{-1} and 1.5 mS cm^{-1}, respectively). Pikaar et al. also observed higher rates of electrooxidation of sulfide at the MMO anodes in domestic wastewater than in the synthetic feed, and attributed it to the presence of metals, as even trace concentrations are capable of enhancing the sulfide oxidation due to the formation of the metal-sulfide complexes [231].

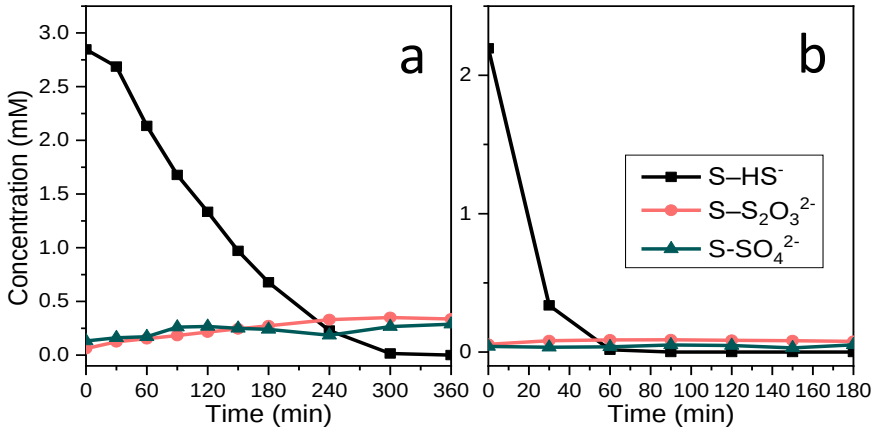

Figure 4.7 Dissolved sulfur species present in the sewage during the electrooxidation of sulfide at + 0.9 V/SHE using the: a) GF, and b) ACF electrode.

ACF was capable of complete sulfide oxidation to sulfur with fast reaction kinetics, whereas the final concentration of the dissolved sulfur species was below 0.1 mM, indicating the formation of elemental sulfur and chemisorption of sulfide to the ACF surface (**Figure 4.7 b**). In addition to the sulfide removal, 53% of COD was removed due to the adsorption of organics on the ACF [326]. Organic compounds, after being adsorbed to the ACF, are likely to interact with the sulfide and form sulfonated hydrocarbons [327]. This additional interaction might be responsible for the slightly higher sulfide removal rates compared to the experiments using the synthetic feed, conducted in the absence of organic compounds.

In the case of the GF electrode, sulfide removal was slower compared to the ACF and occurred after five hours of the treatment, and only slight decrease in COD (i.e., 11% removal) was observed due to the chemical oxidation with the *in situ* generated oxygen. The main mechanism of sulfide removal was its direct oxidation to sulfur, however, indirect sulfide oxidation with also occurred as was indicated by the increase in sulfate and thiosulfate concentrations. Total dissolved sulfur species concentration was 0.43 mM in the electrochemical treatment of real sewage at the GF electrode, significantly higher compared to the synthetic feed (i.e., 0.1 mM), which could occur due to enhanced oxygen evolution reaction at higher conductivity.

4.3.4. Recovery of the sulfur-loaded GF and ACF electrodes

Anodic recovery of the sulfur-loaded GF electrode was performed by its polarization at +1.7 V/SHE, i.e., well above the OER potential (i.e., + 0.9 V/SHE at pH = 7.8-8), and the potential of sulfide oxidation to sulfate observed at GC electrode (+ 0.9 V/SHE, **Figure 4.1**). Despite the high anodic potential applied and the visible formation of oxygen bubbles at the surface of the GF electrode, dissolution of the electrodeposited S^0 did not occur and no sulfur oxyanions could be measured in the solution. This result indicated that further oxidation of elemental sulfur is difficult to achieve. As reported by the previous studies, S^0 was only partially oxidized to S-O species (**Figure 4.6**), which remain at the surface of the electrode and can be easily reduced back to sulfur when lower potential is applied [328-330].

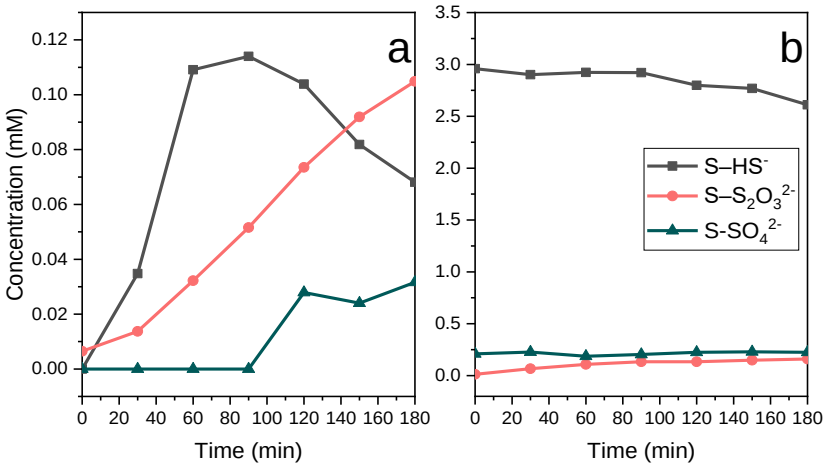

Figure 4.8 Concentration of the dissolved sulfur species measured in the regeneration experiments with sulfur-loaded GF electrode after the: a) cathodic recovery, and b) cathodic recovery in the presence of 2.7 mM HS^-.

The cathodic regeneration of the sulfur-loaded GF electrode was conducted at -1.3 V/SHE, to enable the electrochemical dissolution of sulfur due to its reduction to sulfide, accompanied by the sulfur stripping in the form of hydrogen sulfide with the electrochemically produced hydrogen [331]. About 30% of the previously loaded sulfur was recovered from the GF electrode as a mixture of HS^-, SO_4^2, $S_2O_3^{2-}$ and polyS (**Figure 4.8 a**). This result is also in agreement with the study of Quijada et al. who observed that electrodeposited sulfur can only be removed reductively [332]. Previous studies reported that the electrooxidation of sulfide at the carbon electrodes normally yields weakly and strongly bonded species of sulfur [330, 333]. As proposed by Quijada et al., strongly bound sulfur is represented by the layer of the chemisorbed sulfur, while the top layer consists of the weakly bound bulk elemental sulfur with the S_8 structure [334]. Since the strongly bonded sulfur is not available for the recovery, only partial recovery of the used GF electrode is possible. The XPS high resolution spectra of the GF after the cathodic recovery showed a significant decrease of the signal at 163.7 eV ascribed to the C-S/S_8 (**Figure 4.6 e**). Besides, the

bands at 167.2 and 169.2 eV were absent in the GF material after the recovery, indicating the removal of sulfur oxides species, including C-O and sulfate/sulfite groups. Sulfur that remained at the GF surface after the cathodic polarization consists of C-S/S_8 and C-S-C, which are strongly bound species of sulfur.

Previously, Dutta et al. observed complete cathodic recovery of the sulfur-loaded carbon fiber brush electrodes, despite the much lower cathode potential applied (-0.33 V /SHE) [253] compared to our study (-1.3 V/SHE). Yet, in their study the cathodic recovery was performed in 1-100 mM sulfide solution at high pH, which is particularly favourable for the chemical dissolution of S^0 to polysulfides. During this reaction, sulfide ion is capable of performing a nucleophilic attack and stripping sulfur from the GF electrode in the form of polysulfide [335] as shown in Equation 4.5:

$$HS^- + (n - 1)/8\ S_8 \leftrightarrow S_n^{2-} + H^+ \qquad \text{(Eq. 4.5)}$$

Thus, the cathodic recovery of the sulfur-loaded GF was also conducted in 2.7 mM HS^- solution at pH =11, which is in the lower range of the sulfide concentrations tested by Dutta et al. (**Figure 4.8 b**)[253]. Higher concentrations of sulfide in the regeneration solution were avoided because the on-site storage of such highly concentrated sulfide solutions would imply high health and safety hazards of the electrochemical treatment units. Given that polysulfides are unstable species that are rapidly converted to $S_2O_3^{2-}$, SO_3^{2-} and SO_4^{2-} in the presence of oxygen [25], their concentration could not be determined. Nevertheless, the initial formation of polysulfides was observed due to the appearance of the characteristic yellow colour of the electrolytes in the regeneration of the GF anode.

The sulfur-loaded ACF could not be recovered by any of the strategies tested, as demonstrated by the XPS analyses of the ACF surface (**Figure 4.6 c**). There was also no formation of the dissolved sulfur species, i.e., HS^- in the cathodic recovery and $S_2O_3^{2}$, SO_4^{2-} and polyS in the anodic recovery of sulfur-loaded ACF, as was observed for GF. There was also no polysulfide formation (i.e., yellow colouring of the solution) observed in the case of the cathodic recovery of the ACF electrode in the presence of 2.7 mM HS^-. In the chemisorption of sulfide at the ACF surface, sulfide reacts in a substitution reaction with the oxygen-containing functional groups at the ACF surface, and forms C-S bonds with the eventual complexation to S_8 [320, 321, 324, 336]. Thus, unlike in the case of GF, where some sulfur is only weakly bonded, chemisorption of sulfide at the ACF results in the production of bulky sulfur polymers incorporated into the carbon matrix, making their detachment from the ACF surface very difficult [327, 337]. Indeed, the XPS spectra of the cathodically recovered ACF demonstrates S2p peak of the same intensity as in the material prior to the recovery (**Figure 4.6 c**). Even though no sulfur oxyanions were detected in the electrolyte during the cathodic polarization, the reduction of sulfur to sulfide still occurs as was indicated by the appearance of the peak at 162 eV typical of sulfides, however, in this case sulfide remains at the surface of ACF [314, 315]. Moreover, catalytic oxidation of sulfide at the ACF normally takes place in its micropores as was indicated by the BET analysis, which showed an increase of the mean micropore diameter from 25.2Å in pristine ACF to 29.2Å in the used material [320]. Therefore, the recovery of the sulfur loaded in the microporous structure of the ACF is strongly impeded by the diffusion limitations [320, 327].

4.3.5. The impact of the recovery strategy on the subsequent sulfide removal

As was shown in this study, the GF electrode can only be recovered and the electrodeposited sulfur removed under cathodic polarization. However, the cathodic recovery was not complete, allowing the dissolution only of the weakly physiosorbed top layer of sulfur. Therefore, the GF electrodes that were loaded with sulfur and then subjected to any recovery had some sulfur present at its surface. This sulfur was capable of anchoring sulfide ions in the complexation reaction of polysulfide formation that stayed adsorbed at the surface, which caused slightly enhanced rates of sulfide removal with the used materials compared to the pristine GF. Another confirmation of the fact that the pre-adsorbed sulfur underwent complexation by the sulfide ion rather than the chemical dissolution in the form of polysulfide is the cathodic recovery performed in the presence of HS^-. This recovery strategy had a similar impact on the subsequent sulfide oxidation as any other recovery type, demonstrating that it was not possible to recover the electrodes with chemical sulfur dissolution, on the contrary to what had been previously observed for carbon brush electrodes [253].

Cathodic (-1.3 V/SHE) and in particular anodic (+1.7 V/SHE) polarization of the used GF electrode significantly improved the rates of sulfide removal at 0.4 V/SHE compared to the pristine GF material, i.e., from 0.19 h^{-1} in the pristine GF to 0.67 h^{-1} and 0.44 h^{-1} after anodic and cathodic recovery of the used GF electrode, respectively (**Figure 4.9 a**). As was previously reported, anodic polarization of the GF causes surface etching resulting in a higher surface area, as well as an increased molar ratio of O to C and the number of -COOH functional groups which are capable of catalyzing the sulfide oxidation reaction and improving the electron transfer [338, 339]. In addition, anodic polarization of the GF can improve its wettability [340].

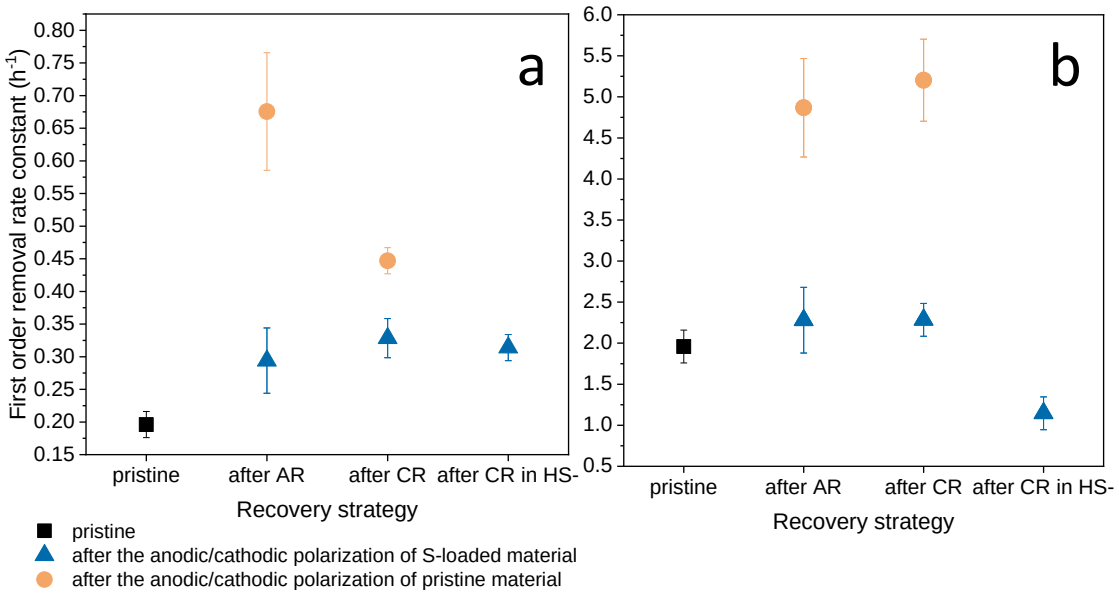

Figure 4.9 First-order sulfide removal rates observed at the: a) GF, and b) ACF electrodes subjected to the three recovery strategies.

Sulfide removal rates observed after both anodic and cathodic regeneration of the sulfur-loaded ACF were similar, i.e., 4.2 h^{-1} and 5.2 h^{-1}, respectively (**Figure 4.9 b**). Even though none of these strategies were successful in recovering sulfur that had been chemisorbed at the ACF surface, sulfide removal rates on sulfur loaded material were slightly higher due to the similar interactions between the sulfur and sulfide to the ones observed at GF. Moreover, cathodic recovery of the ACF electrode in the presence of HS^- led to lower sulfide removal (i.e., 1.1 h^{-1}) compared to pristine ACF (i.e., 1.9 h^{-1}) (**Figure 4.9 b**). In this case, the polymerization of the ACF-bound sulfur in the presence HS^- caused a higher saturation of the ACF and less active sites available for further sulfide sorption [320, 321].

Similar to the GF electrode, anodic and cathodic polarization of the ACF electrode significantly increased the sulfide removal rates from 1.9 h^{-1} for the pristine material to 4.2 h^{-1} and 5.2 h^{-1},

respectively (**Figure 4.9 b**). Studies report that the ACF chemistry is significantly changed under both anodic and cathodic polarization. While the cathodic polarization only results in slight oxidation of the material due to the generation of H_2O_2, anodic polarization induces extensive oxidation of the ACF as well as modification of the porous network [325].

4.4. Conclusion

Both ACF and GF electrodes were capable of selective HS^- oxidation to elemental sulfur in low-conductivity solutions (i.e., <1 mS cm^{-1}), as well as in the raw sewage. The observed HS^- removal rate was ten times faster at the ACF compared with the GF electrode. However, considering that the specific surface area of ACF is significantly higher compared to GF (i.e., 97500 m^2 for ACF and 65 m^2 for GF), the normalised reaction rate constant of sulfide oxidation at ACF was actually lower than at GF electrode (i.e., $3.9 \cdot 10^{-9}$ m^3 h^{-1} m^{-2} for ACF and $9.2 \cdot 10^{-6}$ m^3 h^{-1} m^{-2} for GF).

Out of all tested regeneration strategies, only cathodic polarisation enabled partial regeneration (i.e., 30% efficiency) of the used GF electrode. Sulfur retained at the ACF electrode could not be recovered by any of the investigated strategies. The efficiency of the electrochemical sulfur regeneration was limited due to incorporation of sulfur into the carbon matrix observed at both GF and ACF.

To summarize, sluggish sulfide oxidation kinetics alongside with impossibility of complete electrode recovery makes carbon-based electrodes unattractive for full scale application notwithstanding their competitive cost. Even though partial regeneration achieved at GF is beneficial for sulfide removal in short term, the impossibility to dissolve electrodeposited sulfur completely decreases selectivity of the treatment as it leads to the production of polyS. Although

chemical electrode regeneration strategy achieved through extraction of sulfur with organic solvent was reported to be effective, its application would compromise the sustainability and increase the operating cost of the electrochemical treatment unit [244].

Chapter 5. Manganese oxide-based porous electrodes for rapid and selective (electro)catalytic removal and recovery of sulfide from wastewater

5.1. Background

In this study, we propose for the first time the use of Mn_xO_y-based electrodes for the catalytic sulfide removal, while achieving a continuous regeneration of the Mn_xO_y coating by applying anodic potential. The coating of the electrochemically-deposited manganese oxides over a porous GF was fine-tuned in terms of the precursor concentration and loading to obtain a specific Mn_xO_y oxidation state, loading, morphology and crystallinity and maximize its (electro)catalytic activity and selectivity towards the sulfide oxidation to sulfur. The effect of calcination on the electrodeposited Mn_xO_y and its subsequent performance was also investigated. Gradual loss of the electrode performance due to the formation of the deposited sulfur was also addressed by the application of the cathodic polarization for the dissolution of S^0. Furthermore, the synthesized GF-Mn_xO_y electrodes were employed for the sulfide removal from real sewage to investigate the performance of the Mn_xO_y-based electrodes for sulfide removal under realistic conditions.

5.2. Material and methods

5.2.1. Mn_xO_y-coated electrode synthesis

GF-Mn_xO_y electrodes were synthesized using the anodic electrodeposition technique. The synthesis was performed in a three-electrode setup at ambient temperature (i.e., 24 ± 1 °C), with GF (2 × 1.5 × 0.5 cm) obtained from Final Advanced Materials (France) as a working electrode (anode), carbon foil as a counter electrode and Ag/AgCl (KCl 3 M, Bioanalytical systems, IN) as reference electrode. The electrodeposition medium contained 0.2 M $MnSO_4$ and 0.02 M H_2SO_4 [341]. To investigate the influence of the precursor concentration on the Mn_xO_y coating characteristics, electrodeposition synthesis was also performed using 0.02 M $MnSO_4$ and 0.02 M H_2SO_4. In all synthesis procedures, 0.01 vol % Triton X-100 was used to improve the deposition

efficiency and obtain a more uniform coating on a porous structure of the GF [342]. Deposition was performed in potentiostatic mode at + 1.63 V/SHE. To ensure the reproducibility of each deposition, the mass of the manganese oxide loading was calculated according to Faraday's law and the charge was limited to 200 C or 1000 C. After completion of the synthesis process, material was rinsed thoroughly with distilled water. To ensure a complete removal of the Triton X-100, synthesized material was treated with isopropanol at 60 °C for 15 min, followed by the second rinsing with distilled water. To investigate the effect of the temperature treatment, samples were calcinated at 300, 400 and 500 °C in air for 1 h in a tubular oven (Nabertherm, Germany). "H" in the sample code stands for high precursor concentration (i.e., 0.2 M $MnSO_4$), while "L" means low precursor concentration (i.e., 0.02 M $MnSO_4$). The amount of charge (i.e., 200 C or 1000 C) is also mentioned in the code. Names of the samples, which were subjected to the temperature treatment include "c" for calcinated.

5.2.2. (Electro)catalytic sulfide removal and electrode regeneration tests

Electrochemical experiments were carried out in a glass cell (250 mL) with an air-tight seal. GF or GF-Mn_xO_y materials was used as the anode, Ag/AgCl (3M KCl) as the reference electrode and Pt coil was the counter electrode separated from the anodic compartment by a porous glass frit. Electrochemical cell was purged with nitrogen prior to all experiments to minimize the loss of sulfide due to its reaction with the DO. The experiments were performed in both OC and under constant potential of +0.4 V/SHE to evaluate the sulfide removal using GF and the synthesized GF-Mn_xO_y electrodes. The initial concentration of sulfide was 2.7 mM, with 2.6 mM $NaNO_3$ as a supporting electrolyte (conductivity 3 – 3.2 mS cm^{-1}, pH 8.2). The pH of the supporting electrolyte was maintained at pH 8 – 8.2 during the 2 hours experiments to avoid sulfide stripping. Cathodic regeneration of the sulfur loaded electrodes was performed in the same reactor as described above

under constant potential of -0.8 V/SHE and in a 25 mM $NaNO_3$ electrolyte (conductivity of 3 – 3.2 mS cm^{-1}). All experiments were performed in duplicate and values are expressed as mean with their standard errors.

To investigate the performance of the Mn_xO_y-coated electrodes for sulfide removal under realistic conditions, experiments were performed with real sewage that was filtered using 0.2 μm nylon membrane, deoxygenated and amended with the same initial concentration of sulfide (i.e., 2.7 mM) and adjusted to pH 8.2. The conductivity of the sampled sewage was identical to the supporting electrolyte used in the experiments (i.e., 3.2 mS cm^{-1}).

Surface characterisation of the electrode materials and chemical analysis are described in the Chapter 3.

5.3. Results and discussion

5.3.1. Characterization of the GF-Mn_xO_y electrodes

Figure 5.1 represents the XRD patterns of the synthesized GF-Mn_xO_y materials. As expected, the XRD spectra of the non-calcinated samples did not show any peak that could be attributed to the crystalline phase of the Mn_xO_y, meaning that the electrodeposition alone results in a completely amorphous coating. On the contrary, all calcinated samples showed signals characteristic of an orthorhombic bixbyite crystalline phase, α-Mn_2O_3 (Mn(III)) (**Figure 5.1 a, Figure 5.2**). As can be concluded from the improved signal, increase in the calcination temperature improved the crystallinity of the material. The same oxide type was obtained in the samples synthesized at the higher precursor concentration (**Figure 5.1 b**). Sample in which the Mn_xO_y loading was increased

to 1000 C demonstrated a pattern more typical of the tetragonal hausmannite, Mn_3O_4, comprised of the Mn with two valence states: Mn(III) and Mn(II) (**Figure 5.1 c**). The appearance of Mn(II) can be caused by an increased thickness of the coating obtained by the longer time of the electrodeposition. Deeper layers of such coating are completely isolated from oxygen during the calcination step, thus leading to the Mn_xO_y thermal reduction to lower oxide forms such as Mn(II) [343]

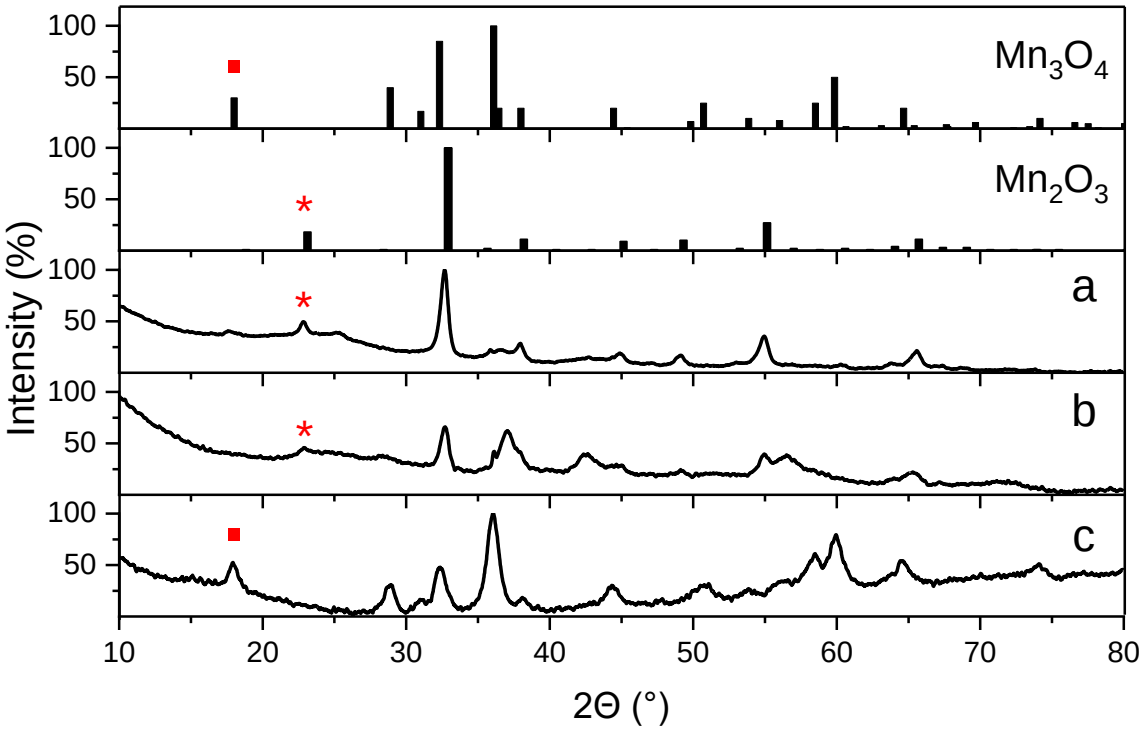

Figure 5.1 The XRD patterns of GF-Mn_xO_y electrodes obtained using different precursor concentrations (i.e., 0.02 M (L) and 0.2 M $MnSO_4$ (H)), electrical charge applied (200 C and 1000 C), followed by the calcination step: a) L-200 C, c., b) H-200 C, c., and c) H-1000 C, c. Reference patterns are depicted at the top for Mn_3O_4 (■), α-Mn_2O_3 (*), where the symbols indicate the respective low-angle reflections.

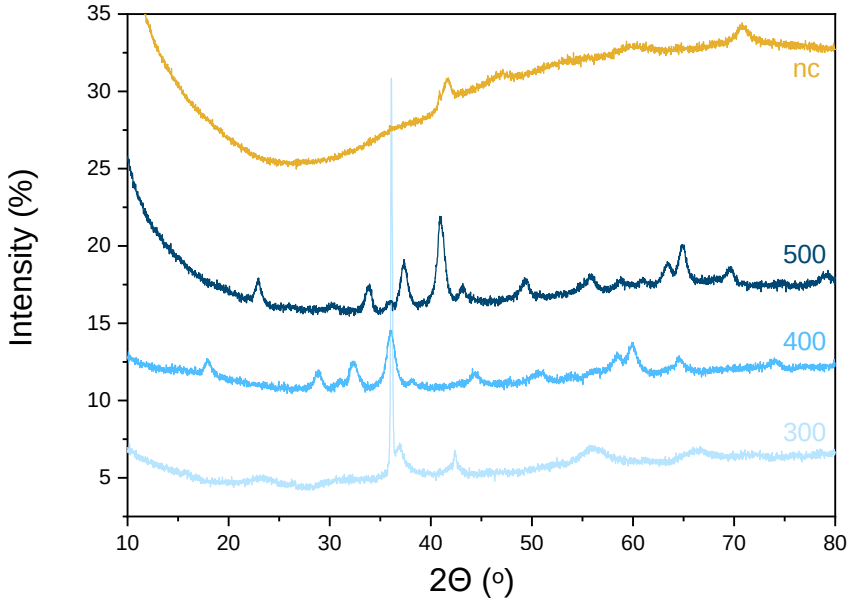

Figure 5.2 The XRD patterns of the non-calcinated GF-Mn_xO_y (H-200 C) and materials obtained using different calcination temperatures (300°C, 400°C and 500°C). nc=non-calcinated sample.

Table 5.1 The XPS peak analyses of the GF-MnxOy electrodes obtained using different precursor concentrations (0.02 M and 0.2 M MnSO4), electrical charge applied (200 C and 1000 C), and with and without the calcination step. The deconvoluted data are shown for the Mn 2p3/2 and Mn 3s.

Sample	Mn $2p_{3/2}$, E_b, eV	Mn 3s			Valence number of Mn
		E_b (1), eV	E_b (2), eV	ΔE, eV	
L-200C	642	88.3	83.7	4.6	4
L-200C, c.	642	89.1	83.9	5.2	3
H-200C	641.9	88.8	84.2	4.6	4
H-200, c.	641.7	89	83.8	5.2	3
H-1000C	641.9	88.4	84.1	4.3	4
H-1000C, cal.	641.6	88.9	83.7	5.2	3

The XPS analysis was also carried out to investigate the surface composition of the amorphous Mn_xO_y coating and to complement the XRD analysis results of the crystalline samples. The Mn valence state was determined based on the Mn 3s doublet peak separation as a more reliable method compared to the one based on the location of the Mn 2p peaks only [342]. Different Mn

3s doublet peak splitting values were previously reported in the literature including 4.5, 5.2, 5.4, and 5.8 eV for MnO_2 (Mn I), Mn_2O_3 (Mn(III)), Mn_3O_4 (Mn(II), Mn(III)), and MnO (Mn(II)), respectively [342, 344, 345]. As can be seen from the Table 5.1, doublet peak separation values for all samples that were not subjected to calcination (i.e., L-200 C, H-200 C, H-1000 C) are in the range common for the MnO_2 (Mn(IV)). This valence state is typical for the Mn-based coatings synthesized via the anodic electrodeposition pathway, and forms via the following reaction [346]:

$$Mn^{2+} + 4OH^- \rightarrow MnO_2 + 2H_2O + 2e^- \quad \text{(Eq. 5.1)}$$

The doublet peak separation increased for the calcinated samples (i.e., L-200 C, c, H-200 C, c, H-1000 C, c) indicating the transformation of the MnO_2 (Mn(IV)) into the Mn_2O_3 (Mn(III)), which is in agreement with the XRD data. This phase transformation took place due to the thermal decomposition of the MnO_2 at 500ºC according to the following reaction [343, 347]:

$$4\ MnO_2 \rightarrow 2Mn_2O_3 + O_2 \quad \text{(Eq. 5.2)}$$

The dominant surface species for the samples with the higher Mn-loading (i.e., 1000 C) was also Mn_2O_3, confirming the assumption that the Mn(II) is mainly present in the inner layers of the coating.

Figure 5.3 compares the morphology of the various Mn_xO_y coatings prepared under different electrodeposition parameters. The Mn_xO_y coating synthesized at higher $MnSO_4$ concentration (i.e., 0.2 M) has a nanorod-like morphology (**Figure 5.3 c, 5.3 d**). When the charge was increased (**Figure 5.3 e, 5.3 f**), the electrode coating became thicker and smoother as nanorods became less pronounced, merging into each other and forming a dense layer. The observed morphological difference can be explained through the mechanism of the Mn_xO_y layer formation. Manganese oxide coating formation using the electrodeposition is a complex process that can be divided into two main steps: *i)* nuclei formation, and *ii)* crystal growth [348]. Nuclei formation and continuous

uptake of the new substrate sites normally occurs within seconds in the initial stage of the electrodeposition, resulting in a very rough coating with high specific surface area. As the electrodeposition continues, the formed nuclei continue to grow in all directions and finally merge into adjacent growth centers, forming Mn_xO_y film over the entire GF substrate surface. Formation of the new nuclei during the continuous crystal growth also occurs, however, this process takes place on the top of the existing Mn_xO_y layer. Thus, the Mn_xO_y layer becomes thicker and smoother, while the specific surface area of the coating decreases due to the presence of less relief in its structure. The Mn_xO_y coating obtained at the lower precursor concentrations (i.e., 0.02 M $MnSO_4$) is characterized by a nanoneedle-like structure mixed with the nanorods of smaller size compared to the samples synthesized at higher precursor concentration (**Figure 5.3 a**). According to Babakhani et al., instantaneous mechanism can be suppressed by limiting the Mn^{2+} concentration at the electrode surface, which results in a material with more compact grains (**Figure 5.3 a, 5.3 b**) [346]. Calcination did not have any significant effect on the morphology of the synthesized materials.

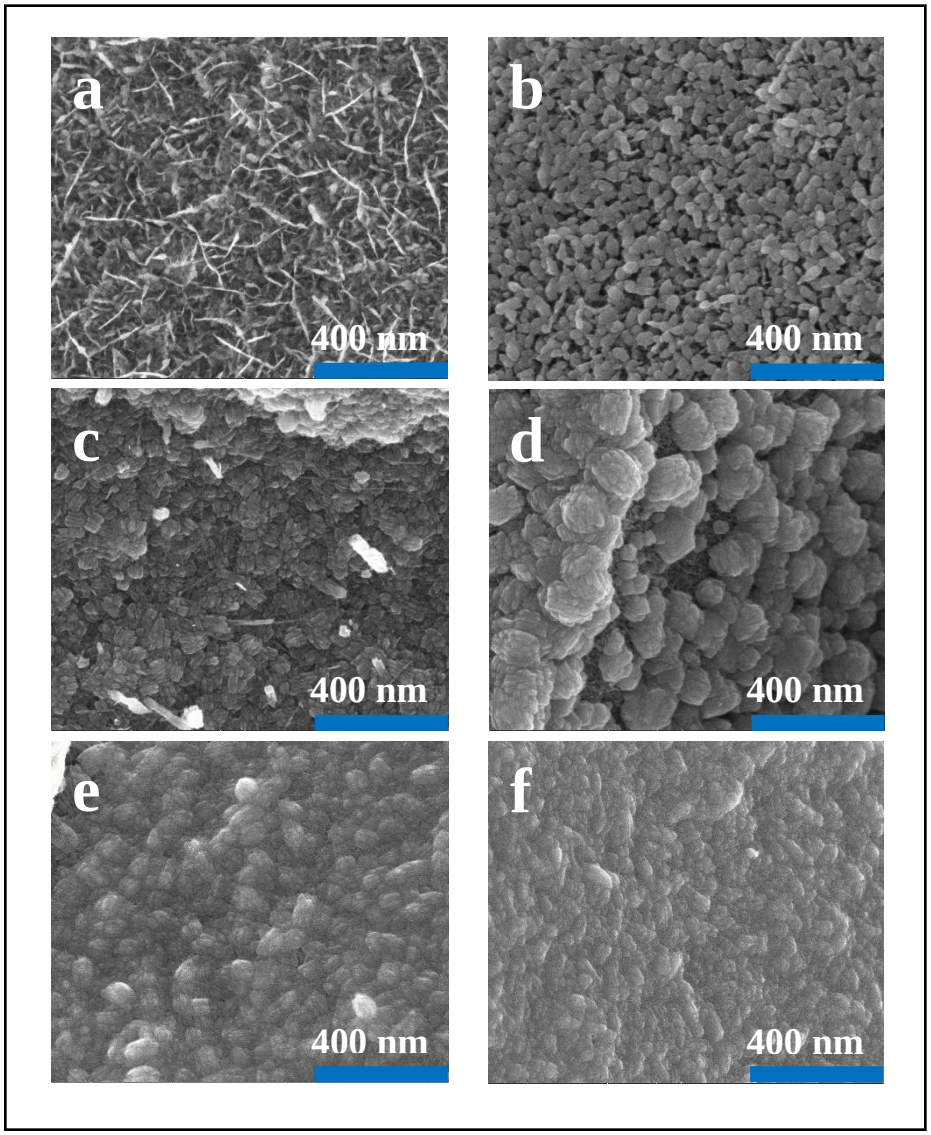

Figure 5.3 SEM images of the GF-Mn_xO_y electrodes synthesized using different electrodeposition conditions and protocols: a) L-200 C, b) L-200 C, c, c) H-200 C, d) H-200 C, c, e) H-1000 C, and f) H-1000 C, c.

5.3.2. Catalytic activity of GF-Mn_xO_y electrodes towards sulfide oxidation

First, catalytic activity of each synthesized material was evaluated in the OC experiments. All electrode materials synthesized demonstrated remarkable catalytic activity of the Mn_xO_y coating towards HS^- oxidation even without applying the potential. More than 80% sulfide removal was achieved within two hours, while no sulfide removal was observed when the pristine GF was used in the OC experiments (**Figure 5.4**). The main final product of the HS^- oxidation was elemental sulfur, with more than 85% yield of S^0. The presence of low concentrations of dissolved sulfur species such as thiosulfate and sulfate was also detected (up to 15% of the initial sulfide concentration). Elemental sulfur produced by the catalytic oxidation by Mn_xO_y coating remained at the electrode surface, as was confirmed by the SEM images, and the EDX (**Figure 5.5**) and XPS analyses.

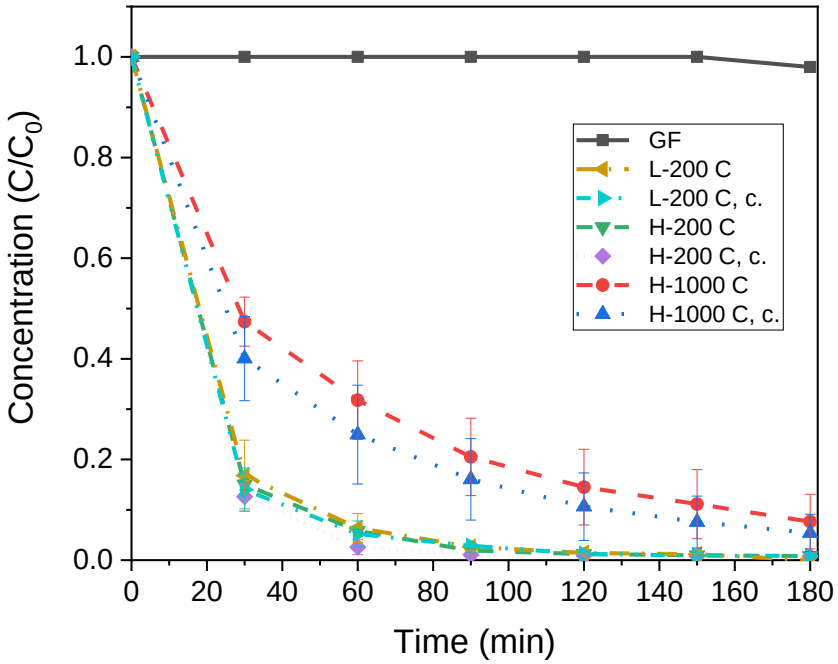

Figure 5.4 The concentrations of sulfide (C) normalized to the initial value (C_0) in the OC experiments using the GF and GF-Mn_xO_y electrodes.

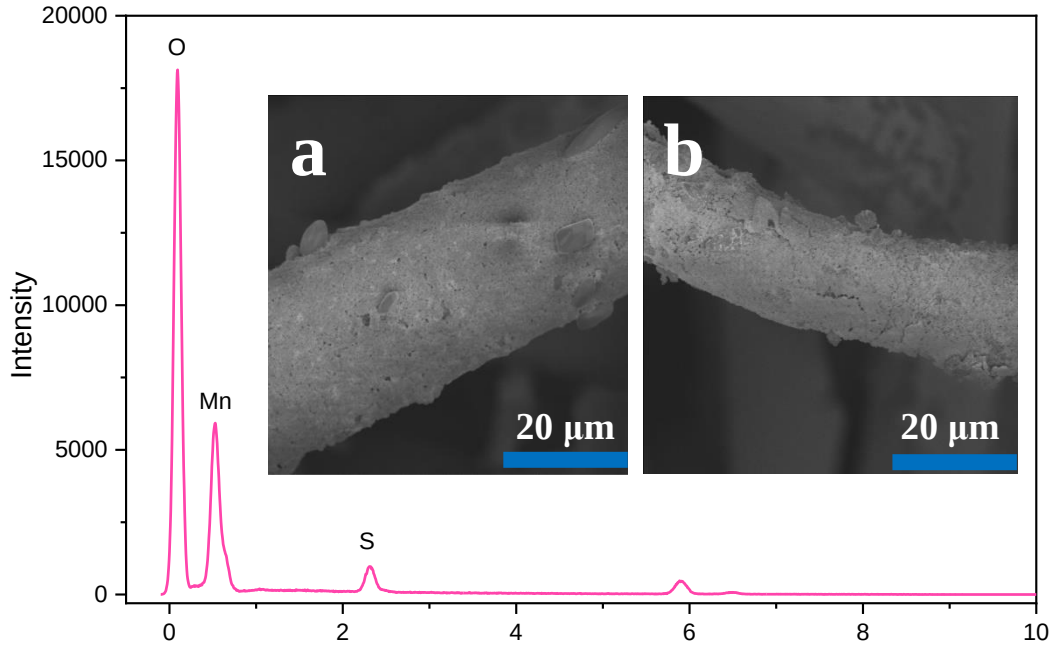

Figure 5.5 The EDX spectra and SEM images of the GF-Mn_xO_y electrodes synthesized using 0.2 M $MnSO_4$, charge loading of 200 C, and calcinated at 500ºC used for sulfide removal in the: a) OC experiments, and b) at 0.4 V/SHE .

The catalytic reaction between sulfide and manganese oxides starts with the HS^- adsorption onto the catalyst surface. Adsorption is followed by the formation of a surface complex (Equation 5.3) and its subsequent oxidation at the surface (Equation 4.4, 4.5) [349]. The electron transfer from Mn(IV) to sulfide occurs in two consecutive steps and involves the formation of the Mn(III) surface complex as a reaction intermediate:

$$Mn(IV)O_2 + HS^- + 4H^+ \leftrightarrow Mn(IV)S^- + 2H_2O \quad \text{(Eq. 5.3)}$$

$$Mn(IV)S^- \rightarrow Mn(III)S \quad \text{(Eq. 5.4)}$$

$$Mn(III)S + e^- \rightarrow Mn(II)S \quad \text{(Eq. 5.5)}$$

$$Mn(II)S \rightarrow Mn(II) + S^0 \quad \text{(Eq. 5.6)}$$

Being the intermediate, Mn(III) itself is capable of rapid catalytic oxidation of sulfide [350]. Even though the initial valence state of the Mn_xO_y catalyst had almost no effect on the sulfide removal, the kinetics of the process for the calcinated samples were slightly faster due to the more crystalline coating (Table 5.2).

Table 5.2 The first-order sulfide removal rate constant (h^{-1}) at the GF-Mn_xO_y electrodes obtained at different calcination temperatures in the OC experiment.

Calcination temperature, ^oC	**First order removal rate constant, h^{-1}**
0	1.83±0.14
300	1.92±0.11
400	1.87±0.27
500	1.89±0.01

The materials synthesized at high and low precursor concentrations (i.e., 0.2 M and 0.02 M $MnSO_4$) showed similar performance in terms of the sulfide removal rates (i.e., 1.83 ± 0.14 h^{-1} and 1.74 ± 0.1 h^{-1}, respectively). The increased charge loading significantly deteriorated the removal rates of sulfide (**Figure 5.4**). When the charge was increased from 200 C to 1000 C, the sulfide removal rate decreased from 1.83 ± 0.14 h^{-1} to 0.63 ± 0.2 h^{-1} (**Figure 5.4**). The performance of each synthesized material greatly depends on the active surface area of the Mn_xO_y coating. Even though the active surface area of the synthesized GF-Mn_xO_y electrodes could not be measured due the fibrous nature of the substrate, it decreases over the electrodeposition process with the nuclei growth, due to the evening out of the surface and less relief in its structure. Therefore, such Mn_xO_y films demonstrate worse performance as they lose active sites available for sulfide oxidation.

Table 5.3 The total dissolved manganese detected after the GF-Mn_xO_y electrode (H-200 C, c.), after 0, 3 and 6 h of (electro)catalytic sulfide oxidation at 0.4 V/SHE, and cathodic recovery at 0.8 V/SHE.

Time, h	Total dissolved Mn, mg L^{-1}	
	at 0.4 V	at -0.8 V
0	0.07	0.04
3	0.1	0.165
6	0.005	0.7

Prior to the application of the GF-Mn_xO_y electrode for electrochemical sulfide oxidation at 0.4 V/SHE, its stability under anodic polarization was verified by performing the experiments at 0.4 V/SHE, while measuring the total dissolved manganese (Table 5.3). The obtained values after 3 and 6 h of anodic polarization showed that there was no release of manganese ions into the electrolyte, thus the stability of the synthesized electrode was confirmed. As can be seen from **Figure 5.6**, the presence of the Mn_xO_y coating yielded an eight-fold higher sulfide removal rate compared to the GF (i.e., 1.83 ± 0.14 h^{-1} for GF-Mn_xO_y and 0.23 ± 0.12 h^{-1} for GF). However, in comparison with the OC experiments performed at the GF-Mn_xO_y electrode, application of potential did not have any significant effect on the HS^- removal rate or the final products of the reaction. As was demonstrated by the XPS, increase of the Mn 3s doublet peak separation of the GF-Mn_xO_y electrodes applied for sulfide removal in the OC indicates the reduction of the catalytic coating from Mn(III) to Mn(II). Mn reduction also occurred when the HS^- removal was performed at 0.4 V/SHE, yet, partial recovery of the catalytic coating was achieved as both Mn(II) and Mn(III) were detected by the XPS analyses (Table 5.4). Therefore, when potential is applied, catalytic HS^- oxidation occurs simultaneously with the oxidation of the reduced Mn-oxide catalytic coating, which can be highly beneficial for the long-term application of such material.

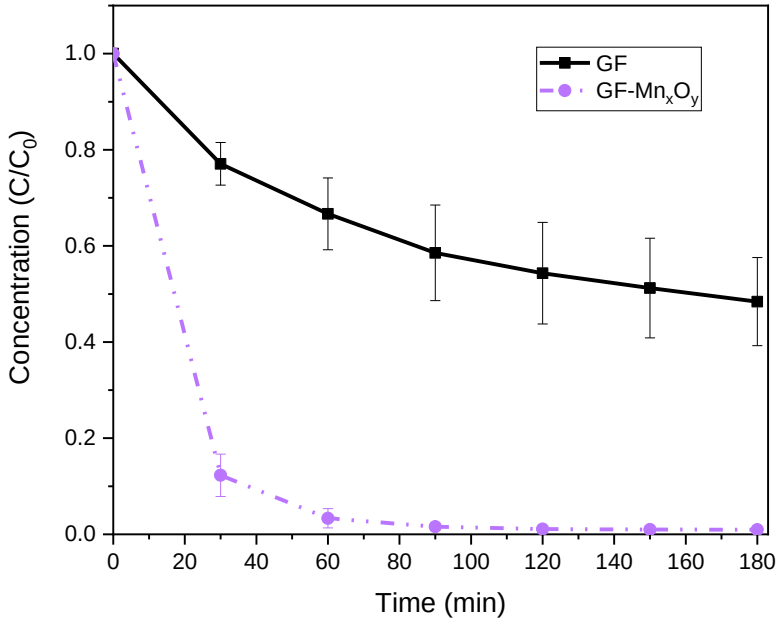

Figure 5.6 HS^- removal rate at 0.4 V/SHE applied to the GF and GF-Mn_2O_3 electrode. The GF-Mn_2O_3 electrode was synthesized using 0.2 M $MnSO_4$, charge loading of 200ºC, and calcinated at 500ºC.

Table 5.4 The XPS peak analysis of the GF-Mn_xO_y electrode (0.2 M $MnSO_4$, 200 C, calcination at 500ºC) as synthesized, GF-Mn_xO_y electrode used in the OC experiment and GF-Mn_xO_y electrode used for electrochemical removal of sulfide at 0.4 V/SHE, both performed in 2.7 mM HS^- and 2.6 mM $NaNO_3$ electrolyte, at pH 8-8.2. The deconvoluted data is shown for the Mn 2p3/2 and Mn 3s spectra.

Sample	Mn 2p$_{3/2}$, E_b, eV	Mn 3s			Valence number of Mn
		E_b (1), eV	E_b (2), eV	ΔE, eV	
pristine	641.7	89	83.8	5.2	3
after OC	641.9	89.3	83.5	5.8	2
after EC	641.7	89	83.6	5.4	2, 3

5.3.3. Repeated application of the GF-Mn_2O_3 electrodes for sulfide removal and sulfur recovery

Repeated application of the GF-Mn_2O_3 electrode (0.2 M $MnSO_4$, 200 C, c) in the OC experiment and at 0.4 V/SHE was performed to investigate the impact of the anodic potential application on the sulfide removal process (**Figure 5.7**). As can be seen from **Figure 5.7 a**, the first order sulfide removal rate in the OC experiments was drastically decreased in each subsequent cycle, from 2.42 ± 0.05 h^{-1} in the first cycle to 0.39 ± 0.02 h^{-1} in the sixth cycle. The performance was partly lost due to the reduction of the catalytically active Mn(III) to Mn(II) and its subsequent release into electrolyte as Mn^{2+}. This loss of the catalyst can be counteracted by the application of low anodic potential, which oxidizes Mn(II) back to Mn(III). Indeed, when the experiments were performed at 0.4 V/SHE, the performance of the GF-Mn_2O_3 electrode was improved as compared with the OC experiment (i.e., 0.39 ± 0.02 h^{-1} and 0.65 ± 0.03 h^{-1} in the sixth cycle in the OC and at 0.4 V, respectively). Significant decrease in the first order removal rate occurred after the fourth application both with and without the applied potential (i.e., 2.42 ± 0.05 h^{-1} in the first cycle to 1.57 ± 0.01 h^{-1} in the fourth cycle), due to the electrode passivation with the electrodeposited elemental sulfur.

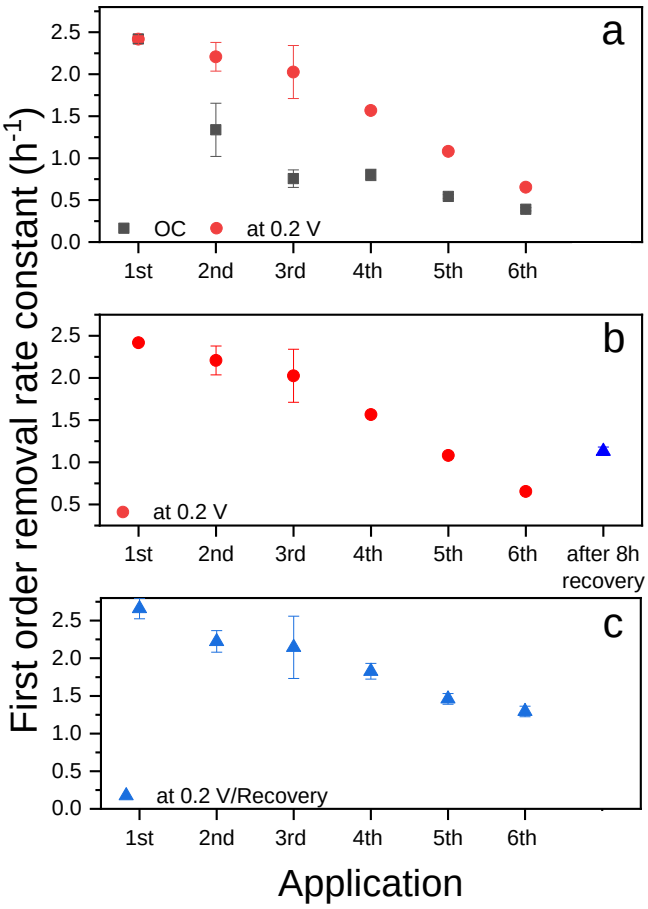

Figure 5.7 The observed first-order sulfide removal rate constant (h^{-1}) at the GF-Mn_2O_3 electrodes (H-200 C, c): a) in the OC experiment and at +0.4 V/SHE of applied anode potential in six subsequent cycles, b) at +0.4 V/SHE in the repeated application with the last cycle preceded by the 8 hours of cathodic recovery at -0.8 V/SHE, c) at +0.4 V/SHE in six subsequent application cycles, when each cycle was followed by 2 h of THE cathodic recovery at -0.8 V/SHE.

Gradual decrease in the electrode performance is a common problem reported by many studies focused on the direct electrochemical oxidation of HS^- [303, 351, 352]. The final product, elemental sulfur, has high electrical resistance (1017 Ω cm^{-1}) [171], and its formation at the electrode surface limits the electron transfer and passivates the electrode. Electrodeposited elemental sulfur also imposes mass transfer limitations, which further aggravates the performance. Therefore, electrochemical sulfide oxidation and separation from the wastewater needs to be coupled with an appropriate strategy for the elemental sulfur recovery. Several studies successfully

applied cathodic polarization for electrochemical dissolution of sulfur and its recovery in the form of sulfide [253, 351]. The recovery was performed at -0.8 V/SHE to enable the reduction of elemental sulfur. Cathodic recovery was performed at potential below the hydrogen evolution potential, to achieve higher coulombic efficiency and minimize any potential damage to the electrode coating. GF-Mn_2O_3, loaded with the elemental sulfur prior to the recovery, was polarized at -0.8 V/SHE for 8 hours and the concentration of HS^- and other dissolved sulfur species was measured. The concentration of HS^- increased linearly over time (i.e., from 0 mM to 1.73±0.01 mM after 8 hours) confirming the possibility of the cathodic sulfur recovery (**Figure 5.9**). In addition to this, the gradual buildup of the yellow color, typical for polysulfide solution, was observed (**Figure 5.8**). Given the difficulties associated with the polysulfide determination, the recovery efficiency could not be calculated only based on the measured concentrations of HS^-. When the recovered material was applied again for the HS^- removal, the sulfide removal rate was partly restored, increasing from 0.65 ± 0.03 h^{-1} to 1.1 ± 0.035 h^{-1}. The initial sulfide removal rate of 2.42 ± 0.05 h^{-1} could not be achieved due to the partial loss of the Mn_2O_3 coating (**Figure 5.7 b**). As was shown by the GF-Mn_2O_3 electrode stability tests, performed at -0.8 V/SHE in the 9 mM $NaNO_3$ supporting electrolyte, the increase of the total dissolved manganese occurred after 3 h of polarization. Even though the measured concentration of manganese represents ≤1% of the total Mn_2O_3 deposited, the duration of the recovery cycles was limited to 2 h to ensure the stability of the GF-Mn_2O_3 electrode.

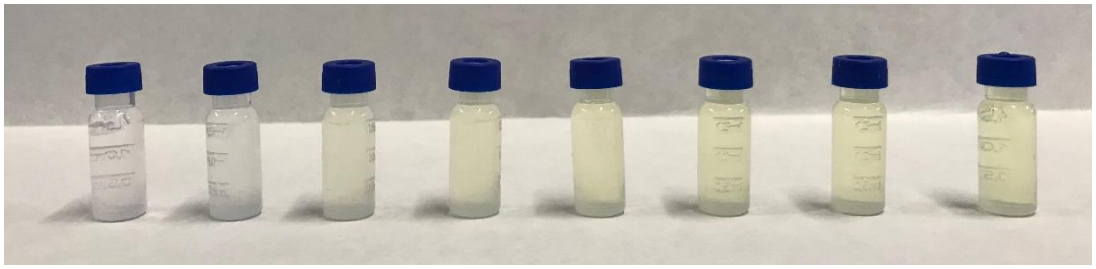

Figure 5.8 Gradual evolution of the yellow color in the electrolyte, used for the recovery of sulfur loaded GF-Mn_2O_3 electrode (H-200 C, c.) by cathodic polarization at -0.8 V/SHE, indicating the increase of polysulfide concentration.

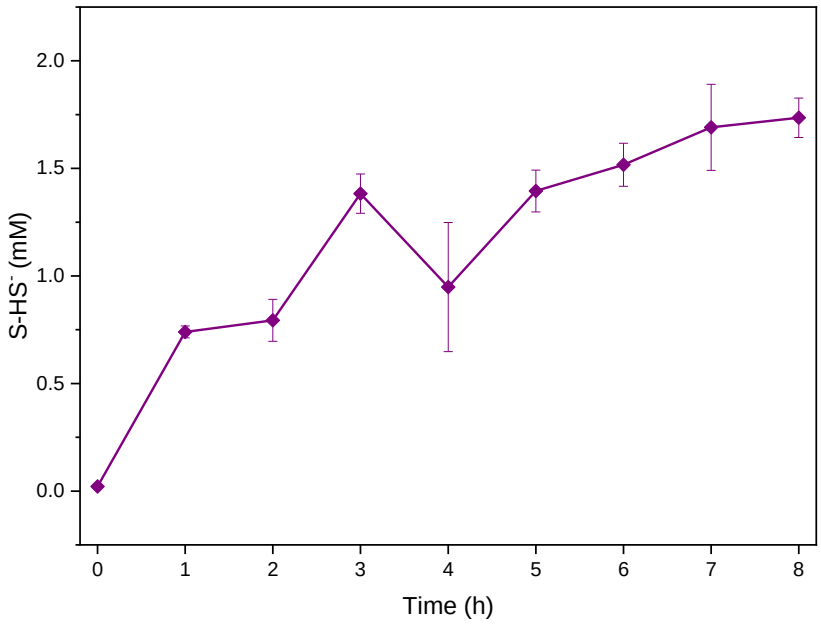

Figure 5.9 The concentration of sulfide released in the recovery cycle of the sulfur-saturated GF-Mn_2O_3 electrode (H-200 C, c.) performed for 8 hours at -0.8 V/SHE.

To investigate the impact of the cathodic recovery on the GF-Mn_2O_3 electrode performance over several cycles, each application for sulfide removal at 0.4 V/SHE was followed by a 2 h recovery cycle at -0.8 V/SHE (**Figure 5.7 c**). The concentration of sulfide released from the electrode in each recovery step was continuously increasing, from 0.042 ± 0.006 mM in the first cycle to 0.92 ± 0.1 mM in the fifth cycle, indicating a gradual saturation of the GF-Mn_2O_3 electrode with the elemental sulfur (**Figure 5.10**) However, as can be seen from **Figure 5.7 c**, even partial recovery had a positive impact on the system performance, yielding higher sulfide removal rates compared with the cycles performed without the recovery (e.g., 1.29 ± 0.07 and 0.65 ± 0.03 h^{-1}, respectively). In addition, these results demonstrate that the shifts between the Mn valence states that could occur under cathodic polarization could be reversed back when the positive potential was applied, as the HS^- removal rates with and without the recovery are comparable during the first cycles of application.

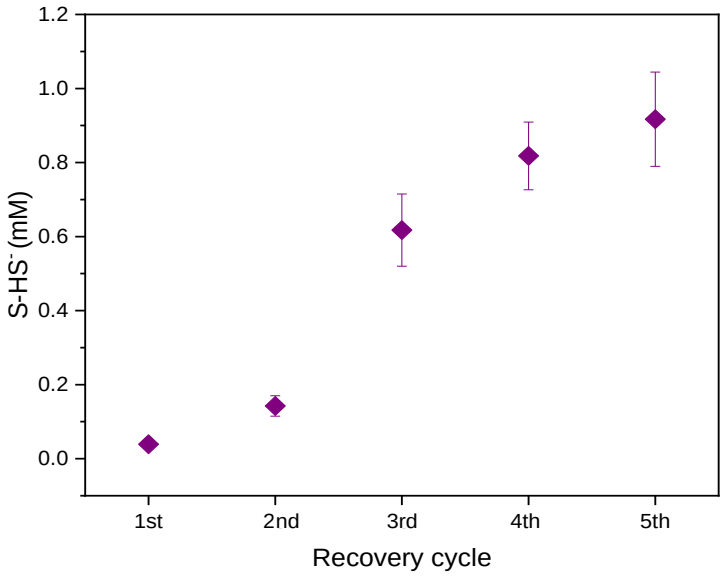

Figure 5.10 Sulfide concentration, released in each recovery cycle of the GF-Mn_2O_3 electrode (H-200 C, c.) performed for 2 hours at -0.8 V/SHE.

5.3.4. Electro-catalytic sulfide removal in real sewage

Sulfide removal rates observed in the experiments with real sewage (0.94 ± 0.13 h^{-1}) were significantly lower compared to the experiments performed in the supporting $NaNO_3$ electrolyte (2.42 ± 0.02 h^{-1}). As was previously mentioned, Mn_yO_x is an excellent catalyst, that is active for different oxidation and reduction reactions, which means that other compounds can interfere and compete with the sulfide ions for active sites. For instance, COD was decreased from 500 mg L^{-1} to 420 mg L^{-1} during 2 h, indicating the oxidation of the organic contaminants.

The selectivity of the process was maintained, as elemental sulfur was the major final product of the treatment. However, its deposition at the surface was partial in the case of real sewage, unlike the case with the supporting electrolyte. Part of the S^0 intermediate, produced at the electrode surface as a result of the sulfide oxidation reaction, can desorb and undergo complexation to S_8 in the bulk of the electrolyte. The complexation to S_8, that took place directly at the surface in the $NaNO_3$ electrolyte, is the reaction controlled by the diffusion rate of sulfide to the electrode surface [349]. Taking into account the presence of other ions such as PO_4^{3-}, which is known for its ability to block the Mn_xO_y active sites, sulfide diffusion towards the electrode was likely impeded [291]. Therefore, part of the S^0 intermediate, being rather unstable, was released into the electrolyte. The desorption of the S^0 intermediate was only partial, as in the recovery cycle gradual increase of sulfide concentration was still observed (i.e., from 0 to 0.2 ± 0.08 mM), indicating the presence of the deposited sulfur. Lower concentration of sulfide released in the recovery cycle compared to the electrode saturated in the $NaNO_3$ electrolyte (0.2 ± 0.08 mM and 0.97 ± 0.12 mM), further confirms that less elemental sulfur was deposited.

As in the case of the $NaNO_3$ electrolyte, sulfide removal from real sewage using GF-Mn_2O_3 electrode was performed over six subsequent cycles, with 2 h cathodic recovery applied in between cycles (**Figure 5.11**). Sulfide removal rate did not change significantly with each cycle (i.e., 0.94 ± 0.13 h^{-1} in the first cycle to 0.82 ± 0.08 h^{-1} in the sixth cycle), unlike when $NaNO_3$ supporting electrolyte was used (**Figure 5.7**). This can be explained by a lower extent of the electrode passivation with elemental sulfur, that occurred due to the partial desorption of the S^0 intermediate. Although the selectivity of the process was partially lost due to the production of colloidal sulfur, it can be recovered by working in the flowthrough mode, thus avoiding diffusion limitations and improving the sulfide mass transfer towards the electrode surface.

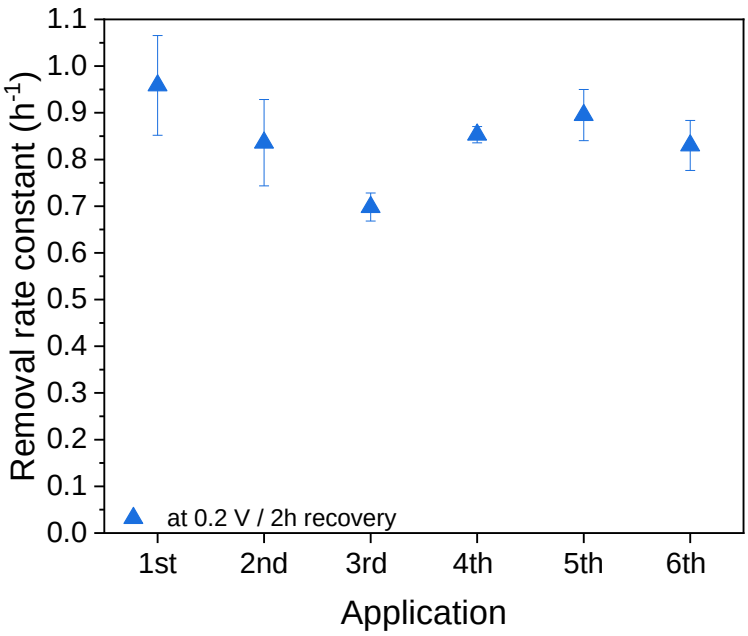

Figure 5.11 Observed first-order sulfide removal rate constant (h^{-1}) at GF-Mn_2O_3 electrodes applied over six subsequent cycles using real sewage.

5.4. Conclusion

Excellent (electro)catalytic activity of the GF-Mn_xO_y yielded drastic increase in sulfide removal rates compared to the pristine GF (i.e., 6 10^{-4} m^3 h^{-1} m^{-2} vs 9.2 10^{-4} m^3 h^{-1} m^{-2} for GF and GF-Mn_xO_y, respectively). Activity of GF-Mn_xO_y electrode, synthesized via electrodeposition pathway, was directly related to the active surface area of material. Since higher MnOx loading decreases active surface area of a material, such materials demonstrated poor performance in terms of hydrogen sulfide removal. Slightly faster sulfide oxidation rate observed at calcinated GF-Mn_xO_y samples was attributed to the enhanced crystallinity of the coating after thermal treatment rather than to the difference in the initial valence state of the catalyst (i.e., Mn(IV) for non-calcinated and Mn(III) for calcinated).

Although anodic polarization at 0.4 V/SHE did not further enhance the sulfide oxidation rate compared to the OC, it enabled a continuous re-oxidation of the reduced Mn_xO_y coating after its reaction with sulfide. The formed elemental sulfur remained at the surface of the GF-Mn_xO_y electrode, leading to a gradual electrode passivation. The deposited sulfur was successfully dissolved by reversing the polarity of the GF-Mn_xO_y electrode to -0.8 V/SHE. However, complete electrode recovery and restoring of the initial sulfide removal rates could not be achieved as prolonged (>3 h) cathodic polarization at -0.8 V/SHE required to remove S^0 also caused a partial dissolution of the Mn_xO_y coating. (Electro)catalytic sulfide removal was somewhat decreased in the case of real sewage. The selectivity of the process towards the deposition of the elemental sulfur was decreased in real sewage due to partial production of colloidal sulfur, which was presumably caused by the diffusion limitations imposed by the presence of other ions. Though the proposed approach demonstrated a promising potential in sulfide control, its further upscaling and application for the treatment of complex wastewater streams requires further efforts to ensure the

electrode stability, to minimize the electrode passivation and allow the recovery of elemental sulfur.

Chapter 6. (Electro)catalytic oxidation of sulfide to colloidal sulfur over manganese oxide coated electrode with TiO_2 nanotubes interlayer

6.1. Background

In order to improve the conductivity of GF substrate and to address the problem of sulfur passivation, in this study the Mn_xO_y coating was deposited on the Ti plate anode with the TiO_2 NTA interlayer. We determined the impact of the operating parameters (i.e., applied potential, pH, sulfide concentration) on the sulfide removal kinetics and the formed reaction products. Furthermore, sulfide oxidation at the synthesized TiO_2 NTA-Mn_xO_y electrodes was investigated in the realistic conditions by performing tests with real sewage.

6.2. Material and methods

6.2.1 Synthesis of the Ti/TiO_2 NTA substrate

4 × 4 cm Ti plates (1 mm, 99.6% purity, Advent Research Materials, U.K.) were mechanically polished until mirror finish. Polished materials were then degreased by sonication in isopropanol, acetone and methanol, rinsed with deionized water and dried in a nitrogen stream. Prior to the anodization, titanium plates were etched in 17% w/w HCl aqueous solution (Scharlab, Spain) at 75^{o}C for 15 min to obtain fresh metal surface for the nanotubes growth. Next, the Ti plates were anodized in a mixture of glycerol and deionized water (50:50 vol.%) with 0.5 wt.% NH_4F, using a two electrode cell configuration and stainless steel mesh as the counter electrode. The potential of the cell was controlled with Autolab 302N potentiostat/galvanostat equipped with the voltage amplifier (Metrohm Autolab B.V., The Netherlands). The anodization procedure included ramping of the potential from the open circuit (OC) to 20 V and maintaining the potential at 20 V during 2

h. After the treatment, the NTA samples were soaked in the deionized water and calcinated in argon at 400°C for 2 h using a tubular oven (Nabertherm, Germany).

6.2.2. Electrodeposition of the Mn_xO_y coating

The Ti/TiO_2 NTA-Mn_xO_y electrodes were synthesized using anodic electrodeposition in a three-electrode setup at ambient temperature (i.e., 24 ± 1°C), using stainless steel mesh as counter and Ag/AgCl (KCl 3M, Bioanalytical systems, the Netherlands) as reference electrode. The electrodeposition medium contained 0.1 M $MnSO_4$, and two different acid concentrations, 0.05 and 0.5 M H_2SO_4, to investigate the influence of the acid concentration on the Mn_xO_y coating characteristics. The electrodeposition was performed in the potentiostatic mode at 1.7 V/SHE (vs Standard Hydrogen Electrode). All the potentials reported in this work are expressed vs SHE and calculated according to Nernst's equation. To ensure the reproducibility of each deposition, the mass of the manganese oxide loading was calculated according to Faraday's law and the charge was limited to 13 C. To investigate the effect of the temperature treatment on the Mn_xO_y coating, some Ti/TiO_2 NTA-Mn_xO_y samples were also calcinated at 500°C in air for 1 h in a tubular oven (Nabertherm, Germany).

6.2.3. Electrochemical removal of sulfide using Ti/TiO_2 NTA- Mn_xO_y electrode

Electrochemical experiments were carried out in a non-divided glass cell (100 mL) with an air-tight seal. The synthesized Ti/TiO_2 NTA-Mn_xO_y electrode was used as an anode, Ag/AgCl (3M KCl) as reference electrode and Ti mesh (DeNora, Italy) as a counter electrode. Electrochemical cells were sealed, and the headspace was under gentle nitrogen purge during the experiments to prevent the intrusion of oxygen and thus loss of sulfide to its oxidation to sulfate. The impact of potential on the sulfide removal was investigated by performing the experiments in the OC and at

0.4 V, 0.6 V or 0.8 V/SHE using a deoxygenated 2.9 mM $NaNO_3$ as supporting electrolyte, with 2 mM Na_2S at pH 12. The diluted supporting electrolyte solution (3.2 mS cm^{-1}) was purposely selected to simulate the conductivity of the real sewage (0.9 – 9 mS cm^{-1}) [309], as low ionic conductivity of real contaminated water is a limiting factor in electrochemical treatment systems. The impact of the initial sulfide concentration on the reaction kinetics was evaluated at 0.8 V/SHE by amending the supporting electrolyte with 0.9 mM, 2 mM or 3.2 mM of sulfide. All of the above-mentioned experiments were performed at the initial pH 12. To investigate the impact of pH, experiments were performed at the initial pH 8 in 2.6 mM $NaNO_3$ and 2 mM of Na_2S. As previously reported, lower initial pH of the solution has a minor effect on the reaction rate of sulfide oxidation with manganese oxides as it is typically followed by the rapid pH increase [294]. Therefore, determination of the pH impact on the oxidation rate required continuous addition of 0.1 M HNO_3 acid to the electrolyte. To investigate the performance of the Ti/TiO_2 NTA-Mn_xO_y electrodes for sulfide removal under realistic conditions, experiments were performed with real sewage that was deoxygenated and amended with 2 mM of sulfide. The conductivity of the sampled sewage was identical to the supporting electrolyte used in the experiments (i.e., 3.2 mS cm^{-1}). All experiments were performed in duplicate, and values are expressed as mean with their standard errors. Surface characterisation of electrode materials and sample analysis are described in the Chapter 3.

6.3. Results and discussion

6.3.1. Characterization of Ti/TiO_2 NTA-Mn_xO_y electrodes

The anodization method employed resulted in uniform and well-aligned aligned TiO_2 NTAs, with outer average diameters of 80–100 nm, wall thickness of 7 – 10 nm and the average length of about 1 μm (**Figure 6.1**)**.** The cross-section of the TiO_2 NTA substrate after the coating with Mn_xO_y (**Figure 6.1 a**) shows that anodic electrodeposition does not lead to any visible change in NTA morphology. The XRD patterns demonstrate that the NTA interlayer consists of pure tetragonal anatase phase, which is typically observed at the TiO_2 NTA after calcination at 400 ^oC **(Figure 6.2)** [353]. The diffraction peaks of the NTA-Mn_xO_y have a similar position compared to the non-coated NTAs, which further confirms that the TiO_2 NTA structure was not affected by the electrodeposition process. Though demonstrating strong signal typical for Ti and TiO_2, the XRD spectra of the coated samples both with and without calcination showed no peaks characteristic for the Mn_xO_y crystalline phase. The absence of the Mn_xO_y signal in the XRD patterns was likely caused by overlapping of the substrate and the Mn_xO_y peaks or by insufficient crystallinity of the Mn_xO_y coating [354]. The presence of Mn_xO_y was confirmed by the XPS analysis, as explained further in the text.

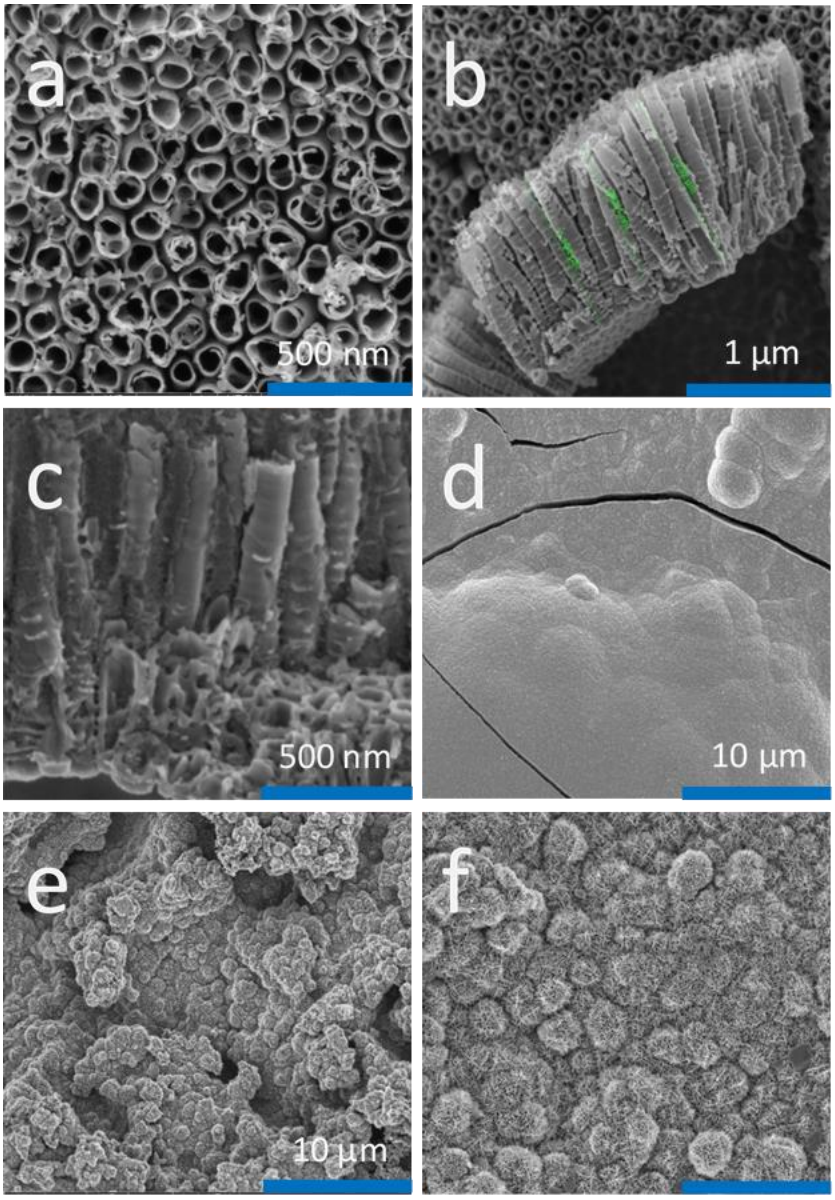

Figure 6.1 The SEM images of the: a) top view of the TiO_2 NTA, b) cross section of the TiO_2 NTA, c) cross section of the TiO_2 NTA filled with the Mn_xO_y; top view of the TiO_2 NTA coated with the Mn_xO_y using precursor solution containing d) 0.1 M $MnSO_4$ and 0.05 M H_2SO_4, e) 0.1 M $MnSO_4$ and 0.5 M H_2SO_4, f) 0.1 M $MnSO_4$ and 0.5 M H_2SO_4 followed by the calcination at 500 ^oC.

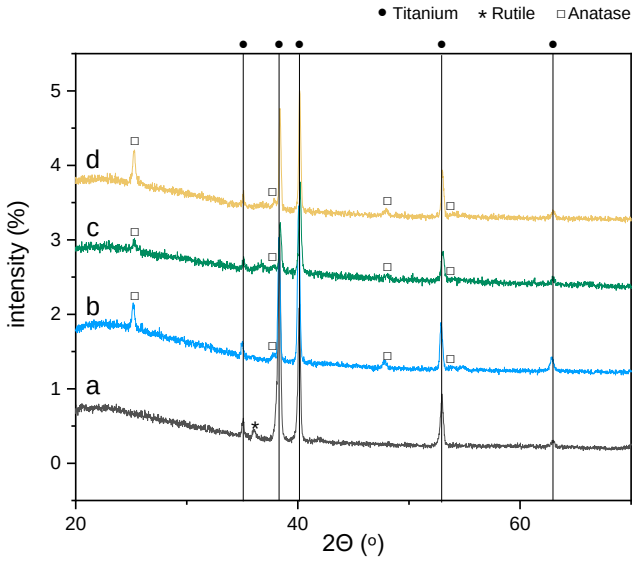

Figure 6.2 The XRD patterns of the: a) Ti plate, b) Ti plate with TiO_2 NTA interlayer, c) TiO_2 NTA coated with THE Mn_xO_y in the presence of 0.5 M H_2SO_4, d) TiO_2 NTA coated with THE Mn_xO_y under high acid concentration (e.g 0.5 M H_2SO_4), followed by the calcination step.

The anodic electrodeposition results in the penetration of Mn_xO_y inside the NTAs (**Figure 6.1 c**), followed by the formation of a uniform Mn_xO_y layer with the approximate thickness of 100 nm on the top of the NTAs. The top view of the Mn_xO_y coatings synthesized at 0.05 M and 0.5 M H_2SO_4 concentration reveals visibly distinct Mn_xO_y morphology. Lower acidity of the precursor solution yields smooth Mn_xO_y coating **(Figure 6.1 d)**, while high acid concentration leads to formation of the coating with rod-like morphology (**Figure 6.1 e**). Shaker et al previously demonstrated that pH is the crucial parameter that can affect the structure, composition, and the morphology of the electrodeposited Mn_xO_y coating [355]. The difference in the pH of the deposition baths (e.g., pH 1.5 for 0.05 M H_2SO_4 and pH 0.5 for 0.5 M H_2SO_4) had a significant effect on the Mn_xO_y coating morphology, as strongly acidic solution enhance the dissolution rate of the Mn_xO_y and lead to the formation of a thinner coating with rod-like morphology [356]. The morphological difference of

the two coatings may also result from the higher ionic conductivity of the strongly acidic bath (i.e., 179.3 mS cm^{-1} for 0.5 M H_2SO_4, vs 24.5 mS cm^{-1} for 0.05 M H_2SO_4), which leads to higher current during the anodic deposition of the Mn_xO_y, and thus significantly reduced deposition time (i.e., 42 s) compared to the less acidic bath (i.e., 74 s) (**Figure 6.3**). As was demonstrated in our previous study [357], prolonged electrodeposition leads to the smoother Mn_xO_y coating surface as nanorods, formed upon initial nucleation, continue to grow in all directions and finally merge into adjacent growth centres. The smooth Mn_xO_y coating is typically characterized by the low specific surface area due to the lack of relief in its structure. In addition to the electrodeposition bath acidity, subsequent calcination of the Ti/TiO_2 NTA-Mn_xO_y had a significant impact on the material morphology, transforming the nanorods into needle like structures with more compact grains (**Figure 6.1 f**).

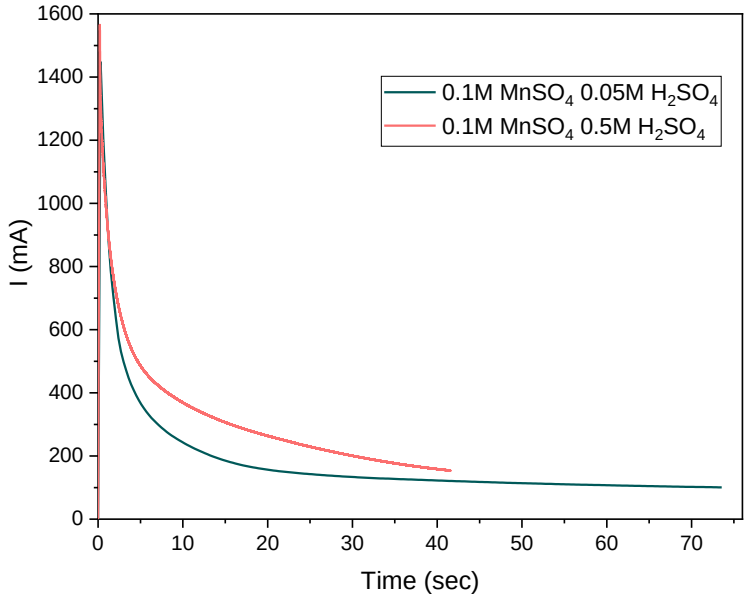

Figure 6.3 Chronoamperometries obtained during the Mn_xO_y coating procedure performed in the electrolyte containing 0.1 M $MnSO_4$ and 0.05 M H_2SO_4 or 0.5 M H_2SO_4.

The composition of the Mn_xO_y coating was investigated using the XPS analysis. The Mn 3s doublet peak separation was used to determine the Mn valence, since this method was reported to be more reliable compared to the one based on the location of the Mn 2p peaks only [342]. Different Mn 3s doublet peak splitting values were previously reported in the literature, including 4.5, 5.2, 5.4, and 5.8 eV for MnO_2 (Mn I), Mn_2O_3 (Mn III), Mn_3O_4 (Mn II, Mn III), and MnO (Mn II), respectively [342, 344, 345]. The doublet peak separation values reported in Table 1 for the non-calcinated samples is typical for MnO_2 (Mn IV). This valence state is common for the Mn_xO_y coatings synthesized via the anodic electrodeposition pathway in strong acidic media, that occurs through the following reaction [346]:

$$Mn^{2+} + 4OH^- \rightarrow MnO_2 + 2H_2O + 2e^- \quad \text{(Eq. 6.1)}$$

The doublet peak separation in the samples subjected to the calcination widened, which indicates the conversion of MnO_2 (Mn(IV)) into Mn_2O_3 (Mn(III)) **(Table 6.1)**. This phase transformation was reported to occur at 500ºC because of the desorption of the lattice oxygen and thermal decomposition according to the following pathway [343, 347]:

$$4\ MnO_2 \rightarrow 2Mn_2O_3 + O_2 \quad \text{(Eq. 6.2)}$$

The impact of the NTA interlayer on the Mn_xO_y coating morphology or composition could not be investigated because the Mn_xO_y coating could not be deposited on a plane Ti plate in any of the investigated deposition conditions. Linear sweep voltammetry performed at the TiO_2 NTA indicates the clear peak at 1.7 V/SHE, which was attributed to the Mn^{2+} oxidation to MnO_2, while bare Ti plate yields very low current with absence of any distinguishable peaks **(Figure 6.4)**. As can be seen from **Figure 6.5**, the resistance of the Ti plate is significantly higher compared to the anodized substrate with the TiO_2 NTAs. Therefore, limited charge transfer at the bare Ti substrate

obstructed the nucleation and subsequent formation of the Mn_xO_y coating, which was only possible when the TiO_2 NTA interlayer was present.

Table 6.1 XPS peak analyses of TiO_2 NTA-Mn_xO_y electrodes obtained using different acid concentrations (e.g 0.5 M and 0.05 M H_2SO_4) in the precursor solution as well as material calcinated at 500 °C after the synthesis. The deconvoluted data are shown for the Mn $2p_{3/2}$ and Mn 3s spectra.

Sample name	Mn $2p_{3/2}$, E_b, eV	Mn3s			Valence number of Mn
		E_b (1), eV	E_b (2), eV	ΔE, eV	
0.05 M H_2SO_4	642.1	88.9	84.2	4.7	4
0.5 M H_2SO_4	642.1	88.9	84.2	4.7	4
0.5 M H_2SO_4, c.	642	89.1	83.9	5.2	3

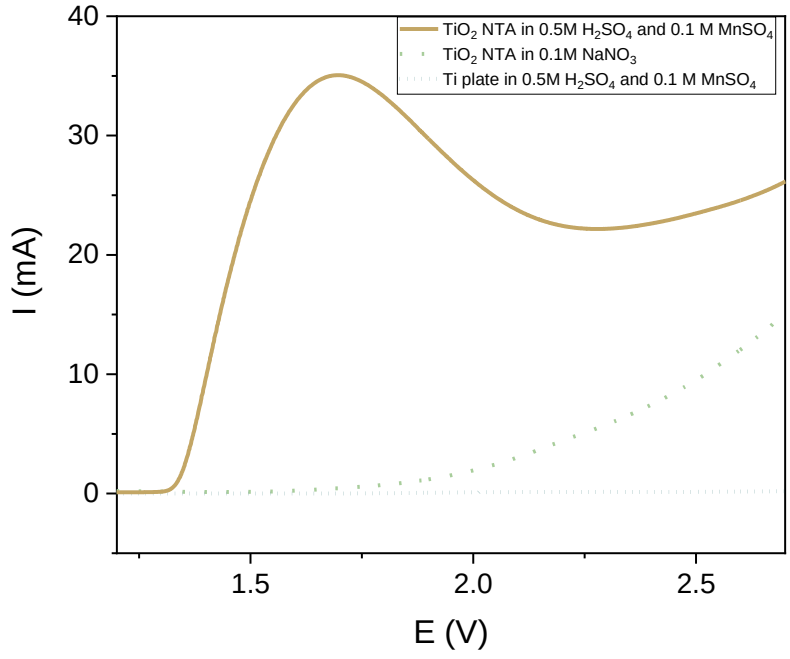

Figure 6.4 Linear sweep voltammograms performed using TiO_2 NTA in 0.5 M H_2SO_4 and 0.1 M $MnSO_4$ or 0.1 M $NaNO_3$ and Ti plate in 0.5 M H_2SO_4 and 0.1 M $MnSO_4$.

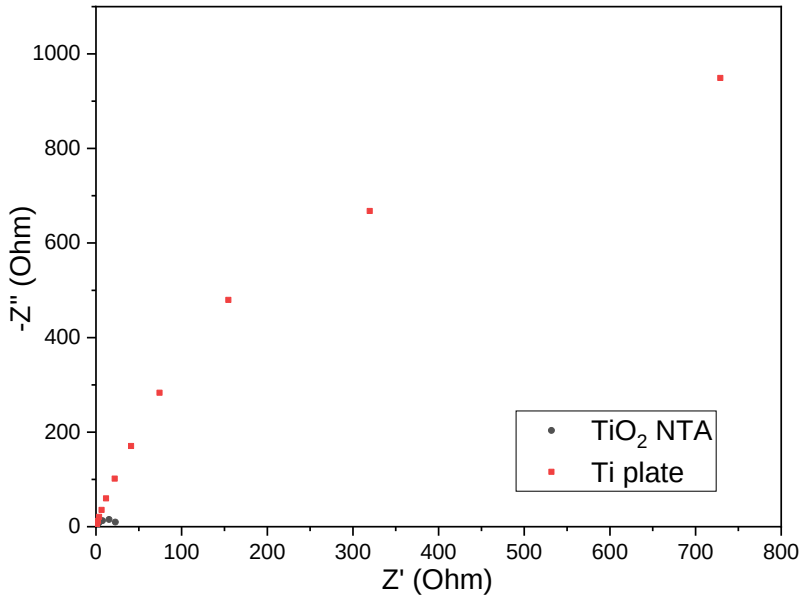

Figure 6.5 Nyquist plots of the EIS measurements at 1.7 V of Ti plate and Ti plate with TiO_2 nts interlayer.

6.3.2. Activity of the Ti/TiO_2 NTA - Mn_xO_y electrodes towards sulfide oxidation

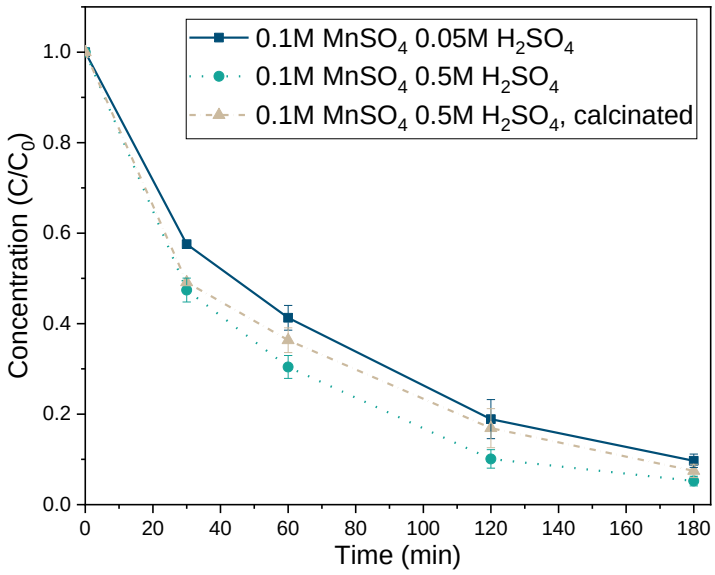

Figure 6.6 Decrease in HS^- concentration (C) normalized to the initial value (C_0) during sulfide removal experiment at 0.8 V/SHE applied to the Ti/TiO_2NTA-Mn_xO_y electrodes.

All of the synthesized Mn_xO_y based materials, polarized at 0.8 V/SHE, caused a rapid sulfide decrease by 90 % within 3 h **(Figure 6.6)**. The main reaction product was elemental sulfur, with 94% yield of S^0. The produced elemental sulfur was deposited at the electrode surface, forming a loosely packed visible layer ($S_{8\ dep}$). According to Luo et al., simultaneous participation of oxygen and manganese oxide in sulfide oxidation favours the formation of thiosulfate over elemental sulfur or sulfate [294]. Therefore, slight increase of $S_2O_3^{2-}$ concentrations (i.e., 0.1 mM or 6% of sulfide removed), observed in all performed experiments was a consequence of the presence of trace amounts of dissolved oxygen in the supporting electrolyte solution. Though several studies assumed that polysulfide is an important intermediate of sulfide oxidation with Mn oxides at basic pH, the solution stayed colourless throughout the experiment indicating the absence of polysulfide formation [293, 358].

The Ti/TiO_2 NTA-MnO_2 synthesized using lower acid concentration in the electrodeposition (i.e., 0.05 M H_2SO_4) performed slightly worse compared to the material synthesized in the presence of 0.5 M H_2SO_4 (i.e., 0.76 ± 0.09 h^{-1} and 0.98 ± 0.14 h^{-1}, respectively) **(Figure 6.6)**. Smooth coating with little relief observed in the SEM images is typically associated with the lower active surface area and leads to a decreased catalytic activity [357]. Indeed, the electrochemically active surface area of the electrodes synthesized at higher acid concentration (i.e., 0.5 M H_2SO_4) was estimated at 408 cm^2, while lower acid concentration yielded material with slightly lower active surface are (i.e., 362 cm^2) (**Figure 6.7**). Thus, the Ti/TiO_2 NTA – MnO_2 electrode synthesized using 0.5 M H_2SO_4 was selected for further experiments.

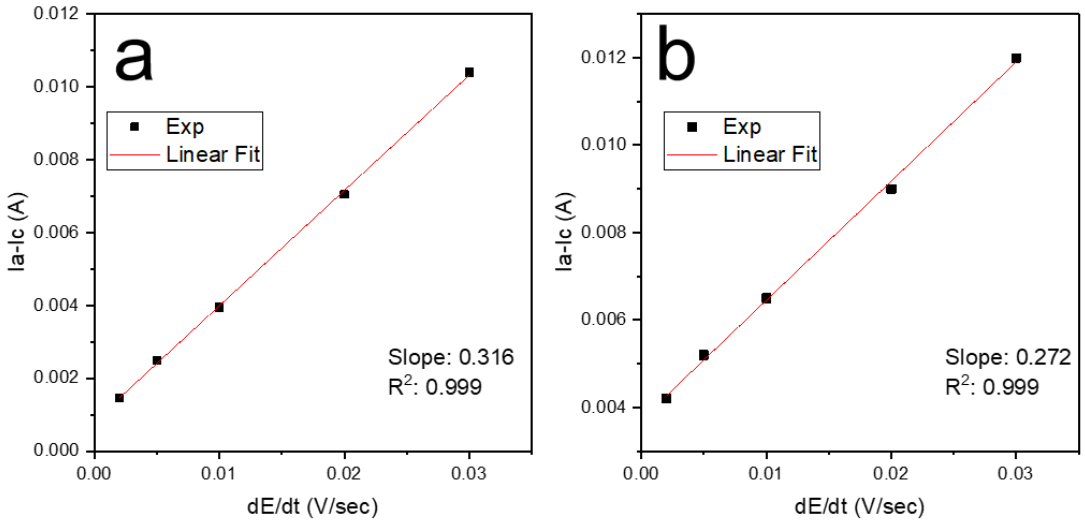

Figure 6.7 Determination of the double-layer capacitance at scan rates between 30 and 2 mV s^{-1} by performing CV in 0.1 M $NaNO_3$ electrolyte. The plots of charging currents versus the scan rates of the: **a)** Ti/TiO_2 NTA-MnO_2 electrodes synthesized in the presence of 0.5 M H_2SO_4, **b)** Ti/TiO_2 NTA-MnO_2 electrodes synthesized in the presence of 0.05 M H_2SO_4.

Catalytic oxidation of sulfide is initiated with the adsorption of HS^- onto the Mn_xOy catalyst surface, followed by the formation of a surface complex, which is then oxidized to adsorbed zero valent sulfur [293]:

$$Mn(IV)O_2 + HS^- + 4H^+ \leftrightarrow Mn(IV)S^- + 2H_2O \quad \text{(Eq. 6.3)}$$

$$Mn(IV)S^- \rightarrow Mn(III)S \quad \text{(Eq. 6.4)}$$

$$Mn(III)S + e^- \rightarrow Mn(II)S \quad \text{(Eq. 6.5)}$$

$$Mn(II)S \rightarrow Mn(II) + S^0 \quad \text{(Eq. 6.6)}$$

The electron transfer from Mn(IV) to sulfide occurs in two consecutive steps and involves the formation of the Mn(III) surface complex as a reaction intermediate. Being the intermediate, Mn(III) itself is capable of rapid catalytic oxidation of sulfide [350]. Although in the case of

Mn(IV) the reaction mechanism requires one additional step, the transition between the surface complexes is so rapid that it does not significantly affect the removal rates, as evidenced from the results obtained with the non-calcined MnO_2 and calcined Mn_2O_3 coatings (i.e., 0.98 ± 0.14 h^{-1} and 0.83 ± 0.01 h^{-1} for Mn(IV) and Mn(III), respectively) **(Figure 6.6)**.

6.3.3. Impact of the applied anode potential

The impact of the anode potential on sulfide oxidation was investigated by performing the experiments in the OC and at 0.4 V, 0.6, 0.8 V/SHE. As can be seen from **Figure 6.8**, in the absence of any applied potential, the Ti/TiO_2 NTA–MnO_2 electrodes lead to a rapid drop in sulfide concentration by 40% within 30 min. Oxidation of sulfide occurs simultaneously with the reduction of the MnO_2 coating, which leads to the production of Mn(II) and its subsequent release into the electrolyte in the form of Mn^{2+} :

$$Mn(II) \rightarrow Mn^{2+}aq + \text{new surface site} \qquad \text{(Eq. 6.7)}$$

After this initial drop, sulfide concentration remained constant, indicating a complete depletion of the MnO_2 catalyst **(Figure 6.8).** Complete dissolution of the coating was also confirmed by ICP-OES analysis of the supporting electrolyte, which detected substantial increase of total dissolved manganese concentration at the end of the experiment **(Table 6.2)**. The measured amount of the dissolved manganese (15.03 mg L^{-1} in 100 mL, i.e., 1.503 mg) is slightly lower than the theoretical weight of the electrodeposited MnO_2 film, calculated according to the Faraday's law (i.e., 1.803 mg).

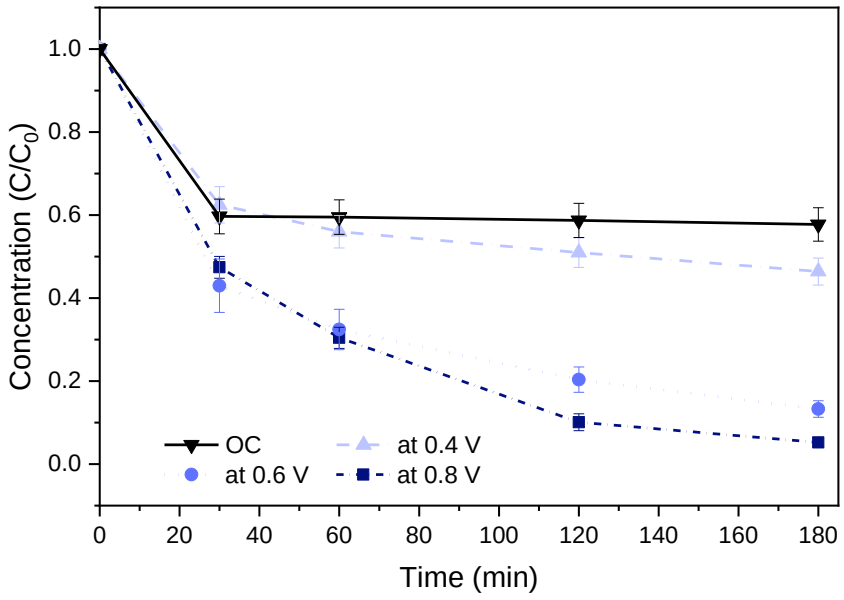

Figure 6.8 Decrease in HS^- concentration (C) normalized to the initial value (C_0) during the OC and electrochemical sulfide removal experiments performed at various potentials in 2.6 mM $NaNO_3$ supporting electrolyte amended with 2 mM of HS^- at pH 12.

Polarization of the Ti/TiO_2 NTA-MnO_2 electrodes at the anodic potential as low as 0.4 V/SHE drastically minimized the loss of the MnO_2 catalyst. The amount of total dissolved manganese detected in the electrolyte (i.e., 0.07 mg) represented only 3.8% of the theoretical coating weight. The coating stabilization was achieved by recovering the reduced Mn(II) back to its initial oxidation state with the application of potential. The Mn 3s doublet peak separation in the samples after the sulfide removal experiments was equal to the pristine TiO_2 NTA-MnO_2 sample **(Table 6.3)**. However, such stabilization could not be achieved without an appropriate substrate such as TiO_2 NTA. The TiO_2 nanostructures not only improve the mechanical stability of the coating through better adhesion, but, more importantly, promote the charge transfer and enhance the conductivity of the electrode [281], which enables a rapid recovery of the Mn catalyst. Rapid restauration of the oxidation state of Mn maintained the catalytic activity of the Ti/TiO_2NTA-MnO_2 electrode as was indicated by the gradual decrease of sulfide concentration during the entire experiment. Further increase of the potential significantly enhanced the sulfide oxidation kinetics

(i.e., 0.21 ± 0.07 h^{-1} at 0.4 V/SHE, 0.53 ± 0.1 h^{-1} at 0.6 V/SHE and 0.98 ± 0.2 h^{-1} at 0.8 V/SHE). This was a consequence of a faster MnO_2 catalyst re-oxidation at higher potentials as the amount of dissolved Mn was decreased even further when potential was increased, with only 0.01 mg of Mn released at 0.8 V/SHE, which represents 0.53% of the theoretical coating weight **(Table 6.2)**. In addition, the reaction kinetics could also be accelerated though faster direct electrolysis of sulfide. For instance, elemental sulfur can be electrochemically oxidized to sulfate at standard redox potential of 0.357 V/SHE, however, no increase of the dissolved sulfur species could be detected [221].

Table 6.2 Total dissolved manganese detected directly after in the OC experiments, and in the chronoamperometric experiments at 0.4 - 0.8 V applied to TiO_2 NTA-MnO_2 anode using 2.6 mM $NaNO_3$ and 2mM HS^- containing electrolyte at pH 12.

	Total dissolved Mn, mg L^{-1}
OC	15.03
at 0.4 V	0.7
at 0.6 V	0.18
at 0.8 V	0.08

Table 6.3 The XPS peak analyses of the Ti/TiO_2 NTA-Mn_xO_y electrodes obtained using different acid concentrations (e.g 0.5 M and 0.05 M H_2SO_4) in the precursor solution as well as for the material calcinated at 500 °C after the synthesis. The deconvoluted data are shown for the Mn $2p_{3/2}$ and Mn 3s spectra.

Sample name	Mn $2p_{3/2}$, E_b, eV	Mn3s			O1s		Valence number of Mn
		E_b (1), eV	E_b (2), eV	ΔE, eV	E_b, eV	Area %	
before test at pH 8	642.2	88.9	84.1	4.8	529.5[a)]	48.4	4
					531.0[b)]	34.8	
					532.9[c)]	16.7	
after test at pH 8	642.3	88.9	84.2	4.7	529.6	40.9	4
					530.9	37.3	
					532.4	21.7	
before test at pH 12	642.2	88.6	83.9	4.7	529.6	46.5	4
					530.9	37.2	
					532.7	16.2	
after test at pH 12	642.2	88.7	83.8	4.9	529.6	50.3	4
					530.7	30.1	
					532.8	19.5	

a) Oxide O^{2-}
b) Surface bounded OH^-
c) Weakly physisorbed O^-

6.3.4. Impact of the initial sulfide concentration and pH

The initial sulfide concentration had a pronounced effect on the sulfide oxidation rate **(Figure 6.9 a).** Lowering the initial sulfide concentration from 2 mM to 0.9 mM did not affect the reaction kinetics, as first-order rate constants were the same (i.e., 1.04 ± 0.05 h^{-1} and 0.98 ± 0.2 h^{-1}, respectively). Increase in the initial sulfide concentration to 3.9 mM led to slower sulfide oxidation kinetics, with rate constants of 0.62 ± 0.1 h^{-1}. Slower removal rates at higher HS^- concentration confirms that the reaction kinetics is determined by the rate at which HS^- ions can form complexes with the MnO_2 catalyst rather than controlled by mass transfer [359]. As can be seen from Table S2, higher HS^- concentration had no negative impact on the MnO_2 coating stability as the total

dissolved manganese detected in the electrolyte (i.e., 0.01 mg) represented less than 0.6% of the theoretical weight of the deposited MnO_2 coating.

At pH 8, sulfide was removed at a higher rate ($1.32 \pm 0.2\ h^{-1}$) compared with the pH 12 experiments ($0.98 \pm 0.2\ h^{-1}$) **(Figure 6.9 b)**. The pH-dependence of the sulfide oxidation rate further confirms that an the interaction between HS^- and the MnO_2 coating occurs through inner-sphere complex formation [293].

The catalytic activity and stability of the MnO_2 catalysts is generally very sensitive towards the pH of the electrolyte [360]. The surface groups of manganese oxides are amphoteric, meaning they can function both as an acid and a base [361]. Hence, the catalyst surface can undergo protonation and/or deprotonation depending on the value of the pH of the solution [362]:

$$Mn^{IV}OH \leftrightarrow Mn^{IV}O^- + H^+ \quad pK_1 = 8.2 \qquad \text{(Eq 6.8)}$$

On the other hand, sulfide speciation is also dependent on the pH as can be seen from the sulfide ionization equilibrium [18]:

$$H_2S_{(aq)} \leftrightarrow HS^- \quad pK_1 = 6.88 \qquad \text{(Eq 6.9)}$$

The formation of a complex is affected by the relative distribution of different sites on the manganese oxide surface and of sulfide in the solution [293, 294]. According to Zhu et al., the pH range between 7 and 8 enables the formation $[Mn^{IV}OH][HS^-]$ complex, which leads to faster sulfide oxidation kinetics compared to $[Mn^{IV}OH][H_2S]$ and $[Mn^{IV}O^-][HS^-]$ [294]. The increase of hydroxide containing surface groups in samples exposed to electrolyte at basic pH was also confirmed by the XPS analysis **(Table 6.3).**

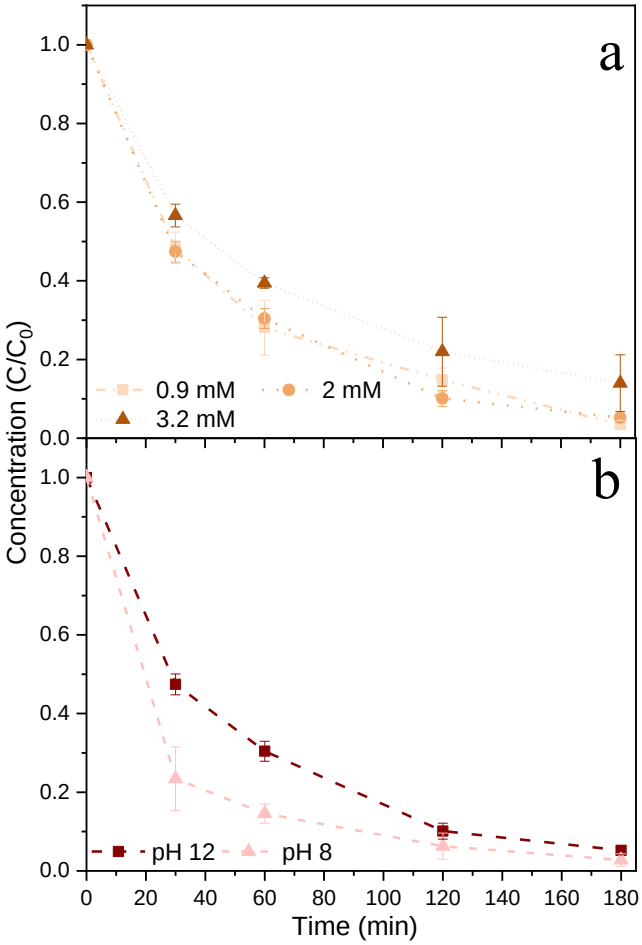

Figure 6.9 Decrease in HS^- concentration (C) normalized to the initial value (C_0) a) during electrochemical experiments performed at 0.8 V/SHE using various initial sulfide concentrations at pH 12, b) during electrochemical experiments performed at 0.8 V/SHE in 2.6 mM $NaNO_3$ supporting electrolyte amended with 2 mM of HS− at pH 8 and pH 12.

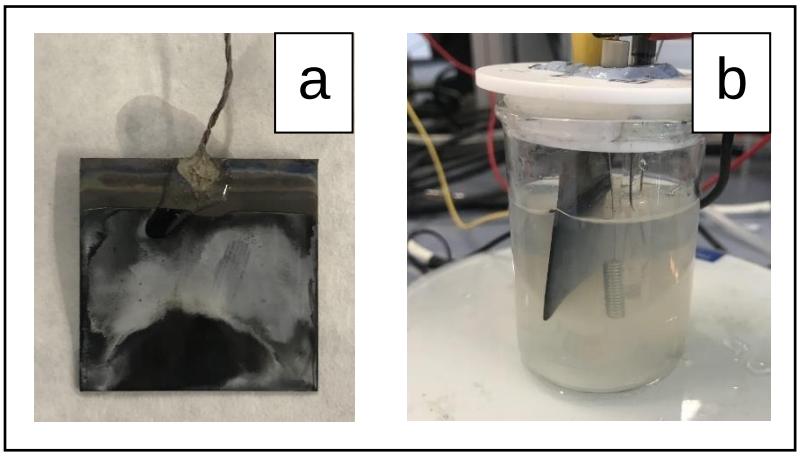

Figure 6.10 Images of the: a) Ti/TiO_2 NTA-Mn_xO_y electrode after the electrochemical sulfide removal test performed at pH 12, b) colloidal sulfur solution produced during electrochemical sulfide removal using Ti/TiO_2 NTA-Mn_xO_y electrodes at pH 8.

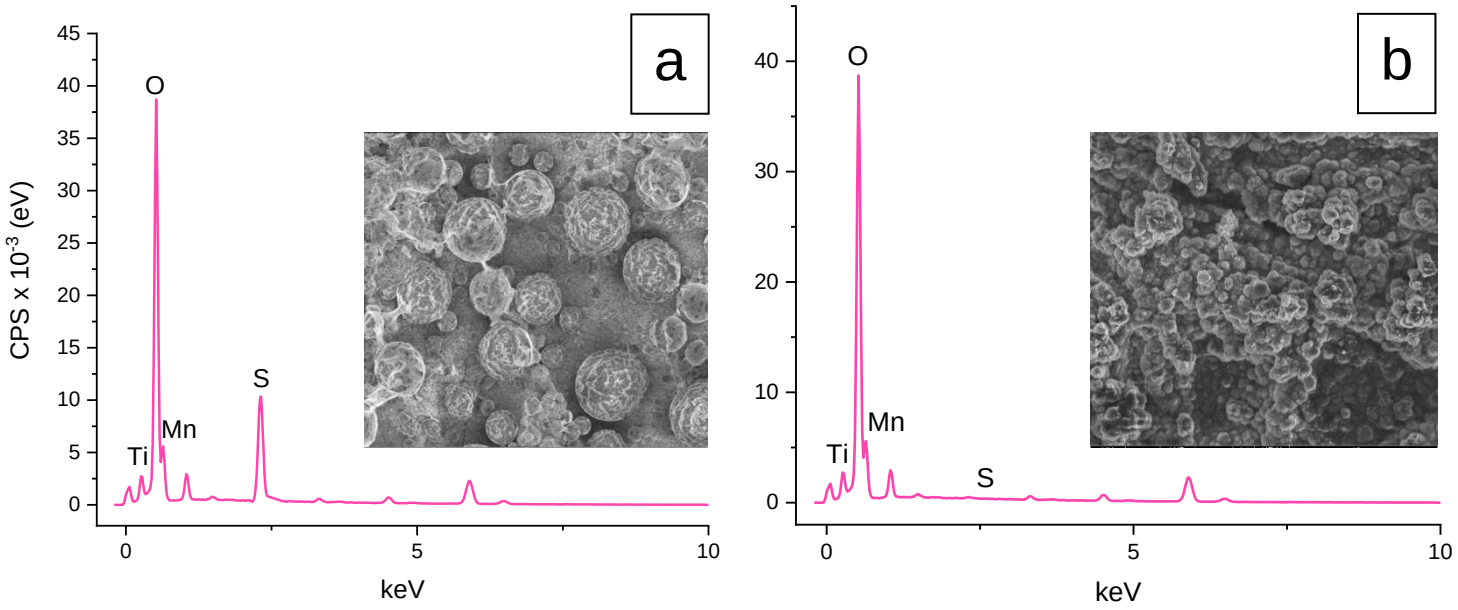

Figure 6.11 The SEM images and the EDX spectra of the: a) Ti/TiO_2 NTA-Mn_xO_y electrode after electrochemical sulfide removal test performed at pH 12, b) TiO_2 NTA-Mn_xO_y electrode after electrochemical sulfide removal test performed at pH 8.

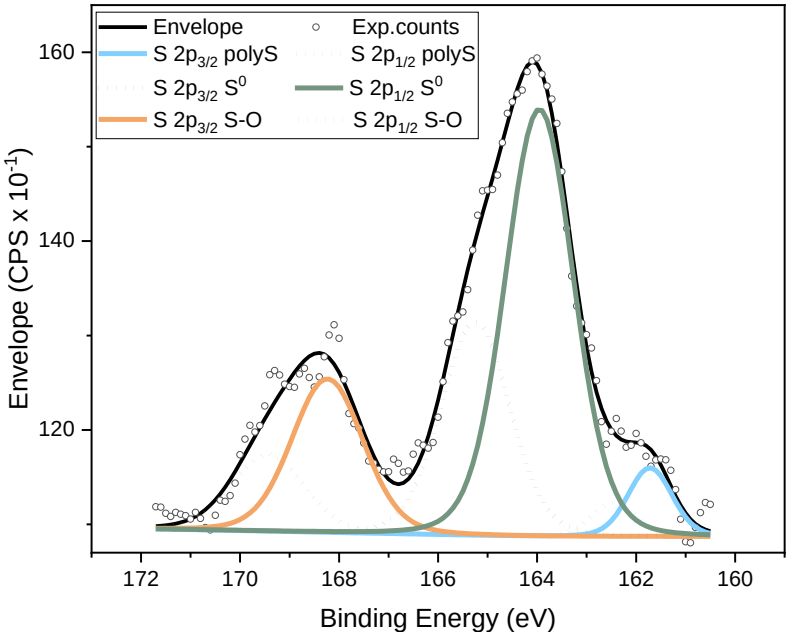

Figure 6.12 High resolution S2p XPS spectra of Ti/TiO_2 NTA-Mn_xO_y electrode after the electrochemical sulfide removal test performed at pH 12.

Even though the final product of the treatment at both pH 8 and 12 was elemental sulfur, at pH 12 sulfur remained adsorbed at the anode surface ($S_{8\ dep}$), while at pH 8 sulfur was formed and instantly desorbed from the anode surface and released into the electrolyte producing colloidal sulfur particles of ~ 0.2 μm ($S_{8\ col}$) **(Figure 6.10)**. Adsorption of the elemental sulfur to the Ti/TiO_2NTA-MnO_2 electrode surface at pH 12 was confirmed by the recorded SEM and EDX **(Figure 6.11)**, as well as XPS analysis **(Figure 6.12)**. The SEM images of the electrode surface after the sulfide removal test at pH 8 demonstrate that the MnO_2 morphology remained unchanged **(Figure 6.11 b)**. Moreover, neither EDX nor XPS detected the presence of sulfur, thus further evidencing that when controlling the supporting electrolyte pH at pH 8, the formed elemental sulfur was not electrodeposited but released as $S_{8\ col}$. The difference in the forms of produced sulfur indicates the shift in the S_8 formation mechanism. As was mentioned in Equation 8, further

oxidation of surface complexes of sulfide ion and manganese yields zero valent sulfur, S^0. At pH 8, zero valent sulfur is desorbed from the anode surface and released into the solution, where it undergoes further complexation to $S_{8\ col}$ [293]. On the contrary, at pH 12, formation of elemental sulfur ($S_{8\ dep}$) becomes diffusion controlled and occurs at the electrode surface.

Direct electrooxidation of sulfide to elemental sulfur is typically associated with the gradual loss of performance, which occurs as a result electrode passivation with the isolating layer of elemental sulfur [221, 253, 351]. In electrooxidation at pH 12 in which $S_{8\ dep}$ remained at the anode surface, rapid decrease in sulfide removal rates was observed within three consecutive applications, i.e., 0.81 ± 0.03 h^{-1}, 0.41 ± 0.06 h^{-1}, and 0.19±0.08 h^{-1} in the first, second and third cycle **(Figure 6.13)**. Moreover, the electrode passivation was further supported by the increase in the energy consumption in each subsequent cycle (i.e., 0.09 Wh L^{-1}, 0.18 Wh L^{-1} and 0.79 Wh L^{-1} in the first, second and third application, respectively). Similar passivation with elemental sulfur was noted in the repetitive applications of the Ti/TiO_2NTA-MnO_2 anode in the experiments without pH control, as pH was rapidly increased from the initial pH 8 to pH 12 (data not shown). On the contrary, when the pH was controlled at pH 8, the Ti/TiO_2NTA-MnO_2 electrode demonstrated rapid and robust sulfide removal in the consecutive cycles, with unchanged sulfide removal rate constants (i.e., 1.01 ± 0.04 h^{-1}, 0.96 ± 0.06 h^{-1}, and 1.06 ± 0.1 h^{-1} in the first, second and third application) and energy consumption (i.e., 0.05 Wh L^{-1}, 0.044 Wh L^{-1} and 0.042 Wh L^{-1} in the first, second and third application, respectively), demonstrating that the electrode passivation was effectively avoided **(Figure 6.13)**.

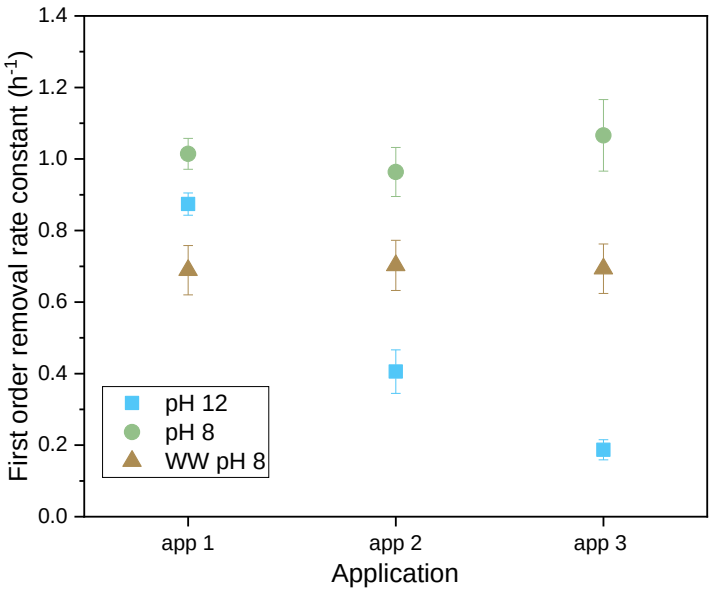

Figure 6.13 Observed first-order sulfide removal constant (h^{-1}) at the Ti/TiO_2 NTA-Mn_xO_y electrodes applied over three subsequent cycles in synthetic electrolyte containing 2.6 mM $NaNO_3$ and 2 mM of HS^-, at pH 12 and pH 8, and in the real sewage at pH 8.

6.3.5 Electro-catalytic sulfide removal in real sewage

Sulfide removal rates observed in the experiments with real sewage were somewhat lower (0.69 ± 0.06 h^{-1}) compared to the experiments performed in the supporting $NaNO_3$ electrolyte (1.01 ± 0.04 h^{-1}) **(Figure 6.13)**, while the energy consumption of the system increased (i.e., 0.05 Wh L^{-1} and 0.29 Wh L^{-1} in the supporting $NaNO_3$ electrolyte and in real sewage, respectively). This can be explained by the participation of the MnO_2 coating in reactions other than sulfide oxidation. A slight decrease (i.e., 8% removal) in chemical oxygen demand (COD) of was observed at the end of the experiments, indicating a partial oxidation of the organic matter by the MnO_2 coating. Nevertheless, sulfide was still completely removed within 3 h, indicating high selectivity of TiO_2 NTA-MnO_2 electrode even in the case of complex matrix such as real sewage. Moreover,

phosphate, typically present in wastewater, can block the MnO_2 surface sites available for the reaction with sulfide and inhibit sulfide removal [363]. The competition between sulfide and phosphate for the MnO_2 sites were further confirmed by the slight decrease of phosphate concentration (i.e., from 0.08 mM to 0.04 mM). Notwithstanding the presence of organics and inorganics in real sewage that are known to react with the Mn-oxide [364, 365] and can cause reductive dissolution of the MnO_2 coating, the electrodes remained stable and no release of Mn^{2+} ions was detected in the ICP-OES analyses.

Given that the buffering capacity of the real sewage avoided an increase in pH during the experiment and maintained it at pH 8, the formation of elemental sulfur proceeded in the same manner as in the experiments performed using $NaNO_3$ electrolyte at pH 8. The final product of the sulfide oxidation in real swage was zero valent sulfur, that underwent complexation to $S_{8\ col}$ in the bulk of the electrolyte. Thus, the passivation of the anode surface with elemental sulfur was completely avoided, and there was no decrease in the sulfide removal rates in subsequent applications (i.e., $0.69 \pm 0.06\ h^{-1}$, $0.70 \pm 0.065\ h^{-1}$, $0.69 \pm 0.09\ h^{-1}$ in the first, second and third cycle) and the energy consumption of the system remained constant (i.e., $0.29\ Wh\ L^{-1}$, $0.26\ Wh\ L^{-1}$, $0.31\ Wh\ L^{-1}$ in the first, second and third cycle) **(Figure 6.13).**

The deposition of sulfur at the electrode surface might be considered beneficial for application in sewer systems as it enables complete separation of sulfur from the stream, thus, avoiding the problems with sulfide reformation [171]. Moreover, direct oxidation of sulfide to sulfur requires low energy input, especially compared to the indirect sulfide oxidation with electrochemically produced oxygen, or via direct electron transfer to sulfate [366]. On the other hand, several studies mentioned that the efficiency of direct sulfide oxidation is significantly deteriorated in sewage

with low sulfur content due to mass transfer limitation, which is a major issue considering that average sulfide concentration is sewage rarely exceeds 3 mM [231]. Besides, gradual loss of performance associated with the sulfur deposition is another important drawback which prevents the implementation of this approach in practice [221, 253, 351]. Previously proposed strategies aimed at the mitigation of the electrode passivation such as extraction of sulfur with organic solvents [244], use of surfactants [245], and cathodic dissolution of the electrodeposited sulfur [253, 351] are either incapable of full restauration of sulfide removal capacity, economically unattractive or environmentally hazardous. Hence, switching to electrochemical production of colloidal sulfur at low applied potentials can help maintain low energy requirements of direct sulfide oxidation to sulfur, while avoiding problems with passivation and decreased efficiency in waste streams with low sulfide content. Even though colloidal sulfur remains in the stream, it is unlikely to lead to sulfide reformation due to its low bioavailability, especially when compared to other dissolved sulfur species [13].

6.4. Conclusion

The TiO_2 NTA interlayer enabled the electrodeposition of the Mn_xO_y coating by providing a conductive substrate with high specific surface area. The electrodeposition of the Mn_xO_y led to filling of the TiO_2 nanotubes without damaging their morphology. Higher concentration of acid in Mn_xO_y precursor solution yielded coating with higher specific surface area that demonstrated slightly better sulfide oxidation kinetics. Initial valence state of the catalyst (i.e., Mn(IV) and Mn(III)) generally had little effect on the removal kinetics.

The Ti/TiO_2NTA-MnO_2 anode demonstrated excellent catalytic activity towards sulfide oxidation, yielding a thirty-fold higher normalized reaction rate compared to Mn_2O_3-coated GF anodes (i.e.,

$175 \cdot 10^{-4}$ m^3 h^{-1} m^{-2} and $6 \cdot 10^{-4}$ m^3 h^{-1} m^{-2} for Ti/TiO_2NTA-MnO_2 and GF-Mn_2O_3, respectively) [357]. Oxidation of sulfide on MnO_2 coating occurred through formation of the inner sphere complex, yielding elemental sulfur as the final product. Coating dissolution, observed in the OC experiment due to the Mn_xO_y reduction, was effectively prevented by the continuous recovery of the catalyst under low applied potentials. The pH of the electrolyte not only affected the reaction kinetics, but also determined the form of the resulting elemental sulfur. At pH 12, zero valent sulfur remained adsorbed at the anode surface, whereas at pH 8 it was desorbed and further complexed to S_8, thus avoiding completely the anode passivation. The electrochemical production of colloidal sulfur instead of its electrodeposition at the anode surface enabled a sustained (electro)catalytic activity of the Ti/TiO_2NTA-MnO_2 anode in the subsequent applications in $NaNO_3$ electrolyte at constant pH 8, as well as in the real sewage in which constant pH 8 was maintained by the buffering capacity of sewage.

This unprecedented performance of the Ti/TiO_2NTA-Mn_xO_y anodes developed in this study enabled rapid sulfide oxidation and selectivity towards colloidal sulfur in the conditions relevant for sewage treatment and other processes where removal of dissolved sulfide is of interest (e.g., sulfide removal from alkaline solutions used in biogas scrubbers, at pH 8-9). Continuous electrocatalytic recovery of the coating is of crucial importance for reusing a catalyst that is otherwise rapidly depleted when used in a homogeneous oxidation process. Electrocatalytic sulfide removal using Ti/TiO_2NTA-Mn_xO_y anodes overcomes two major limitations of conventional direct electrochemical sulfide oxidation: low efficiency for diluted sulfide solutions, and electrode passivation with sulfur, while maintaining low energy input requirements (0.29 kWh m^{-3}). Taking into consideration the easiness of the electrode synthesis procedure, low cost of the earth-abundant

manganese, low energy consumption, low bioavailability of electrochemically produced sulfur, modularity and possibility of automated, remote operation of the electrooxidation of sulfide at $Ti/TiO_2NTA\text{-}MnO_2$ electrodes, the proposed approach can potentially become a game-changing technology of sulfide control in sewer systems and other applications.

Chapter 7. General discussion

Sulfide causes various problems in both urban and industrial wastewater systems. Apart from its characteristic malodour, the hydrogen sulfide toxicity represents a serious threat for the health of workers involved in the sanitary sewer systems maintenance. Moreover, sulfide-induced corrosion can lead to a rapid deterioration of the structural integrity of the wastewater collection system. Though sulfide-related problems in sewers have long been recognized, the sulfide control technologies available at the market are still characterised by the numerous limitations and drawbacks including high operating costs due to the need for the continuous chemical supply, formation of toxic metal-containing sludge and sulfide reformation at the end of the pipeline [171].

Electrochemical processes are an attractive alternative to the existing technologies for sulfide removal, as they offer a robust removal of hydrogen sulfide *in situ* and avoid the costs and risks related to dosing, transportation and storage of chemicals [171]. Indeed, sulfide can be electrochemically oxidized to the electrodeposited elemental sulfur, thus avoiding sulfide reformation or formation of secondary waste streams. On the other hand, considering high electrical resistance of elemental sulfur (1017 Ω cm^{-1}), its deposition at the anode surface leads to a gradual loss of performance and eventually halts the process [221, 253]. Previously proposed strategies aimed at the mitigation of the electrode passivation such as extraction of sulfur with organic solvents [244], use of surfactants [245], and cathodic dissolution of the electrodeposited sulfur [253, 351] are either incapable of the full restauration of the sulfide removal capacity, economically unattractive or environmentally hazardous. Therefore, the application of direct electrochemical sulfide control systems for treatment of sewage or other types of wastewater is feasible if an appropriate anode recovery strategy is developed [1, 367].

Chapter 4 of this thesis is focused on the direct electrochemical sulfide oxidation using activated carbon felt and graphite felt as anode. These low-cost carbon-based materials were selected due to their high surface area, which is always beneficial for electrochemical applications. Moreover, activated carbon felt is capable of catalytic sulfide oxidation to sulfur, which can potentially enhance the sulfide removal rate. Previously, Dutta et al. observed complete dissolution of sulfur deposited on the carbon fibre brush electrodes under cathodic polarisation and in the presence of 1 – 100 mM sulfide, which enabled the chemical dissolution of S^0 to polysulfides [253]. Thus, to explore further electrochemical sulfur recovery, three strategies for the electrode regeneration were investigated in our study: *i)* further oxidation of S^0 to soluble species (e.g., $S_2O_3^{2}$, SO_3^{2-}, SO_4^{2-}) via anodic polarization in the absence of HS^-, *ii)* reduction of S^0 back to sulfide via cathodic recovery in the absence of HS^-, and *iii)* cathodic recovery in the presence of HS^-, to determine the role of the chemical dissolution of S^0 in the electrode regeneration process performed in the work of Dutta et al [253].

Chapter 5 is dedicated to the improvement of the sulfide oxidation kinetics with graphite felt anode through the introduction of the catalytically active MnO_2 coating. The ability of manganese oxide to oxidize sulfide was previously studied as a natural process that occurs in sediments [294]. However, high affinity of manganese oxides towards sulfide oxidation was never exploited in wastewater treatment. Some studies proposed sulfide oxidation with potassium permanganate, which yields fast sulfide removal but is also inherently limited by the gradual depletion of the catalyst [298-300]. This chapter also explores the performance of the cathodic regeneration of the sulfur-loaded GF-MnO_2 electrode, which was found to be the only efficient recovery approach in the first chapter.

Finally, Chapter 6 addresses major limitations of the carbon-based electrodes: *i)* insufficient electrical conductivity of the carbon-based substrate (i.e., graphite felt or others), which requires the use of current collectors and limits the efficiency of Mn regeneration, and *ii)* formation of the isolating layer of elemental sulfur at the surface of the anode. To avoid these drawbacks, MnO_2 was electrodeposited on a Ti/TiO_2 NTA substrate. In addition to this, the influence of the operating parameters (e.g., anode potential, initial sulfide concentration and solution pH) on the process kinetics and final products was determined.

Table 7.1 Summary of data for various electrode materials employed for sulfide removal in real sewage amended with ∼2.7 mM HS^- at pH 8.

Material	**Removal efficiency**	**Observed reaction rate, h^{-1}**	**Electrode /Electrolyte, $m^2\ m^{-3}$**	**Normalized reaction rate, $m^3\ h^{-1}\ m^{-2}$**	**E_{anode}, V**	**E_{cell}, V**	**I, mA**	**CE, %**	**E_{eo}, kW h m^{-3}**
ACF	91%	3.8	$975 \cdot 10^6$	$3.9 \cdot 10^{-9}$	0.9	2.2	36	525	0.04
GF	92%	0.6	$65 \cdot 10^3$	$9.2 \cdot 10^{-6}$	0.9	2.7	10	63	1
GF - Mn_xO_y	90%	0.94	1536	$6 \cdot 10^{-4}$	0.4	4.7[1)]	4	407	0.44
NTA - Mn_xO_y	80%	0.7	40	$175 \cdot 10^{-4}$	0.8	2	5	115	0.3

1) Cell divided by a porous glass frit

7.1. Direct sulfide oxidation using porous, carbon-based electrodes

Although both tested anode materials are based on carbon, the observed mechanism of sulfide oxidation was fundamentally different. Electrochemical sulfide oxidation to sulfur was possible using graphite felt anode due to the direct electron transfer. The current efficiency of the sulfide removal with graphite felt was estimated at 63%. Sulfide oxidation rates were impacted by the applied potential, yielding higher rates upon the anode potential increase. Sulfur, electrodeposited

at the anode surface, consisted of two layers: chemisorbed layer underneath a weakly physisorbed bulk elemental sulfur. The passivating sulfur layer was resistant to all regeneration strategies, except for the cathodic dissolution. The weakly physiosorbed layer of S^0 could be dissolved under negative potential, enabling a partial recovery (i.e., 30%) and decreasing the electrode passivation. The removal of sulfide at the activated carbon felt anode was governed purely by the oxidative chemisorption both with and without applying the potential. The final product of sulfide chemisorption on activated carbon felt was elemental sulfur, deposited in its micropores as a result of sulfide oxidation with the dissociative adsorbed oxygen [320]. The mechanism of sulfide removal was also confirmed by the insignificant effect of the applied potential on the sulfide removal kinetics, current efficiency significantly above 100% and significantly lower energy consumption compared to the graphite felt anode (**Table 7.1**). None of the tested electrochemical and chemical recovery strategies could remove the sulfur retained in the micropores of the activated carbon felt anode due to its incorporation into the carbon matrix and diffusion limitations caused by the microporosity of the material. Both graphite felt and activated carbon felt showed good performance when applied for the sulfide oxidation in real sewage, with the observed sulfide removal rates of 0.6 and 3.8 h^{-1} at 0.7 V/SHE, respectively.

Chapter 4 demonstrates that hydrogen sulfide can be selectively oxidized and removed in the form of sulfur using both graphite felt and activated carbon felt electrodes, and in the synthetic HS^- solution and real sewage. Though activated carbon felt is capable of sulfide oxidation to elemental sulfur even in the absence of potential, the chemisorbed sulfur retained in the microporous network of the material is resistant towards electrochemical, chemical and thermal regeneration strategies, thus making complete regeneration of activated carbon felt impossible [327, 368]. An

electrochemical system that requires frequent replacement of the anode would incur high capital and maintenance costs, which makes the implementation of such system unattractive. Though partial regeneration of graphite felt was achieved, its limited efficiency would not be able to sustain robust sulfide removal in long term. Moreover, the presence of the sulfur in the system compromises the selectivity of the treatment, favouring polyS production. Alternatively, carbon-based electrodes loaded with sulfur can be regenerated using organic solvents, however, this strategy is unlikely to be applied in the field of wastewater treatment as it is associated with increased level of environmental hazard. Finally, sulfide oxidation kinetics at carbon-based electrodes was rather slow. Therefore, alternative strategies focused on the material modification should be considered to obtain a porous, high surface area electrode capable of selective oxidation of sulfide to sulfur.

7.2. Electrocatalytic sulfide removal using MnO_2-coated GF electrodes

The sluggish sulfide oxidation kinetics observed at graphite felt electrodes was significantly improved through its modification with MnO_2 coating catalytically active towards sulfide oxidation (i.e., $9.2 \cdot 10^{-6}$ m^3 h^{-1} m^{-2} and $6 \cdot 10^{-4}$ m^3 h^{-1} m^{-2} for graphite felt and GF-MnO_2, respectively) (**Table 7.1**). The catalytic activity of the GF-MnO_2 electrode synthesized via the electrodeposition pathway was directly related to the active surface area of the material, with the lower MnO_2 loading yielding more relief in the coating and higher HS^- removal rates. Even though the application of low potential did not enhance sulfide oxidation, it enabled the continuous regeneration of the reduced manganese after its reaction with the sulfide ion.

Cathodic recovery, that could effectively dissolve elemental sulfur deposited at graphite felt, was also tested at the GF-MnO_2. Cathodic polarisation of sulfur-loaded GF-MnO_2 slowed down its

passivation and the gradual performance deterioration. However, complete recovery could not be accomplished because of the reductive dissolution of the MnO_2 coating observed during prolonged cathodic polarization. The electrocatalytic sulfide oxidation in real sewage also resulted in rapid sulfide removal, yet somewhat lower rates were obtained compared with the synthetic electrolyte (i.e., 0.94 ± 0.13 and 2.42 ± 0.02 for real sewage and synthetic electrolyte, respectively) due to the competing electrosorption of anions and/or reaction of organics present in the sewage with the MnO_2 coating.

Electrochemical recovery of the MnO_2 achieved in this study, is highly important as it enables the continuous recovery of the catalyst that is otherwise rapidly depleted when used in a conventional homogeneous catalytic reaction. The simplicity of the electrode material synthesis and low cost of the graphite felt and Mn_xO_y precursor (i.e., 50 – 55 € per m^2 of GF and 0.25 – 0.50 € per kg of $MnSO_4$) are crucial parameters for the application of the proposed electrodes and up-scaling of the electrochemical system. Even though graphite felt provides high surface area, suitable porosity and permeability for the MnO_2 deposition and subsequent sulfide removal, its limited electrical conductivity ($3 \cdot 10^{-5}$ S/m) constraints not only the application and scale-up of electrochemical system, but also the rate of the MnO_2 coating regeneration and compromise its stability [369]. Another important issue to consider prior to the application of electrochemical sulfide removal is the electrode regeneration strategy. Although cathodic polarisation can slightly alleviate the passivation of the electrode surface by partly dissolving the layer of the deposited sulfur, it also causes gradual dissolution of the MnO_2 catalyst. Numerous studies from the field of energy storage intended to tackle the MnO_2-based cathode instability, proposing a wide range of the MnO_2 stabilization methods [370, 371]. However, even if the MnO_2 dissolution is successfully prevented

and complete removal of the passivating layer of elemental sulfur is achieved, the lifetime of such electrode will still be limited due to the poor cyclability of the manganese oxides [372]. Therefore, solution for the electrode passivation by sulfur requires a different approach, for instance, development of the electrode material that would avoid deposition of sulfur on its surface.

7.3. (Electro)catalytic oxidation of sulfide to colloidal sulfur over manganese oxide-coated electrode with the TiO_2 nanotubes interlayer

To address the problems associated with insufficient conductivity of graphite felt substrate and electrode passivation with elemental sulfur, in this study the Mn_xO_y coating was deposited on the Ti plate anode with the TiO_2 NTA interlayer.

The TiO_2 NTAs were coated with the manganese oxide without damaging the nanotube morphology via the developed electrodeposition procedure. Similar to the results reported in the Chapter 5, the MnO_2 coating demonstrated excellent catalytic activity for the sulfide oxidation, yielding elemental sulfur as the final product. Notwithstanding the lower specific surface area of the Ti/TiO_2 NTA-MnO_2 electrode (i.e., 32 cm^2 of Ti plate vs 1000 cm^2 of graphite felt or 9 10^8 cm^2 of activated carbon felt), its performance is comparable to the high surface porous materials as a result of the improved electron transfer between the MnO_2 coating and the substrate (**Table 7.1**). The dissolution of the coating observed in the OC experiment due to the MnO_2 reduction was effectively prevented by the continuous recovery of the catalyst under low applied potentials. The pH of the electrolyte not only affected the reaction kinetics, but also determined the form of the resulting elemental sulfur. At pH 12, the produced elemental sulfur remained adsorbed at the anode surface ($S_{8\ dep}$), whereas at pH 8 the zero valent sulfur (S^0) was desorbed and further complexed to elemental sulfur ($S_{8\ col}$) in the electrolyte, thus avoiding completely the anode passivation. Production of the colloidal sulfur instead of its electrodeposition at the anode surface enabled a

sustained (electro)catalytic activity of the Ti/TiO_2 NTA-MnO_2 anode in the subsequent applications in $NaNO_3$ electrolyte at constant pH 8, as well as in the real sewage in which constant pH 8 was maintained by the buffering capacity of sewage.

The Chapter 6 demonstrates that the sulfide removal using the Ti/TiO_2 NTA-MnO_2 anode offers several important advantages over the anode materials discussed in the previous chapters. As a result of the improved electron transfer between the substrate and the Mn_xO_y coating, an electrochemical cell equipped with the Ti/TiO_2 NTA-MnO_2 anodes demonstrated the highest normalised removal rates, while maintaining low energy consumption (i.e., 0.3 kWh m^{-3}) of the system (**Table 7.1**). Given that at the pH 8 and in the real sewage, the Ti/TiO_2 NTA-MnO_2 anode selectively oxidizes sulfide to elemental sulfur in its colloidal form, there is no passivation of the anode surface, which is typically observed at other electrode materials, including carbon-based electrodes. Considering the modularity, versatility, high efficiency and selectivity for sulfide oxidation of the electrocatalytic sulfide removal, as well as the omission of the continuous chemical dosing, the approach proposed in the present study has potential for upscaling and implementation for sulfide control in real sewers. Oxidation of sulfide to elemental sulfur followed by its precipitation is expected to minimize the problem of sulfide reformation especially when compared to other possible sulfide oxidation products (e.g., $S_2O_3^{2-}$, SO_3^{2-}, SO_4^{2-}). Finally, electrocatalytic system is characterised by small footprint, which implies the possibility of its coupling with the solar photovoltaic panels, making it very well suited for the decentralized treatment of waste streams [234]. However, several operating problems such as blockage, ragging, accumulation of particles and biofilm growth caused by harsh environment of sewers must be

seriously considered prior to implementation of the Ti/TiO_2 NTA-MnO_2 anode based treatment unit in full scale.

Chapter 8. Future perspectives

The bench scale experiments described in this thesis demonstrated the feasibility of electrocatalytic sulfide control approach. However, further upscaling and implementation of such system requires thorough analysis of the engineering parameters as well as possible issues that can arise during the operation of the proposed system. Therefore, this chapter addresses the most critical process and engineering considerations. Finally, the future prospective and opportunities for electrochemical sulfide abatement strategies are discussed.

8.1 Considerations of the reactor configuration

The versatility and the mechanical stability of the Ti/TiO_2 NTA-MnO_2 electrodes enable a great degree of flexibility in the reactor design, which can be specifically tailored towards given dimensions, lengths and daily flow of a sewer pipe. For instance, anode size can be easily scaled up or down based on the flow rate or sulfide concentration in the stream. Moreover, depending on the orientation, the arrangement and the shape of the electrodes, the reactor can be designed for flow through or flow by operation in multiple or single channels. Besides plane electrodes, Ti/TiO_2 NTA-MnO_2 can be synthesized over Ti cylinder, tube or impeller. Finally, the proposed system does not require IEM, which helps to avoid excessive capital cost and operating problems such as scaling and clogging. Given the simplicity and the diversity of possible reactor configurations as well as the selectivity of the developed electrodes towards sulfide oxidation, the electrochemical cell equipped with the Ti/TiO_2 NTA-MnO_2 can be installed directly inside a sewer pipe. This configuration does not require installation of a separate pumping station, which helps to drastically reduce capital and operating costs and avoids associated operating problems.

The optimal placement of the cell in the sewer network is another crucial aspect to consider. Hydrogen sulfide concentration typically reaches its peak downstream and gets released into gaseous phase at the points of increased turbulence intensity (i.e junctions, waterfalls, drops etc.).

Therefore, placement of the electrochemical cell prior to the sewer hydraulic structures, especially those located downstream of the pipeline, can prevent the release of gaseous hydrogen sulfide, thus avoiding related odour and corrosion issues. The Ti/TiO_2 NTA-MnO_2 based systems can be also installed prior to the discharge of the stream into the primary tank, to prevent the occurrence of odour nuisance at the wastewater treatment utility.

8.2 Estimation of operating and capital costs

A cost calculation was performed to investigate the economic potential of the proposed electrochemical system based on Ti/TiO_2 NTA-Mn_xO_y anode. The cost of the 1 m^2 of Ti/TiO_2 NTA-Mn_xO_y was calculated based on the assumption that the distance between the anode and the cathode during the NTA synthesis and coating procedures is 4 cm. Overview of the required materials together with prices can be seen in **Table 8.1**.

Table 8.1 Estimation of the total cost of synthesis of 1 m^2 Ti/TiO_2 NTA-Mn_xO_y anode.

Item	Quantity	Price	Cost, €
Ti plate, thickness 1mm	1 m^2	20 – 25 € per m^2	20 – 25 €
Glycerol	25 kg	0.6 – 1.4 € per kg	15 – 35 €
NH_4F	0.23 kg	2.55 – 3.39 € per kg	0.58 – 0.77 €
Energy required for anodization	2 kW h	0.8 € per kW h	1.6 €
Argon	20 L	1.78 – 1.86 € per L	35.6 – 37.32 €
Energy required for calcination	12 kW h	0.8 € per kW h	9.6 €
$MnSO_4$	0.34 kg	0.25 – 0.50 € per kg	0.085 – 0.17 €
H_2SO_4	1 kg	0.25 € per kg	0.25 €
Energy required for Mn_xO_y coating	0.5 kW h	0.8 € per kW h	0.4 €
Estimated total cost per m^2			**83 – 110 €**

In order to perform the calculation of the investment and operational costs of an upscaled system installed inside a sewer, several assumptions were made. First, it was assumed that the required total surface area of an anode is 50 m^2. Secondly, the duration of the treatment required to prevent the release of gaseous sulfide was assumed to be 12 hours a day, 7 days a week. The wastewater stream was assumed to contain 30 mg L^{-1} of sulfide at the flow rate of 10000 m^3 day^{-1}. In **Table 8.2** an overview of all the assumptions used in the calculation of the investment and operational costs are presented.

Table 8.2 Assumptions for the calculation of the investment and operational costs of an electrochemical cell equipped with Ti/TiO_2 NTA-Mn_xO_y anode.

Investment costs	Unit	Value
Cost of anode material	euro m^{-2}	110
Cell potential	V	2
Current density	mA cm^{-2}	0.15
Cost kW h	€	0.8
Duration of treatment	h	12
Frequency of treatment	times per week	7
Flow rate	m^3 day^{-1}	10000
Sulfide concentration	mg L^{-1}	30

Table 8.3 Estimation of the capital and operating costs for sulfide removal from sewage based on the assumption that the required anode surface area is 100 m^2.

Investment costs	**Unit**	**Value**
Required anode surface area	m^2	50
Anode and cathode costs [a)]	€	5325
Additional costs [b)]	€	1600
Total estimated investment costs	€	6922.5
Operational costs	**Unit**	**Value**
Power input	W	312
Energy input	kW h day^{-1}	3.75
Estimated energy costs	€ $year^{-1}$	1095
Total cost (annual basis)	**Unit**	**Value**
Total cost (estimated lifetime 1 year)	€ m^{-3}	0.0021
	€ kg^{-1} S	0.073
Total cost (estimated lifetime 5 years)	€ m^{-3}	0.0006
	€ kg^{-1} S	0.022

[a)]Assuming that the counter electrode is made of stainless-steel mesh with surface area of 50 m^2, [b)]Based on the assumption that the additional costs represent 20% of the total cost of the electrochemical system.

Zhang et al. estimated that the cost of sulfide removal by chemical addition at € 1.9 – 7.2 kg^{-1} S without consideration of the capital costs and costs associated with the storage of chemicals. The cost of the electrochemical abatement of sulfide was calculated at € 0.53 – 0.75 kg^{-1} S. According to the calculations presented here, the developed electrochemical system based on the Ti/TiO_2 NTA-Mn_xO_y can further reduce the cost of sulfide control to € 0.073 kg^{-1} S even if an electrode lifetime is only 1 year. Ti/TiO_2 NTA-Mn_xO_y anodes are expected to be highly selective towards sulfide oxidation since removal of organic matter evaluated as COD removal in the batch experiments was minimal. Moreover, considering low energy requirements of the cell, solar panel can be used to drive the electrochemical cell. In this way, the system can be independent of the electrical grid. However, long-

term experiments at larger scale are required to validate the process parameters including the exact electrode lifetime, and accurately assess the costs of the proposed approach.

8.3 Engineering and process considerations

Wastewater flow through sewer networks varies significantly over time following the diurnal pattern. Flow rates in the sewer systems typically correspond with the human activity, reaching the highest velocities in the morning and evening hours. The up-flow velocity during the night is the lowest due to the absence of any pumping events. Considering the highest flow and thus the lowest sulfide concentration during the daytime, and the longest hydraulic retention time (HRT) during the night-time, the electrochemical cell can operate during night-time only.

The harsh environments of sewer networks may lead to considerable operational problems for an electrochemical system installed directly inside the pipeline. For instance, wastewater stream often contains grease or debris that can build up causing blockages and obstructing cell operation. Solution of such problem would require external intervention and down-time of the system, therefore, the potential occurrence of build-up must be prevented at the stage of the cell design. Practice shows that the dimensions of the flow channels of at least 50 mm can effectively avoid the blockage of the system. Such configuration can be achieved by placing the sequence of parallel plates with the distance of 50 mm in flow by mode or by operating in flow through mode using mesh anodes with the opening of 50 mm. However, the surface area of the mesh anodes with such dimensions might not be sufficient to achieve the desired level of sulfide removal. The system equipped with cylinder, tube or impeller-shaped electrodes is prone to blockages. Furthermore, the anode configuration that enables its rotation (i.e., cylinder, tube or impeller) can enhance the mass transfer to the surface of the electrode and substantially improve the sulfide removal kinetics,

which is especially beneficial considering low flow rate typically observed during the night-time. Finally, such smoothly shaped electrodes without any sharp or uneven points can effectively avoid ragging, which may arise from accumulation and wrapping of fibrous materials. Alternatively, the chance of blockage and ragging can be successfully minimized by preconditioning of a non-dispersible waste through grinding prior to the electrochemical unit, though, this approach elevates capital and operating costs of the system.

Further practical problems can arise from settling and accumulation of the particles including colloids naturally present in the waste stream (e.g., organics matter, clay particles, plankton and other dispersed moieties) as well as the colloidal sulfur produced as a result of the treatment. The accumulation of the colloidal particles can be prevented by flushing that occurs if the up-flow velocity of the stream is sufficiently high (i.e., > 0.8 m s^{-1}). Hence, the particles, that are settled overnight can be effectively removed at elevated flow-through velocity typical for "morning flush". Another potential operating problem is associated with the biofilm growth, which often occurs at anodes with low potential. The formation of a biofilm containing electrochemical active bacteria favors the removal of organics and decreases the sulfide removal efficiency. Since strong oxidizing potential is unfavourable for bacterial growth, biofilm accumulation can be prevented by regular increase of anodic potential.

8.4 Opportunities for future research

1) According to the calculations presented in the previous chapter, substitution of the conventional MMO anodes with the Ti/TiO_2 NTA-MnO_2 can reduce the cost of the sulfide control in sewer systems from € 0.53 – 0.75 kg^{-1} S to € 0.073 – 0.022 kg^{-1} S, thus, clearly demonstrating promising economic potential of the developed approach. However, the obtained cost is based on the

results of the bench scale experiments as well as several simplified assumptions. Therefore, the next obvious step is to verify the calculated number by performing the experiment at larger scale over long period of time. If possible, these experiments should be performed at the scale that would enable the sulfide control in the entire raising main section, which would allow the realistic comparison between the proposed approach and other strategies for sulfide control and removal. Moreover, such test would enable the evaluation of the Ti/TiO_2 NTA-MnO_2 anode and reliable estimation of its lifetime under realistic conditions.

2) After ensuring the efficiency of the Ti/TiO_2 NTA-MnO_2 anodes at bigger scale over a long time, its excellent performance can be exploited beyond the sulfide control in sewers. For instance, numerous industries including pulp and paper, tanning and petrochemical generate effluent rich in sulfide, which also leads to severe corrosion of the pipe network as well as malodour and toxicity issues. Unlike sewage, industrial wastewater is characterised by the high conductivity and moderate to high sulfide concentrations. For instance, spent caustic streams typically have a conductivity of 93 mS cm^{-1} and sulfide concentrations of 240 mM, while geothermal brines often contain 60 mM of sulfide. The safe discharge of such streams into water bodies requires removal of sulfide, which is typically achieved by either wet air oxidation at high temperatures and pressure or by addition of chemicals. As was discussed in Chapter 1, such sulfide removal techniques are associated with high energy input requirements, continuous need for chemical dosing or formation of toxic sludge that requires post treatment. Several studies demonstrated that electrochemical technique is an attractive alternative to conventional methods for sulfide removal from industrial wastewater as it achieves effective sulfide control at reduced capital and operating costs. However, substitution of conventional anode material (i.e MMO) with low-cost Ti/TiO_2 NTA-MnO_2 can make an electrochemical approach even more attractive by decreasing the energy input and avoiding electrode passivation with sulfur. Low content of suspended solids allows application of high surface area three-dimensional structures such as Ti

foam or entangled Ti, which can improve the performance of the cell for highly concentrated sulfide solutions.

3) Hydrogen sulfide also represents a serious problem in anaerobic digestion [373]. Hydrogen sulfide, produced by the SRB, tends to volatilize from the liquid phase and mix with the produced methane, reaching concentrations of up to 20000 ppm in extreme cases [374]. Even though the hydrogen sulfide content typically observed in the biogas is normally lower (e.g., 500-5000 ppm), it still causes severe corrosion of piping and pumps associated with the biogas transportation and storage [374, 375]. Furthermore, upon combustion, hydrogen sulfide leads to the corrosion of the engines, rapid degradation of the engine lube oil and sulfur dioxide emissions. To comply with the equipment tolerance, the maximum allowed hydrogen sulfide concentration in the biogas utilized in the internal combustion engine is limited between 200 and 500 ppm [374, 376]. In the case of direct injection of the upgraded biomethane into the natural gas pipeline, hydrogen sulfide content must be reduced below 4 ppm [377].

The most popular approach for the hydrogen sulfide removal from the biogas is Claus process, which is based on multistage catalytic oxidation of hydrogen sulfide at 1000-1200ºC [378, 379]. This simple and easy to operate process enables robust sulfide removal coupled with sulfur recovery [380]. However, Claus process is very energy intensive, moreover, it requires gas stream with high hydrogen sulfide content at high flow through velocity [381]. The desulfurization of the biogas can be achieved using physico-chemical (i.e., precipitation with iron salts, absorption or adsorption) or biological methods (i.e., microaeration, biofiltration or bioscrubbing) [382, 383]. Physicochemical treatment processes have high chemical and energy consumption, making biological desulfurization techniques such as Thiopaq® (Paques, The Netherlands) and Sulfothane™ (Veolia, France) the preferred biogas treatment options at small scale, for low- and

medium-strength sulfide-containing gas streams Even though the bioscrubbers are capable of effective and robust sulfide removal and recovery, they are associated with several important limitations. For example, bioscrubbing requires gas streams with high hydrogen sulfide content, while insufficient sulfide concentration in the feed may lead to failure of the biological processes [384, 385]. Moreover, low sulfide concentration can significantly reduce the selectivity of the process, leading to the accumulation of sulfate and thiosulfate in the absorbent [384, 385]. Prevention of the processes failure due to the accumulation of the dissolved sulfur species requires a bleed stream, with further increases substantially the operational costs associated with this approach [386].

Given the small footprint, low cost, stability, high efficiency and selectivity of the Ti/TiO_2 NTA-MnO_2 anodes for sulfide oxidation to elemental sulfur, the sulfide control approach proposed in this study can become a technology for the biogas desulfurization and upgrading. Unlike most of the existing biogas desulfurization methods, electrocatalytic approach does not require a continuous dosage of chemicals, which makes it more economical and sustainable. Moreover, low sulfide concentration, which typically leads to serious operation problems in the bioscrubbers, does not affect the efficiency or selectivity of the electrocatalytic treatment developed in this thesis. The resulting elemental sulfur can be easily separated from the suspension by simple sedimentation, hence, enabling a complete recovery and subsequent recirculation of the alkaline absorbent. Finally, sulfur, produced with the proposed approach can be reused as a fertilizer or as a valuable industrial chemical reincorporated into the production lines of other industries. This approach for biogas desulfurization has the potential to develop into a true green technology, that not only provides enormous savings in operational costs especially in comparison with technologies currently available at the market, but also enables extraction of a valuable product.

Chapter 9. Conclusions

The present thesis explored the potential of electrochemical and electrocatalytic techniques for sulfide control in sewer systems. For this purpose, the performance low-cost carbon-based felts applied for sulfide oxidation was evaluated. Furthermore, novel electrode materials such as graphite felt coated with catalytically active MnO_2 or Ti plate with TiO_2 nanotube array interlayer coated with MnO_2 were developed and applied for sulfide oxidation. The problem of sulfur passivation, typically observed in direct electrochemical sulfide oxidation processes, was also addressed by testing different regeneration strategies and approaches.

The main conclusions of this thesis are:

Electrochemical sulfide oxidation can be performed at the high surface carbon-based electrodes such as graphite and activated carbon felts, however, the kinetics of sulfide oxidation at such electrodes is rather slow. Moreover, long-term application of carbon-based electrodes is limited due to accumulation of sulfur, which will eventually lead to the process failure as complete sulfur recovery could not be achieved using simple approaches based on aqueous solutions:

- The graphite felt anode oxidizes sulfide to sulfur even at low anode potentials.
- The chemisorption of sulfide is the major removal mechanism at the activated carbon felt, and the application of the anode potential did not significantly increase the sulfide removal rates.
- The elemental sulfur chemisorbed at the activated carbon felt could not be removed by any of the investigated strategies due to the incorporation of sulfur into the carbon matrix, and its removal would likely require the use of organic solvents.

- Only partial dissolution of the sulfur electrodeposited at the graphite felt could be achieved under cathodic polarization.

- Electrochemical sulfide oxidation to elemental sulfur was also achieved using real sewage as a supporting electrolyte.

The application of the GF-MnO_2 electrodes significantly enhanced the sulfide removal kinetics compared to carbon-based electrodes. Notwithstanding that continuous regeneration of the MnO_2 catalyst that was achieved by anodic polarisation of the electrode, the initial catalytic activity GF-MnO_2 electrodes was decreased upon sulfur loading. The electrode activity could not be fully restored through cathodic polarisation due to its negative impact on MnO_2 coating stability:

- The GF-MnO_2 electrodes demonstrated excellent (electro)catalytic activity and selectivity for sulfide oxidation to sulfur at significantly higher rates compared to bare graphite felt (i.e., $9.2 \cdot 10^{-6}\ m^3\ h^{-1}\ m^{-2}$ and $6 \cdot 10^{-4}\ m^3\ h^{-1}\ m^{-2}$ for graphite felt and GF-MnO_2, respectively).

- The anodic polarization at low potentials (i.e., 0.4-0.8 V/SHE) did not enhance the sulfide oxidation rate, however, it enabled a continuous re-oxidation of the reduced MnO_2 coating after its reaction with sulfide.

- Gradual electrode passivation with the deposited sulfur was slowed down by the cathodic recovery, however, complete recovery and dissolution of the elemental sulfur layer at the electrode surface could not be achieved due to the associated dissolution of the MnO_2 coating during the cathodic polarization.

- In real sewage, deposition of sulfur at the electrode surface was only partial as production of colloidal sulfur was also observed.

The Ti/TiO_2 NTA-MnO_2 anodes demonstrated excellent stability, catalytic activity for sulfide oxidation and high selectivity towards elemental sulfur in different experimental condition. The produced elemental sulfur was desorbed from the electrode surface, thus avoiding the gradual performance loss:

- The enhanced electron transfer between the Ti/TiO_2 NTA substrate and the MnO_2 coating resulted in fast sulfide oxidation kinetics comparable to materials with high specific surface area (i.e., $175 \cdot 10^{-4}$ m^3 h^{-1} m^{-2} and $6 \cdot 10^{-4}$ m^3 h^{-1} m^{-2} for Ti/TiO_2NTA-MnO_2 and GF-Mn_2O_3, respectively).

- Sulfide can be rapidly removed even at very lower sulfide concentrations (i.e., <1 mM).

- Increase of potential from 0.4 V to 0.8 V/SHE accelerated the MnO_2 re-oxidation and enhanced the sulfide removal kinetics.

- Decreasing the pH from pH 12 to pH 8 accelerated the sulfide removal rates and enabled the desorption of the elemental sulfur from the anode surface, which helped prevent the electrode passivation.

- The sulfide oxidation rate was slightly decreased in the real sewage due to the competition imposed by the presence of other ions. Similar to the synthetic electrolyte at pH 8, the final product of the treatment was colloidal sulfur.

References

[1] I. Pikaar, R.A. Rozendal, Z. Yuan, J. Keller, K. Rabaey, Electrochemical sulfide oxidation from domestic wastewater using mixed metal-coated titanium electrodes, Water Research, 45 (2011) 5381-5388.
[2] B. Meyer, Elemental sulfur, Chemical Reviews, 76 (1976) 367-388.
[3] R. Steudel, Aqueous Sulfur Sols, in: R. Steudel (Ed.) Elemental Sulfur and Sulfur-Rich Compounds I, Springer Berlin Heidelberg, Berlin, Heidelberg, 2003, pp. 153-166.
[4] R. Steudel, B. Eckert, Solid Sulfur Allotropes, 2003, pp. 1-80.
[5] R. Steudel, Sulfur-rich oxides SnO and SnO2 (n > 1), 2003, pp. 203-230.
[6] V.V. Brazhkin, S.V. Popova, R.N. Voloshin, Pressure–temperature phase diagram of molten elements: selenium, sulfur and iodine, Physica B: Condensed Matter, 265 (1999) 64-71.
[7] R. Steudel, Liquid Sulfur, 2003, pp. 81-116.
[8] R.J. Huxtable, The Chemistry of Sulfur, Biochemistry of Sulfur, Springer US, Boston, MA, 1986, pp. 1-9.
[9] M. Pourbaix, Atlas of electrochemical equilibria in aqueous solutions, First English edition. ed., Pergamon Press, Oxford, 1966.
[10] N.N. Greenwood, A. Earnshaw, 15 - Sulfur, Chemistry of the Elements (Second Edition), Butterworth-Heinemann, Oxford, 1997, pp. 645-746.
[11] R. Steudel, Homocyclic sulfur molecules, Inorganic Ring Systems, Springer Berlin Heidelberg, Berlin, Heidelberg, 1982, pp. 149-176.
[12] J.J. Griebel, R.S. Glass, K. Char, J. Pyun, Polymerizations with elemental sulfur: A novel route to high sulfur content polymers for sustainability, energy and defense, Progress in Polymer Science, 58 (2016) 90-125.
[13] A. Le Faou, B.S. Rajagopal, L. Daniels, G. Fauque, Thiosulfate, polythionates and elemental sulfur assimilation and reduction in the bacterial world, FEMS Microbiology Letters, 75 (1990) 351-382.
[14] S. Ralf, G. Thomas, H. Gabriele, The Molecular Composition of Hydrophilic Sulfur Sols Prepared by Acid Decomposition of Thiosulfate [1], Zeitschrift für Naturforschung B, 43 (1988) 203-218.
[15] A.A. Garcia, Jr., G.K. Druschel, Elemental sulfur coarsening kinetics, Geochem Trans, 15 (2014) 11-11.
[16] W.E. Kleinjan, A. de Keizer, A.J.H. Janssen, Biologically Produced Sulfur, in: R. Steudel (Ed.) Elemental Sulfur and Sulfur-Rich Compounds I, Springer Berlin Heidelberg, Berlin, Heidelberg, 2003, pp. 167-188.
[17] F.-C.A. Kafantaris, G.K. Druschel, Kinetics of the nucleophilic dissolution of hydrophobic and hydrophilic elemental sulfur sols by sulfide, Geochimica et Cosmochimica Acta, 269 (2020) 554-565.
[18] M. Abdollahi, A. Hosseini, Hydrogen Sulfide, in: P. Wexler (Ed.) Encyclopedia of Toxicology (Third Edition), Academic Press, Oxford, 2014, pp. 971-974.
[19] O. Kabil, R. Banerjee, Redox biochemistry of hydrogen sulfide, The Journal of biological chemistry, 285 (2010) 21903-21907.
[20] F.J. Millero, The thermodynamics and kinetics of the hydrogen sulfide system in natural waters, Marine Chemistry, 18 (1986) 121-147.
[21] E. Cuevasanta, M.N. Moller, B. Alvarez, Biological chemistry of hydrogen sulfide and persulfides, Archives of biochemistry and biophysics, 617 (2017) 9-25.

[22] A.A. Douabul, J.P. Riley, The solubility of gases in distilled water and seawater—V. hydrogen sulphide, Deep Sea Research Part A. Oceanographic Research Papers, 26 (1979) 259-268.
[23] S. Riahi, C.N. Rowley, Solvation of Hydrogen Sulfide in Liquid Water and at the Water–Vapor Interface Using a Polarizable Force Field, The Journal of Physical Chemistry B, 118 (2014) 1373-1380.
[24] R.C. Ropp, Chapter 3 - Group 16 (O, S, Se, Te) Alkaline Earth Compounds, in: R.C. Ropp (Ed.) Encyclopedia of the Alkaline Earth Compounds, Elsevier, Amsterdam, 2013, pp. 105-197.
[25] K.Y. Chen, J.C. Morris, Kinetics of oxidation of aqueous sulfide by oxygen, Environmental Science & Technology, 6 (1972) 529-537.
[26] W. Giggenbach, Optical spectra of highly alkaline sulfide solutions and the second dissociation constant of hydrogen sulfide, Inorganic Chemistry, 10 (1971) 1333-1338.
[27] D. Peramunage, F. Forouzan, S. Licht, Activity and spectroscopic analysis of concentrated solutions of potassium sulfide, Analytical Chemistry, 66 (1994) 378-383.
[28] P.M. May, D. Batka, G. Hefter, E. Königsberger, D. Rowland, Goodbye to S2− in aqueous solution, Chemical Communications, 54 (2018) 1980-1983.
[29] M. Holmer, H. Hasler-Sheetal, Sulfide intrusion in seagrasses assessed by stable sulfur isotopes-A synthesis of current results, Frontiers in Marine Science, 1 (2014).
[30] E.R. DeLeon, G.F. Stoy, K.R. Olson, Passive loss of hydrogen sulfide in biological experiments, Analytical biochemistry, 421 (2012) 203-207.
[31] Q. Li, J.R. Lancaster, Chemical foundations of hydrogen sulfide biology, Nitric Oxide, 35 (2013) 21-34.
[32] F.J. Millero, A. LeFerriere, M. Fernandez, S. Hubinger, J.P. Hershey, Oxidation of hydrogen sulfide with hydrogen peroxide in natural waters, Environmental Science & Technology, 23 (1989) 209-213.
[33] H. Golchoubian, F. Hosseinpoor, Effective oxidation of sulfides to sulfoxides with hydrogen peroxide under transition-metal-free conditions, Molecules, 12 (2007) 304-311.
[34] A.P. Black, J.B. Goodson, The Oxidation of Sulfides by Chlorine in Dilute Aqueous Solutions, Journal (American Water Works Association), 44 (1952) 309-316.
[35] S. Glavas, S. Toby, Reaction between ozone and hydrogen sulfide, The Journal of Physical Chemistry, 79 (1975) 779-782.
[36] A.H.M. Veeken, L. Akoto, L.W. Hulshoff Pol, J. Weijma, Control of the sulfide (S2−) concentration for optimal zinc removal by sulfide precipitation in a continuously stirred tank reactor, Water Research, 37 (2003) 3709-3717.
[37] L. Altaş, H. Büyükgüngör, Sulfide removal in petroleum refinery wastewater by chemical precipitation, Journal of Hazardous Materials, 153 (2008) 462-469.
[38] N. Karbanee, R.P. van Hille, A.E. Lewis, Controlled Nickel Sulfide Precipitation Using Gaseous Hydrogen Sulfide, Industrial & Engineering Chemistry Research, 47 (2008) 1596-1602.
[39] J. Gun, A.D. Modestov, A. Kamyshny, D. Ryzkov, V. Gitis, A. Goifman, O. Lev, V. Hultsch, T. Grischek, E. Worch, Electrospray Ionization Mass Spectrometric Analysis of Aqueous Polysulfide Solutions, Microchimica Acta, 146 (2004) 229-237.
[40] A. Kamyshny, A. Goifman, J. Gun, D. Rizkov, O. Lev, Equilibrium Distribution of Polysulfide Ions in Aqueous Solutions at 25 °C: A New Approach for the Study of Polysulfides' Equilibria, Environmental Science & Technology, 38 (2004) 6633-6644.

[41] K. Avetisyan, T. Buchshtav, A. Kamyshny, Kinetics and mechanism of polysulfides formation by a reaction between hydrogen sulfide and orthorhombic cyclooctasulfur, Geochimica et Cosmochimica Acta, 247 (2019) 96-105.
[42] K.Y. Chen, S.K. Gupta, Formation of Polysulfides in Aqueous Solution, Environmental Letters, 4 (1973) 187-200.
[43] C.G. Lindsay, G.V. Gibbs, A molecular orbital study of bonding in sulfate molecules: Implications for sulfate crystal structures, Physics and Chemistry of Minerals, 15 (1988) 260-270.
[44] H.W. Ruben, D.H. Templeton, R.D. Rosenstein, I. Olovsson, Crystal Structure and Entropy of Sodium Sulfate Decahydrate, Journal of the American Chemical Society, 83 (1961) 820-824.
[45] D. Rickard, Chapter 2 - Sulfur Chemistry in Aqueous Solutions, in: D. Rickard (Ed.) Developments in Sedimentology, Elsevier2012, pp. 31-83.
[46] T.A. Hansen, Metabolism of sulfate-reducing prokaryotes, Antonie van Leeuwenhoek, 66 (1994) 165-185.
[47] V.V. Trachevskii, S.V. Zimina, E.P. Rodina, Thiosulfate metal complexes, Russian Journal of Coordination Chemistry, 34 (2008) 664.
[48] R.H. Dinegar, R.H. Smellie, V.K.L. Mer, Kinetics of the Acid Decomposition of Sodium Thiosulfate in Dilute Solutions, Journal of the American Chemical Society, 73 (1951) 2050-2054.
[49] F.P. Terraglio, R.M. Manganelli, The Absorption of Atmospheric Sulfur Dioxide by Water Solutions, Journal of the Air Pollution Control Association, 17 (1967) 403-406.
[50] E.C. Fuller, R.H. Crist, The Rate of Oxidation of Sulfite Ions by Oxygen, Journal of the American Chemical Society, 63 (1941) 1644-1650.
[51] Y. Li, K. Tang, L. Zhang, Z. Zhao, X. Xie, C.-T.A. Chen, D. Wang, N. Jiao, Y. Zhang, Coupled Carbon, Sulfur, and Nitrogen Cycles Mediated by Microorganisms in the Water Column of a Shallow-Water Hydrothermal Ecosystem, Frontiers in microbiology, 9 (2018).
[52] B.B. Jørgensen, A.J. Findlay, A. Pellerin, The Biogeochemical Sulfur Cycle of Marine Sediments, Frontiers in microbiology, 10 (2019).
[53] M. Jahanbani Veshareh, H.M. Nick, A sulfur and nitrogen cycle informed model to simulate nitrate treatment of reservoir souring, Scientific Reports, 9 (2019) 7546.
[54] R. Berner, S. Petsch, The Sulfur Cycle and Atmospheric Oxygen, Science, 282 (1998) 1426-1427.
[55] D.E. Canfield, K. Erik, T. Bo, The Sulfur Cycle, in: D.E. Canfield, E. Kristensen, B. Thamdrup (Eds.) Advances in Marine Biology, Academic Press2005, pp. 313-381.
[56] S.H. Bottrell, R.J. Newton, Reconstruction of changes in global sulfur cycling from marine sulfate isotopes, Earth-Science Reviews, 75 (2006) 59-83.
[57] P. Brimblecombe, The Global Sulfur Cycle, Treatise on Geochemistry: Second Edition, Elsevier Inc.2013, pp. 559-591.
[58] Y. Gao, M. Ma, T. Yang, W. Chen, T. Yang, Global atmospheric sulfur deposition and associated impaction on nitrogen cycling in ecosystems, Journal of Cleaner Production, 195 (2018) 1-9.
[59] P.A. Loka Bharathi, Sulfur Cycle, in: S.E. Jørgensen, B.D. Fath (Eds.) Encyclopedia of Ecology, Academic Press, Oxford, 2008, pp. 3424-3431.
[60] I. Cardoso Pereira, M. Martins, Sulfate-reducing bacteria as new microorganisms for biological hydrogen production, International Journal of Hydrogen Energy, 38 (2013) 12294-12301.

[61] B. Thamdrup, H. Fossing, B.B. Jørgensen, Manganese, iron and sulfur cycling in a coastal marine sediment, Aarhus bay, Denmark, Geochimica et Cosmochimica Acta, 58 (1994) 5115-5129.
[62] W.F. Guerin, R.S. Braman, Patterns of organic and inorganic sulfur transformations in sediments, Organic Geochemistry, 8 (1985) 259-268.
[63] H.L. Ehrlich, Geomicrobiology, The Quarterly Review of Biology, 78 (2003) 229-229.
[64] L.L. Barton, M.-L. Fardeau, G.D. Fauque, Hydrogen Sulfide: A Toxic Gas Produced by Dissimilatory Sulfate and Sulfur Reduction and Consumed by Microbial Oxidation, in: P.M.H. Kroneck, M.E.S. Torres (Eds.) The Metal-Driven Biogeochemistry of Gaseous Compounds in the Environment, Springer Netherlands, Dordrecht, 2014, pp. 237-277.
[65] L.L. Barton, G.D. Fauque, Chapter 2 Biochemistry, Physiology and Biotechnology of Sulfate-Reducing Bacteria, Advances in Applied Microbiology, Academic Press2009, pp. 41-98.
[66] P.A. Trudinger, Assimilatory and Dissimilatory Metabolism of Inorganic Sulphur Compounds by Micro-Organisms, in: A.H. Rose, J.F. Wilkinson (Eds.) Advances in Microbial Physiology, Academic Press1969, pp. 111-158.
[67] E. Bertran, W.D. Leavitt, A. Pellerin, G.M. Zane, J.D. Wall, I. Halevy, B.A. Wing, D.T. Johnston, Deconstructing the Dissimilatory Sulfate Reduction Pathway: Isotope Fractionation of a Mutant Unable of Growth on Sulfate, Frontiers in microbiology, 9 (2018).
[68] V. Krukenberg, D. Riedel, H.R. Gruber-Vodicka, P.L. Buttigieg, H.E. Tegetmeyer, A. Boetius, G. Wegener, Gene expression and ultrastructure of meso- and thermophilic methanotrophic consortia, Environmental Microbiology, 20 (2018) 1651-1666.
[69] J.M. Shively, L. Barton, Variations in autotrophic life, Academic Press, London; San Diego; New York, 1991.
[70] M. Dworkin, The prokaryotes. a handbook on the biology of bacteria Vol. 2, Vol. 2, Springer, New York, 2007.
[71] J. Boulegue, Solubility of Elemental Sulfur in Water at 298 K, Phosphorus and Sulfur and the Related Elements, 5 (1978) 127-128.
[72] D. Pokorna, J. Zabranska, Sulfur-oxidizing bacteria in environmental technology, Biotechnology Advances, 33 (2015) 1246-1259.
[73] L.A. Robertson, J.G. Kuenen, The Colorless Sulfur Bacteria, in: M. Dworkin, S. Falkow, E. Rosenberg, K.-H. Schleifer, E. Stackebrandt (Eds.) The Prokaryotes: Volume 2: Ecophysiology and Biochemistry, Springer New York, New York, NY, 2006, pp. 985-1011.
[74] B. De Gusseme, P. De Schryver, M. De Cooman, K. Verbeken, P. Boeckx, W. Verstraete, N. Boon, Nitrate-reducing, sulfide-oxidizing bacteria as microbial oxidants for rapid biological sulfide removal, FEMS Microbiology Ecology, 67 (2009) 151-161.
[75] A.J.H. Janssen, S. Meijer, J. Bontsema, G. Lettinga, Application of the redox potential for controling a sulfide oxidizing bioreactor, Biotechnology and bioengineering, 60 (1998) 147-155.
[76] K. Finster, W. Liesack, B. Thamdrup, Elemental Sulfur and Thiosulfate Disproportionation by Desulfocapsa sulfoexigens sp. nov., a New Anaerobic Bacterium Isolated from Marine Surface Sediment, Applied and Environmental Microbiology, 64 (1998) 119-125.
[77] H. Cypionka, A.M. Smock, M.E. Böttcher, A combined pathway of sulfur compound disproportionation in Desulfovibrio desulfuricans, FEMS Microbiology Letters, 166 (1998) 181-186.

[78] L.P.M. Lamers, H.B.M. Tomassen, J.G.M. Roelofs, Sulfate-Induced Eutrophication and Phytotoxicity in Freshwater Wetlands, Environmental Science & Technology, 32 (1998) 199-205.
[79] W.D. Heizer, R.S. Sandler, E. Seal, Jr., S.C. Murray, M.G. Busby, B.G. Schliebe, S.N. Pusek, Intestinal effects of sulfate in drinking water on normal human subjects, Digestive diseases and sciences, 42 (1997) 1055-1061.
[80] D.J. Soucek, A.J. Kennedy, Effects of hardness, chloride, and acclimation on the acute toxicity of sulfate to freshwater invertebrates, Environ Toxicol Chem, 24 (2005) 1204-1210.
[81] D. Acha C, S. Guedron, D. Amouroux, D. Point, X. Lazzaro, P. Fernandez, G. Sarret, Algal Bloom Exacerbates Hydrogen Sulfide and Methylmercury Contamination in the Emblematic High-Altitude Lake Titicaca, Geosciences (Switzerland), 8 (2018) 438.
[82] R. Tostevin, A.V. Turchyn, J. Farquhar, D.T. Johnston, D.L. Eldridge, J.K.B. Bishop, M. McIlvin, Multiple sulfur isotope constraints on the modern sulfur cycle, Earth and Planetary Science Letters, 396 (2014) 14-21.
[83] H. Wang, Q. Zhang, Research Advances in Identifying Sulfate Contamination Sources of Water Environment by Using Stable Isotopes, Int J Environ Res Public Health, 16 (2019) 1914.
[84] D. Julian, K.L. April, S. Patel, J.R. Stein, S.E. Wohlgemuth, Mitochondrial depolarization following hydrogen sulfide exposure in erythrocytes from a sulfide-tolerant marine invertebrate, The Journal of experimental biology, 208 (2005) 4109-4122.
[85] D. Kraus, J. Doeller, C. Powell, Sulfide may directly modify cytoplasmic hemoglobin deoxygenation in Solemya reidi gills, The Journal of experimental biology, 199 (1996) 1343-1352.
[86] T. Bagarinao, Sulfide as an environmental factor and toxicant: tolerance and adaptations in aquatic organisms, Aquatic Toxicology, 24 (1992) 21-62.
[87] P. Nicholls, D.C. Marshall, C.E. Cooper, M.T. Wilson, Sulfide inhibition of and metabolism by cytochrome c oxidase, Biochemical Society transactions, 41 (2013) 1312-1316.
[88] B. Boström, J.M. Andersen, S. Fleischer, M. Jansson, Exchange of phosphorus across the sediment-water interface, Hydrobiologia, 170 (1988) 229-244.
[89] N.F. Caraco, J.J. Cole, G.E. Likens, Evidence for sulphate-controlled phosphorus release from sediments of aquatic systems, Nature, 341 (1989) 316-318.
[90] B. Doujaiji, J.A. Al-Tawfiq, Hydrogen sulfide exposure in an adult male, Ann Saudi Med, 30 (2010) 76-80.
[91] Å.D. Austigard, K. Svendsen, K.K. Heldal, Hydrogen sulphide exposure in waste water treatment, J Occup Med Toxicol, 13 (2018) 10-10.
[92] J. Stanek, J. Gift, G. Woodall, G. Foureman, Hydrogen Sulfide: Integrative Analysis of Acute Toxicity Data for Estimating Human Health Risk⋆⋆This article has been reviewed by the National Center for Environmental Assessment, US Environmental Protection Agency, and approved for publication. Approval does not signify that the contents necessarily reflect the views and policies of the agency, nor does the mention of trade names or commercial products constitute endorsement or recommendation for use, in: J.O. Nriagu (Ed.) Encyclopedia of Environmental Health, Elsevier, Burlington, 2011, pp. 124-139.
[93] S. Rahnama-Moghadam, L.D. Hillis, R.A. Lange, Chapter 3 - Environmental Toxins and the Heart, in: M. Ramachandran (Ed.) Heart and Toxins, Academic Press, Boston, 2015, pp. 75-132.
[94] S. Nogué, R. Pou, J. Fernández, P. Sanz-Gallén, Fatal hydrogen sulphide poisoning in unconfined spaces, Occupational Medicine, 61 (2011) 212-214.

[95] O. World Health, Guidelines for drinking-water quality: fourth edition incorporating first addendum, 4th ed + 1st add ed., World Health Organization, Geneva, 2017.
[96] S. Tavakoli Kivi, R.T. Bailey, Modeling sulfur cycling and sulfate reactive transport in an agricultural groundwater system, Agricultural Water Management, 185 (2017) 78-92.
[97] D. Kaown, D.-C. Koh, B. Mayer, K.-K. Lee, Identification of nitrate and sulfate sources in groundwater using dual stable isotope approaches for an agricultural area with different land use (Chuncheon, mid-eastern Korea), Agriculture, Ecosystems & Environment, 132 (2009) 223-231.
[98] J.L. Huisman, G. Schouten, C. Schultz, Biologically produced sulphide for purification of process streams, effluent treatment and recovery of metals in the metal and mining industry, Hydrometallurgy, 83 (2006) 106-113.
[99] P.K. Dutta, K. Rabaey, Z. Yuan, R.A. Rozendal, J. Keller, Electrochemical sulfide removal and recovery from paper mill anaerobic treatment effluent, Water Research, 44 (2010) 2563-2571.
[100] E. Genschow, W. Hegemann, C. Maschke, Biological sulfate removal from tannery wastewater in a two-stage anaerobic treatment, Water Research, 30 (1996) 2072-2078.
[101] R. Bowell, A review of sulfate removal options for mine waters, Proceedings of Mine Water 2004-Process, Policy and Progress, (2004).
[102] C.A. Bondi, J.L. Marks, L.B. Wroblewski, H.S. Raatikainen, S.R. Lenox, K.E. Gebhardt, Human and Environmental Toxicity of Sodium Lauryl Sulfate (SLS): Evidence for Safe Use in Household Cleaning Products, Environ Health Insights, 9 (2015) 27-32.
[103] W. Rauch, M. Kleidorfer, Replace contamination, not the pipes, Science, 345 (2014) 734-735.
[104] R. Leung, D. Li, W. Yu, H. Chui, T. Lee, M. van Loosdrecht, G. Chen, Integration of seawater and grey water reuse to maximize alternative water resource for coastal areas: The case of the Hong Kong International Airport, Water science and technology : a journal of the International Association on Water Pollution Research, 65 (2012) 410-417.
[105] M. van Loosdrecht, D. Brdjanovic, H.K. Chui, G.H. Chen, A source for toilet flushing and for cooling, sewage treatment benefits, and phosphorus recovery: direct use of seawater in an age of rapid urbanisation, Water21, 21 (2012) 17-19.
[106] P.L. Ward, Sulfur dioxide initiates global climate change in four ways, Thin Solid Films, 517 (2009) 3188-3203.
[107] H. Rodhe, Human impact on the atmospheric sulfur balance, Tellus B: Chemical and Physical Meteorology, 51 (1999) 110-122.
[108] S. Kapitány, D. Nagy, J. Posta, Á. Béni, Determination of atmospheric sulphur dioxide and sulphuric acid traces by indirect flame atomic absorption method, Microchemical Journal, (2020) 104853.
[109] J.J. Su, Y.J. Chen, Monitoring of sulfur dioxide emission resulting from biogas utilization on commercial pig farms in Taiwan, Environmental monitoring and assessment, 187 (2015) 4109.
[110] R. Raiswell, Evolution of the global biogeochemical sulphur cycle, scope 39 edited by P. Brimblecombe and A. Y. Lein. John Wiley and Sons, Chichester, 1989. No. of pages: 241. Price: £56.95 (hardback), Geological Journal, 27 (1992) 192-193.
[111] C.N. Hewitt, The atmospheric chemistry of sulphur and nitrogen in power station plumes, Atmospheric Environment, 35 (2001) 1155-1170.

[112] R.K. Jain, Z.C. Cui, J.K. Domen, Chapter 4 - Environmental Impacts of Mining, in: R.K. Jain, Z.C. Cui, J.K. Domen (Eds.) Environmental Impact of Mining and Mineral Processing, Butterworth-Heinemann, Boston, 2016, pp. 53-157.
[113] A.L. Barach, Treatment of Sulfur Dioxide Poisoning, JAMA, 215 (1971) 485-485.
[114] H.-M. Hung, M.R. Hoffmann, Oxidation of Gas-Phase SO2 on the Surfaces of Acidic Microdroplets: Implications for Sulfate and Sulfate Radical Anion Formation in the Atmospheric Liquid Phase, Environmental Science & Technology, 49 (2015) 13768-13776.
[115] L. Yao, O. Garmash, F. Bianchi, J. Zheng, C. Yan, J. Kontkanen, H. Junninen, S.B. Mazon, M. Ehn, P. Paasonen, M. Sipilä, M. Wang, X. Wang, S. Xiao, H. Chen, Y. Lu, B. Zhang, D. Wang, Q. Fu, F. Geng, L. Li, H. Wang, L. Qiao, X. Yang, J. Chen, V.-M. Kerminen, T. Petäjä, D.R. Worsnop, M. Kulmala, L. Wang, Atmospheric new particle formation from sulfuric acid and amines in a Chinese megacity, Science, 361 (2018) 278-281.
[116] M. Yang, T.G. Bell, F.E. Hopkins, T.J. Smyth, Attribution of atmospheric sulfur dioxide over the English Channel to dimethyl sulfide and changing ship emissions, Atmos. Chem. Phys., 16 (2016) 4771-4783.
[117] M. Sipilä, T. Berndt, T. Petäjä, D. Brus, J. Vanhanen, F. Stratmann, J. Patokoski, R.L. Mauldin, A.-P. Hyvärinen, H. Lihavainen, M. Kulmala, The Role of Sulfuric Acid in Atmospheric Nucleation, Science, 327 (2010) 1243-1246.
[118] M. Lippmann, Background on health effects of acid aerosols, Environmental health perspectives, 79 (1989) 3-6.
[119] A.K. Pattantyus, S. Businger, S.G. Howell, Review of sulfur dioxide to sulfate aerosol chemistry at Kīlauea Volcano, Hawai'i, Atmospheric Environment, 185 (2018) 262-271.
[120] A. Molnár, E. Mészáros, K. Imre, A. Rüll, Trends in visibility over Hungary between 1996 and 2002, Atmospheric Environment, 42 (2008) 2621-2629.
[121] W. Aas, A. Mortier, V. Bowersox, R. Cherian, G. Faluvegi, H. Fagerli, J. Hand, Z. Klimont, C. Galy-Lacaux, C.M.B. Lehmann, C.L. Myhre, G. Myhre, D. Olivié, K. Sato, J. Quaas, P.S.P. Rao, M. Schulz, D. Shindell, R.B. Skeie, A. Stein, T. Takemura, S. Tsyro, R. Vet, X. Xu, Global and regional trends of atmospheric sulfur, Scientific Reports, 9 (2019) 953.
[122] G. Gudjonsson, J. Vollertsen, T. Hvitved-Jacobsen, Dissolved oxygen in gravity sewers--measurement and simulation, Water Sci Technol, 45 (2002) 35-44.
[123] P.H. Nielsen, K. Raunkjær, N.H. Norsker, N.A. Jensen, T. Hvitved-Jacobsen, Transformation of Wastewater in Sewer Systems – A Review, Water Science and Technology, 25 (1992) 17-31.
[124] T. Hvitved-Jacobsen, J. Vollertsen, C. Yongsiri, A. Nielsen, S. Abdul-Talib, Sewer microbial processes, emissions and impacts, 2002.
[125] A.M. Alani, A. Faramarzi, M. Mahmoodian, K.F. Tee, Prediction of sulphide build-up in filled sewer pipes, Environmental technology, 35 (2014) 1721-1728.
[126] A. Sarti, M. Zaiat, Anaerobic treatment of sulfate-rich wastewater in an anaerobic sequential batch reactor (AnSBR) using butanol as the carbon source, Journal of Environmental Management, 92 (2011) 1537-1541.
[127] J. Vollertsen, T. Hvitved-Jacobsen, I. McGregor, R. Ashley, Aerobic microbial transformations of pipe and silt trap sediments from combined sewers, Water Science and Technology, 38 (1998) 249-256.
[128] T. Hvitved-Jacobsen, J. Vollertsen, A. Nielsen, Sewer Processes: Microbial and Chemical Process Engineering of Sewer Networks, 2013.

[129] A. Romanova, D.M. Mahmoodian, M. Alani, Influence and Interaction of Temperature, H2S and pH on Concrete Sewer Pipe Corrosion, International Journal of Civil, Architectural, Structural and Construction Engineering, 8 (2014) 592-595.
[130] C. Yongsiri, J. Vollertsen, T. Hvitved-Jacobsen, Effect of Temperature on Air-Water Transfer of Hydrogen Sulfide, Journal of Environmental Engineering-asce - J ENVIRON ENG-ASCE, 130 (2004).
[131] L. Carrera, F. Springer, G. Lipeme-Kouyi, P. Buffiere, A review of sulfide emissions in sewer networks: overall approach and systemic modelling, Water science and technology : a journal of the International Association on Water Pollution Research, 73 (2016) 1231-1242.
[132] A.H. Nielsen, T. Hvitved-Jacobsen, J. Vollertsen, Recent findings on sinks for sulfide in gravity sewer networks, Water science and technology : a journal of the International Association on Water Pollution Research, 54 (2006) 127-134.
[133] S. Okabe, M. Odagiri, T. Ito, H. Satoh, Succession of Sulfur-Oxidizing Bacteria in the Microbial Community on Corroding Concrete in Sewer Systems, Applied and Environmental Microbiology, 73 (2007) 971-980.
[134] M. Wu, T. Wang, K. Wu, L. Kan, Microbiologically induced corrosion of concrete in sewer structures: A review of the mechanisms and phenomena, Construction and Building Materials, 239 (2020) 117813.
[135] D.J. Roberts, D. Nica, G. Zuo, J.L. Davis, Quantifying microbially induced deterioration of concrete: initial studies, International Biodeterioration & Biodegradation, 49 (2002) 227-234.
[136] C. Parker, THE CORROSION OF CONCRETE, Australian Journal of Experimental Biology and Medical Science, 23 (1945) 91-98.
[137] I. Fernandes, M. Pericão, P. Hagelia, F. Noronha, M. Ribeiro, J. Maia, Identification of acid attack on concrete of a sewage system, Materials and Structures - MATER STRUCT, 45 (2012).
[138] J.L. Davis, D. Nica, K. Shields, D.J. Roberts, Analysis of concrete from corroded sewer pipe, International Biodeterioration & Biodegradation, 42 (1998) 75-84.
[139] R.L. Islander, J.S. Devinny, F. Mansfeld, A. Postyn, H. Shih, Microbial Ecology of Crown Corrosion in Sewers, Journal of Environmental Engineering, 117 (1991) 751-770.
[140] M. House, W. Weiss, Review of Microbially Induced Corrosion and Comments on Needs Related to Testing Procedures, 2014.
[141] A. Yousefi, A. Allahverdi, P. Hejazi, Accelerated biodegradation of cured cement paste by Thiobacillus species under simulation condition, International Biodeterioration & Biodegradation, 86 (2014) 317-326.
[142] A.P. Harrison, Jr., The acidophilic thiobacilli and other acidophilic bacteria that share their habitat, Annual review of microbiology, 38 (1984) 265-292.
[143] D. Nica, J.L. Davis, L. Kirby, G. Zuo, D.J. Roberts, Isolation and characterization of microorganisms involved in the biodeterioration of concrete in sewers, International Biodeterioration & Biodegradation, 46 (2000) 61-68.
[144] X. Li, U. Kappler, G. Jiang, P.L. Bond, The Ecology of Acidophilic Microorganisms in the Corroding Concrete Sewer Environment, Frontiers in Microbiology, 8 (2017).
[145] X. Li, L. O'Moore, Y. Song, P.L. Bond, Z. Yuan, S. Wilkie, L. Hanzic, G. Jiang, The rapid chemically induced corrosion of concrete sewers at high H2S concentration, Water research, 162 (2019) 95-104.

[146] T. Yamanaka, I. Aso, S. Togashi, M. Tanigawa, K. Shoji, T. Watanabe, N. Watanabe, K. Maki, H. Suzuki, Corrosion by bacteria of concrete in sewerage systems and inhibitory effects of formates on their growth, Water Research, 36 (2002) 2636-2642.
[147] G. Jiang, J. Keller, P.L. Bond, Determining the long-term effects of H(2)S concentration, relative humidity and air temperature on concrete sewer corrosion, Water Res, 65 (2014) 157-169.
[148] A.K. Parande, P.L. Ramsamy, S. Ethirajan, C.R.K. Rao, N. Palanisamy, Deterioration of reinforced concrete in sewer environments, Proceedings of the Institution of Civil Engineers - Municipal Engineer, 159 (2006) 11-20.
[149] J. Monteny, E. Vincke, A. Beeldens, N. De Belie, L. Taerwe, D. Van Gemert, W. Verstraete, Chemical, microbiological, and in situ test methods for biogenic sulfuric acid corrosion of concrete, Cement and Concrete Research, 30 (2000) 623-634.
[150] T. Wells, R.E. Melchers, P. Bond, Factors involved in the long term corrosion of concrete sewers, 49th Annual Conference of the Australasian Corrosion Association 2009: Corrosion and Prevention 2009, (2009).
[151] Y. Song, E. Wightman, Y. Tian, K. Jack, X. Li, H. Zhong, P.L. Bond, Z. Yuan, G. Jiang, Corrosion of reinforcing steel in concrete sewers, The Science of the total environment, 649 (2019) 739-748.
[152] A. Vostrikov, O. Fedyaeva, A. Shishkin, M. Sokol, Oxidation of hydrogen sulfide and corrosion of stainless steel in gas mixtures containing H2S, O2, H2O, and CO2, Journal of Engineering Thermophysics, 26 (2017) 314-324.
[153] E. Vahidi, E. Jin, M. Das, M. Singh, F. Zhao, Environmental life cycle analysis of pipe materials for sewer systems, Sustainable Cities and Society, 27 (2016) 167-174.
[154] A.H. Nielsen, J. Vollertsen, H.S. Jensen, T. Wium-Andersen, T. Hvitved-Jacobsen, Influence of pipe material and surfaces on sulfide related odor and corrosion in sewers, Water Research, 42 (2008) 4206-4214.
[155] K. Scrivener, D. Damidot, C. Famy, Possible Mechanisms of Expansion of Concrete Exposed to Elevated Temperatures During Curing (Also Known as DEF) and Implications for Avoidance of Field Problems, Cement, Concrete and Aggregates, 21 (1999) 93-101.
[156] L. Zhang, P. De Schryver, B. De Gusseme, W. De Muynck, N. Boon, W. Verstraete, Chemical and biological technologies for hydrogen sulfide emission control in sewer systems: A review, Water Research, 42 (2008) 1-12.
[157] R. Ganigue, O. Gutierrez, R. Rootsey, Z. Yuan, Chemical dosing for sulfide control in Australia: An industry survey, Water Research, 45 (2011) 6564-6574.
[158] H.-W. Lin, Y. Lu, R. Ganigué, K.R. Sharma, K. Rabaey, Z. Yuan, I. Pikaar, Simultaneous use of caustic and oxygen for efficient sulfide control in sewers, Science of The Total Environment, 601-602 (2017) 776-783.
[159] O. Auguet, M. Pijuan, H. Guasch-Balcells, C.M. Borrego, O. Gutierrez, Implications of Downstream Nitrate Dosage in anaerobic sewers to control sulfide and methane emissions, Water Research, 68 (2015) 522-532.
[160] Y. Liu, C. Wu, X. Zhou, D.Z. Zhu, H. Shi, Sulfide elimination by intermittent nitrate dosing in sewer sediments, Journal of environmental sciences (China), 27 (2015) 259-265.
[161] J. Mohanakrishnan, O. Gutierrez, R. Meyer, Z. Yuan, Nitrite effectively inhibits sulfide and methane production in a laboratory scale sewer reactor, Water research, 42 (2008) 3961-3971.

[162] O. Gutierrez, D. Park, K. Sharma, Z. Yuan, Effects of long-term pH elevation on the sulfate-reducing and methanogenic activities of anaerobic sewer biofilms, Water Research, 43 (2009) 2549-2557.
[163] O. Gutierrez, G. Sudarjanto, G. Ren, R. Ganigué, G. Jiang, Z. Yuan, Assessment of pH shock as a method for controlling sulfide and methane formation in pressure main sewer systems, Water Research, 48 (2014) 569-578.
[164] Q. Beimenr, W. Chenguang, C. Xiaoju, Y. Yixing, The Disinfection Efficacy of Chlorine on Sulfate-reducing Bacteria and Iron Bacteria in Water Supply Systems, Proceedings of the 2012 Second International Conference on Electric Technology and Civil Engineering, IEEE Computer Society, 2012, pp. 3095–3098.
[165] C.W.S. Cheung, I.B. Beech, The use of biocides to control sulphate-reducing bacteria in biofilms on mild steel surfaces, Biofouling, 9 (1996) 231-249.
[166] X. Yan, J. Sun, A. Kenjiahan, X. Dai, B.-J. Ni, Z. Yuan, Rapid and strong biocidal effect of ferrate on sulfidogenic and methanogenic sewer biofilms, Water Research, 169 (2020) 115208.
[167] G. Jiang, O. Gutierrez, Z. Yuan, The strong biocidal effect of free nitrous acid on anaerobic sewer biofilms, Water Research, 45 (2011) 3735-3743.
[168] B. Kiilerich, W. Van de Ven, A.H. Nielsen, J. Vollertsen, Sulfide Precipitation in Wastewater at Short Timescales, Water, 9 (2017).
[169] B. Kiilerich, A.H. Nielsen, J. Vollertsen, Kinetics of sulfide precipitation with ferrous and ferric iron in wastewater, Water science and technology : a journal of the International Association on Water Pollution Research, 78 (2018) 1071-1081.
[170] O. Gutierrez, D. Park, K.R. Sharma, Z. Yuan, Iron salts dosage for sulfide control in sewers induces chemical phosphorus removal during wastewater treatment, Water Research, 44 (2010) 3467-3475.
[171] I. Pikaar, E.M. Likosova, S. Freguia, J. Keller, K. Rabaey, Z. Yuan, Electrochemical Abatement of Hydrogen Sulfide from Waste Streams, Critical Reviews in Environmental Science and Technology, 45 (2015) 1555-1578.
[172] I. Pikaar, M. Flugen, H.-W. Lin, S. Salehin, J. Li, B.C. Donose, P.G. Dennis, L. Bethke, I. Johnson, K. Rabaey, Z. Yuan, Full-scale investigation of in-situ iron and alkalinity generation for efficient sulfide control, Water Research, 167 (2019) 115032.
[173] C. Marschall, P. Frenzel, H. Cypionka, Influence of oxygen on sulfate reduction and growth of sulfate-reducing bacteria, Archives of Microbiology, 159 (1993) 168-173.
[174] A.H. Nielsen, J. Vollertsen, T. Hvitved-Jacobsen, Determination of Kinetics and Stoichiometry of Chemical Sulfide Oxidation in Wastewater of Sewer Networks, Environmental Science & Technology, 37 (2003) 3853-3858.
[175] D.J. O'Brien, F.B. Birkner, Kinetics of oxygenation of reduced sulfur species in aqueous solution, Environmental Science & Technology, 11 (1977) 1114-1120.
[176] P. Sigalevich, M.V. Baev, A. Teske, Y. Cohen, Sulfate reduction and possible aerobic metabolism of the sulfate-reducing bacterium Desulfovibrio oxyclinae in a chemostat coculture with Marinobacter sp. Strain MB under exposure to increasing oxygen concentrations, Appl Environ Microbiol, 66 (2000) 5013-5018.
[177] A. Dolla, M. Fournier, Z. Dermoun, Oxygen defense in sulfate-reducing bacteria, Journal of Biotechnology, 126 (2006) 87-100.
[178] K.U. Kjeldsen, C. Joulian, K. Ingvorsen, Oxygen Tolerance of Sulfate-Reducing Bacteria in Activated Sludge, Environmental Science & Technology, 38 (2004) 2038-2043.

[179] E.D. Coulter, D.M. Kurtz, A Role for Rubredoxin in Oxidative Stress Protection in Desulfovibrio vulgaris: Catalytic Electron Transfer to Rubrerythrin and Two-Iron Superoxide Reductase, Archives of Biochemistry and Biophysics, 394 (2001) 76-86.
[180] M. Santana, Presence and expression of terminal oxygen reductases in strictly anaerobic sulfate-reducing bacteria isolated from salt-marsh sediments, Anaerobe, 14 (2008) 145-156.
[181] H. Santos, P. Fareleira, A.V. Xavier, L. Chen, M.Y. Liu, J. Legall, Aerobic Metabolism of Carbon Reserves by the "Obligate Anaerobe" Desulfovibrio gigas, Biochemical and Biophysical Research Communications, 195 (1993) 551-557.
[182] O. Gutierrez, J. Mohanakrishnan, K.R. Sharma, R.L. Meyer, J. Keller, Z. Yuan, Evaluation of oxygen injection as a means of controlling sulfide production in a sewer system, Water Research, 42 (2008) 4549-4561.
[183] D. Rathnayake, A. Sathasivan, G. Kastl, K.C. Bal Krishna, Hydrogen sulphide control in sewers by catalysing the reaction with oxygen, Science of The Total Environment, 689 (2019) 1192-1200.
[184] C. Buisman, P. Uspeert, A. Janssen, G. Lettinga, Kinetics of chemical and biological sulphide oxidation in aqueous solutions, Water Research, 24 (1990) 667-671.
[185] H. Heukelekian, Effect of the Addition of Sodium Nitrate to Sewage on Hydrogen Sulfide Production and B.O.D. Reduction, Sewage Works Journal, 15 (1943) 255-261.
[186] T. Aoyagi, M. Kimura, N. Yamada, R.R. Navarro, H. Itoh, A. Ogata, A. Sakoda, Y. Katayama, M. Takasaki, T. Hori, Dynamic transition of chemolithotrophic sulfur-oxidizing bacteria in response to amendment with nitrate in deposited marine sediments, Front Microbiol, 6 (2015) 426-426.
[187] J. Mohanakrishnan, O. Gutierrez, K.R. Sharma, A. Guisasola, U. Werner, R.L. Meyer, J. Keller, Z. Yuan, Impact of nitrate addition on biofilm properties and activities in rising main sewers, Water Research, 43 (2009) 4225-4237.
[188] J. O'Gorman, I. Purssell, G. Iori, Caustic soda washing of a sewer pressure main, Water, 38 (2011) 83-87.
[189] P.E. Wiley, Reduction of hydrogen sulfide gas in a small wastewater collection system using sodium hydroxide, Water Environment Research, 91 (2019) 483-490.
[190] Y. Cui, Y. Qin, D. Dilimulati, Y. Wang, The Effect of Chlorine Ion on Metal Corrosion Behavior under the Scratch Defect of Coating, International Journal of Corrosion, 2019 (2019) 7982893.
[191] M. Deborde, U. von Gunten, Reactions of chlorine with inorganic and organic compounds during water treatment-Kinetics and mechanisms: a critical review, Water Res, 42 (2008) 13-51.
[192] J. Chen, X. Xu, X. Zeng, M. Feng, R. Qu, Z. Wang, N. Nesnas, V.K. Sharma, Ferrate(VI) oxidation of polychlorinated diphenyl sulfides: Kinetics, degradation, and oxidized products, Water Res, 143 (2018) 1-9.
[193] J. Chen, N. Wu, X. Xu, R. Qu, C. Li, X. Pan, Z. Wei, Z. Wang, Fe(VI)-Mediated Single-Electron Coupling Processes for the Removal of Chlorophene: A Combined Experimental and Computational Study, Environ Sci Technol, 52 (2018) 12592-12601.
[194] J. Fagan, T.D. Waite, Notes. Biofouling control with ferrate(VI), Environmental Science & Technology, 17 (1983) 123-125.
[195] V.K. Sharma, J.O. Smith, F.J. Millero, Ferrate(VI) Oxidation of Hydrogen Sulfide, Environmental Science & Technology, 31 (1997) 2486-2491.
[196] S. Papić, N. Koprivanac, A.L. Božić, Removal of reactive dyes from wastewater using Fe(III) coagulant, Coloration Technology, 116 (2000) 352-358.

[197] V. Keasler, R.M. De Paula, G. Nilsen, L. Grunwald, T.J. Tidwell, 23 - Biocides overview and applications in petroleum microbiology, in: A.M. El-Sherik (Ed.) Trends in Oil and Gas Corrosion Research and Technologies, Woodhead Publishing, Boston, 2017, pp. 539-562.
[198] B. Legube, Ozonation By-Products, in: A.D. Nikolaou (Ed.) Haloforms and Related Compounds in Drinking Water, Springer Berlin Heidelberg, Berlin, Heidelberg, 2003, pp. 95-116.
[199] C.-H. Wei, Z. Fengzhen, Y. Hu, C. Feng, H. Wu, Ozonation in water treatment: The generation, basic properties of ozone and its practical application, Reviews in Chemical Engineering, 33 (2017).
[200] Z. Zuo, M. Zheng, J. Chang, D. Ren, X. Huang, Z. Yuan, Y. Liu, Free nitrous acid-based suppression of sulfide production in sewer sediments: In-situ effect mechanism, Science of The Total Environment, 715 (2020) 136871.
[201] G. Jiang, O. Gutierrez, K.R. Sharma, J. Keller, Z. Yuan, Optimization of intermittent, simultaneous dosage of nitrite and hydrochloric acid to control sulfide and methane productions in sewers, Water Res, 45 (2011) 6163-6172.
[202] Z. Cao, M. Hibino, H. Goda, Effect of Nitrite Ions on Steel Corrosion Induced by Chloride or Sulfate Ions, International Journal of Corrosion, 2013 (2013) 853730.
[203] L.R. Gardner, P.S. Stewart, Action of glutaraldehyde and nitrite against sulfate-reducing bacterial biofilms, Journal of industrial microbiology & biotechnology, 29 (2002) 354-360.
[204] M.H. Isa, G.K. Anderson, Molybdate inhibition of sulphate reduction in two-phase anaerobic digestion, Process Biochemistry, 40 (2005) 2079-2089.
[205] S. Zahedi, D. Sales, L.-I. Romero, R. Solera, Biomethanization from sulfate-containing municipal solid waste: effect of molybdate on microbial consortium, Journal of Chemical Technology & Biotechnology, 89 (2014) 1379-1387.
[206] J. Witherspoon, D. Apgar, M. Ward, C. Easter, Minimization of Odors and Related Corrosion in Collection Systems: A Summary of the Ongoing Water Environment Research Foundation Project 04-CTS-1, Proceedings of the Water Environment Federation, 2008 (2008) 82-97.
[207] R. Ganigué, G. Jiang, Y. Liu, K. Sharma, Y.-C. Wang, J. Gonzalez, T. Nguyen, Z. Yuan, Improved sulfide mitigation in sewers through on-line control of ferrous salt dosing, Water Research, 135 (2018) 302-310.
[208] D. Firer, E. Friedler, O. Lahav, Control of sulfide in sewer systems by dosage of iron salts: comparison between theoretical and experimental results, and practical implications, The Science of the total environment, 392 (2008) 145-156.
[209] J. Cao, L. Zhang, J. Hong, J. Sun, F. Jiang, Different ferric dosing strategies could result in different control mechanisms of sulfide and methane production in sediments of gravity sewers, Water Research, 164 (2019) 114914.
[210] L. Zhang, J. Keller, Z. Yuan, Inhibition of sulfate-reducing and methanogenic activities of anaerobic sewer biofilms by ferric iron dosing, Water Research, 43 (2009) 4123-4132.
[211] S.K. Khanal, J.C. Huang, Online oxygen control for sulfide oxidation in anaerobic treatment of high-sulfate wastewater, Water environment research : a research publication of the Water Environment Federation, 78 (2006) 397-408.
[212] H. Ge, L. Zhang, D. Batstone, J. Keller, Z. Yuan, Impact of Iron Salt Dosage to Sewers on Downstream Anaerobic Sludge Digesters: Sulfide Control and Methane Production, Journal of Environmental Engineering, 139 (2012) 594-601.

[213] K. Rajeshwar, J.G. Ibanez, - Chapter Two, in: K. Rajeshwar, J.G. Ibanez (Eds.) Environmental Electrochemistry, Academic Press, San Diego, 1997, pp. 57-126.
[214] Allen J. Bard and Larry R. Faulkner, Electrochemical Methods: Fundamentals and Applications, New York: Wiley, 2001, 2nd ed, Russian Journal of Electrochemistry, 38 (2002) 1364-1365.
[215] N. Elgrishi, K.J. Rountree, B.D. McCarthy, E.S. Rountree, T.T. Eisenhart, J.L. Dempsey, A Practical Beginner's Guide to Cyclic Voltammetry, Journal of Chemical Education, 95 (2018) 197-206.
[216] R. Holze, C.M.A. Brett, A.M.O. Brett: Electrochemistry — Principles, methods and applications, OXford University Press, Oxford, ISBN 0-19-855388-9, 1993, 427 pages, £ 25.00, Berichte der Bunsengesellschaft für physikalische Chemie, 98 (1994) 1350-1350.
[217] V.S. Bagotsky, Fundamentals of electrochemistry, 2nd ed. ed., Hoboken : Wiley-Interscience, Hoboken, 2006.
[218] J.S. Newman, K.E. Thomas-Alyea, Electrochemical systems, 3rd ed. ed., J. Wiley, Hoboken, N.J., 2004.
[219] C.G. Zoski, Handbook of electrochemistry, 1st ed. ed., Elsevier, Amsterdam ;, 2007.
[220] J.O.M. Bockris, A.K.N. Reddy, M.E. Gamboa-Aldeco, Modern electrochemistry / John O'M. Bockris and Amulya K.N. Reddy, 2nd ed. ed., Plenum Press, New York, 1998.
[221] B. Ateya, F. AlKharafi, A. Al-Azab, Electrodeposition of Sulfur from Sulfide Contaminated Brines, Electrochemical and Solid State Letters - ELECTROCHEM SOLID STATE LETT, 6 (2003).
[222] Reference Electrodes, 2020.
[223] S. Nayak, B.P. Chaplin, Fabrication and characterization of porous, conductive, monolithic Ti4O7 electrodes, Electrochimica Acta, 263 (2018) 299-310.
[224] M. Rolle, R. Sprocati, M. Masi, B. Jin, M. Muniruzzaman, Nernst-Planck Based Description of Transport, Coulombic Interactions and Geochemical Reactions in Porous Media: Modeling Approach and Benchmark Experiments, Water Resources Research, 54 (2018).
[225] E.J.F. Dickinson, A.J. Wain, The Butler-Volmer equation in electrochemical theory: Origins, value, and practical application, Journal of Electroanalytical Chemistry, 872 (2020) 114145.
[226] Y.-H. Fang, Z.-P. Liu, Tafel Kinetics of Electrocatalytic Reactions: From Experiment to First-Principles, ACS Catalysis, 4 (2014) 4364-4376.
[227] Y.A. Gandomi, D.S. Aaron, J.R. Houser, M.C. Daugherty, J.T. Clement, A.M. Pezeshki, T.Y. Ertugrul, D.P. Moseley, M.M. Mench, Critical Review—Experimental Diagnostics and Material Characterization Techniques Used on Redox Flow Batteries, Journal of The Electrochemical Society, 165 (2018) A970-A1010.
[228] W. Wang, X. Wei, D. Choi, X. Lu, G. Yang, C. Sun, Chapter 1 - Electrochemical cells for medium- and large-scale energy storage: fundamentals, in: C. Menictas, M. Skyllas-Kazacos, T.M. Lim (Eds.) Advances in Batteries for Medium and Large-Scale Energy Storage, Woodhead Publishing2015, pp. 3-28.
[229] M. Panizza, G. Cerisola, Direct And Mediated Anodic Oxidation of Organic Pollutants, Chemical Reviews, 109 (2009) 6541-6569.
[230] K. Kolbrecka, J. Przyluski, Sub-stoichiometric titanium oxides as ceramic electrodes for oxygen evolution—structural aspects of the voltammetric behaviour of TinO2n−1, Electrochimica Acta, 39 (1994) 1591-1595.

[231] I. Pikaar, R.A. Rozendal, Z. Yuan, J. Keller, K. Rabaey, Electrochemical sulfide removal from synthetic and real domestic wastewater at high current densities, Water Research, 45 (2011) 2281-2289.
[232] I. Pikaar, E. Li, R. Rozendal, Z. Yuan, J. Keller, K. Rabaey, Long-term field test of an electrochemical method for sulfide removal from sewage, Water research, 46 (2012) 3085-3093.
[233] B.G. Ateya, F.M. AlKharafi, A.S. Alazab, A.M. Abdullah, Kinetics of the electrochemical deposition of sulfur from sulfide polluted brines, Journal of Applied Electrochemistry, 37 (2007) 395-404.
[234] J. Radjenovic, D.L. Sedlak, Challenges and Opportunities for Electrochemical Processes as Next-Generation Technologies for the Treatment of Contaminated Water, Environmental Science & Technology, 49 (2015) 11292-11302.
[235] M. Panizza, Importance of Electrode Material in the Electrochemical Treatment of Wastewater Containing Organic Pollutants, in: C. Comninellis, G. Chen (Eds.) Electrochemistry for the Environment, Springer New York, New York, NY, 2010, pp. 25-54.
[236] T. Muddemann, D. Haupt, M. Sievers, U. Kunz, Electrochemical Reactors for Wastewater Treatment, ChemBioEng Reviews, 6 (2019) 142-156.
[237] P.C. Caliari, M.J. Pacheco, L.F. Ciríaco, A.M.C. Lopes, Anodic Oxidation of Sulfide to Sulfate: Effect of the Current Density on the Process Kinetics, Journal of the Brazilian Chemical Society, 28 (2017) 557-566.
[238] L. Szpyrkowicz, S.N. Kaul, R.N. Neti, S. Satyanarayan, Influence of anode material on electrochemical oxidation for the treatment of tannery wastewater, Water Research, 39 (2005) 1601-1613.
[239] J.R. Hall, M.H. Schoenfisch, Direct Electrochemical Sensing of Hydrogen Sulfide without Sulfur Poisoning, Anal Chem, 90 (2018) 5194-5200.
[240] N. Zhang, W. Han, L. Wang, Anodic Oxidation of Alkaline Sulfide Solution at a Low Potential, Advanced Materials Research, 356-360 (2011) 1367-1370.
[241] P. Dutta, R. Rozendal, Z. Yuan, K. Rabaey, J. Keller, Electrochemical regeneration of sulfur loaded electrodes, Electrochemistry Communications, 11 (2009) 1437-1440.
[242] B.G. Ateya, F.M. Al-Kharafi, Anodic Oxidation of Sulfide Ions from Chloride Brines, Electrochemistry Communications, 4 (2002) 231-238.
[243] P.K. Dutta, J. Keller, Z. Yuan, R.A. Rozendal, K. Rabaey, Role of Sulfur during Acetate Oxidation in Biological Anodes, Environmental Science & Technology, 43 (2009) 3839-3845.
[244] Y.S. Shih, J.L. Lee, Continuous solvent extraction of sulfur from the electrochemical oxidation of a basic sulfide solution in the CSTER system, Industrial & Engineering Chemistry Process Design and Development, 25 (1986) 834-836.
[245] Yi Qing, Chen Qi, Zhang Ping, Electrochemical study of sulfide solution in the presence of surfactants, Journal of Environmental Sciences, 10 372-377.
[246] W. Shi, B. Yi, M. Hou, F. Jing, P. Ming, Hydrogen sulfide poisoning and recovery of PEMFC Pt-anodes, Journal of Power Sources, 165 (2007) 814-818.
[247] J. Haner, D. Bejan, N. Bunce, Electrochemical Oxidation of Sulfide Ion at a Ti/IrO2–Ta2O5 Anode in the Presence and Absence of Naphthenic Acids, Journal of Applied Electrochemistry - J APPL ELECTROCHEM, 39 (2009) 1733-1738.
[248] E. Ntagia, E. Fiset, L. Truong Cong Hong, E. Vaiopoulou, K. Rabaey, Electrochemical treatment of industrial sulfidic spent caustic streams for sulfide removal and caustic recovery, J Hazard Mater, 388 (2020) 121770.

[249] K. Waterston, D. Bejan, N.J. Bunce, Electrochemical oxidation of sulfide ion at a boron-doped diamond anode, Journal of Applied Electrochemistry, 37 (2007) 367-373.
[250] S.J. Cobb, Z.J. Ayres, J.V. Macpherson, Boron Doped Diamond: A Designer Electrode Material for the Twenty-First Century, Annual Review of Analytical Chemistry, 11 (2018) 463-484.
[251] S. You, B. Liu, Y. Gao, Y. Wang, C. Tang, Y. Huang, N.-Q. Ren, Monolithic Porous Magnéli-phase Ti4O7 for Electro-oxidation Treatment of Industrial Wastewater, Electrochimica Acta, 214 (2016).
[252] S. El-Sherif, D. Bejan, N.J. Bunce, Electrochemical oxidation of sulfide ion in synthetic sour brines using periodic polarity reversal at Ebonex® electrodes, Canadian Journal of Chemistry, 88 (2010) 928-936.
[253] P.K. Dutta, R.A. Rozendal, Z. Yuan, K. Rabaey, J. Keller, Electrochemical regeneration of sulfur loaded electrodes, Electrochemistry Communications, 11 (2009) 1437-1440.
[254] L.-C. Chiang, J.-E. Chang, T.-C. Wen, Indirect oxidation effect in electrochemical oxidation treatment of landfill leachate, Water Research, 29 (1995) 671-678.
[255] G. Chen, Electrochemical technologies in wastewater treatment, Separation and Purification Technology, 38 (2004) 11-41.
[256] E. Vaiopoulou, T. Provijn, A. Prévoteau, I. Pikaar, K. Rabaey, Electrochemical sulfide removal and caustic recovery from spent caustic streams, Water Research, 92 (2016) 38-43.
[257] E. Ntagia, E. Fiset, L. da Silva Lima, I. Pikaar, X. Zhang, A.W. Jeremiasse, A. Prévoteau, K. Rabaey, Anode materials for sulfide oxidation in alkaline wastewater: An activity and stability performance comparison, Water Res, 149 (2019) 111-119.
[258] K. Park, H. Lee, S. Phelan, S. Liyanaarachchi, N. Marleni, D. Navaratna, V. Jegatheesan, L. Shu, Mitigation strategies of hydrogen sulphide emission in sewer networks – A review, International Biodeterioration & Biodegradation, 95 (2014) 251-261.
[259] H.-J. Lee, M.-K. Hong, S.-D. Han, S.-H. Cho, S.-H. Moon, Fouling of an anion exchange membrane in the electrodialysis desalination process in the presence of organic foulants, Desalination, 238 (2009).
[260] M.M. Emamjomeh, M. Sivakumar, Review of pollutants removed by electrocoagulation and electrocoagulation/flotation processes, Journal of Environmental Management, 90 (2009) 1663-1679.
[261] O. Apaydin, U. Kurt, M. Gonüllü, An Investigation on the treatment of tannery wastewater by Electrocoagulation, Global NEST Journal, 11 (2009) 546-555.
[262] R.D.W. Kemmitt, 37 - MANGANESE, in: R.D.W. Kemmitt, R.D. Peacock (Eds.) The Chemistry of Manganese, Technetium and Rhenium, Pergamon1973, pp. 771-876.
[263] J.D. Hem, Rates of manganese oxidation in aqueous systems, Geochimica et Cosmochimica Acta, 45 (1981) 1369-1374.
[264] C.M. Julien, A. Mauger, Nanostructured MnO_2 as Electrode Materials for Energy Storage, Nanomaterials (Basel), 7 (2017) 396.
[265] G. Davies, Some aspects of the chemistry of manganese(III) in aqueous solution, Coordination Chemistry Reviews, 4 (1969) 199-224.
[266] B. Zhang, L. Sun, Why nature chose the Mn4CaO5 cluster as water-splitting catalyst in photosystem II: a new hypothesis for the mechanism of O-O bond formation, Dalton Trans, 47 (2018) 14381-14387.
[267] J.E. Post, Manganese oxide minerals: Crystal structures and economic and environmental significance, Proceedings of the National Academy of Sciences, 96 (1999) 3447-3454.

[268] Y. Yuan, C. Liu, B.W. Byles, W. Yao, B. Song, M. Cheng, Z. Huang, K. Amine, E. Pomerantseva, R. Shahbazian-Yassar, J. Lu, Ordering Heterogeneity of [MnO6] Octahedra in Tunnel-Structured MnO2 and Its Influence on Ion Storage, Joule, 3 (2019) 471-484.
[269] S. Park, Y. Lee, S. Choi, H. Seo, M. Lee, M. Balamurugan, K.T. Nam, Manganese Oxide-based Heterogeneous Electrocatalysts for Water Oxidation, Energy & Environmental Science, 13 (2020).
[270] Y. Huang, Y. Dong, S. Li, J. Lee, C. Wang, Z. Zhu, W. Xue, Y. Li, J. Li, Lithium Manganese Spinel Cathodes for Lithium-Ion Batteries, Advanced Energy Materials, n/a (2020) 2000997.
[271] P. Vanaphuti, J. Chen, J. Cao, K. Bigham, B. Chen, L. Yang, H. Chen, Y. Wang, Enhanced Electrochemical Performance of the Lithium-Manganese-Rich Cathode for Li-Ion Batteries with Na and F CoDoping, ACS Applied Materials & Interfaces, 11 (2019) 37842-37849.
[272] M. Yoshio, H. Noguchi, SECONDARY BATTERIES – LITHIUM RECHARGEABLE SYSTEMS – LITHIUM-ION | Positive Electrode: Manganese Oxides, in: J. Garche (Ed.) Encyclopedia of Electrochemical Power Sources, Elsevier, Amsterdam, 2009, pp. 307-317.
[273] W. Taucher, K. Kordesch, Alkaline Manganese Dioxide - Zinc Batterdes Primary and Rechargeable Cells with and Without Mercury, in: C.A.C. Sequeira (Ed.) Studies in Environmental Science, Elsevier1994, pp. 163-202.
[274] K. Mette, A. Bergmann, J.-P. Tessonnier, M. Hävecker, L. Yao, T. Ressler, R. Schlögl, P. Strasser, M. Behrens, Nanostructured Manganese Oxide Supported on Carbon Nanotubes for Electrocatalytic Water Splitting, ChemCatChem, 4 (2012) 851-862.
[275] P. Menezes, A. Indra, P. Littlewood, M. Schwarze, C. Göbel, R. Schomäcker, M. Driess, Nanostructured Manganese Oxides as Highly Active Water Oxidation Catalysts: A Boost from Manganese Precursor Chemistry, ChemSusChem, 7 (2014).
[276] M.D. Sampson, C.P. Kubiak, Electrocatalytic Dihydrogen Production by an Earth-Abundant Manganese Bipyridine Catalyst, Inorganic Chemistry, 54 (2015) 6674-6676.
[277] R. Simon, C. Niklas, S. Jennifer, Manganese Oxides in Heterogeneous (Photo)Catalysis: Possibilities and Challenges, Green, 5 (2015) 23-41.
[278] W. Xiao, P. Zhou, X. Mao, D. Wang, Ultrahigh aniline-removal capacity of hierarchically structured layered manganese oxides: trapping aniline between interlayers, Journal of Materials Chemistry A, 3 (2015) 8676-8682.
[279] J. Wang, J. Li, C. Jiang, P. Zhou, P. Zhang, J. Yu, The effect of manganese vacancy in birnessite-type MnO2 on room-temperature oxidation of formaldehyde in air, Applied Catalysis B: Environmental, 204 (2017) 147-155.
[280] J. Wang, G. Zhang, P. Zhang, Graphene-assisted photothermal effect on promoting catalytic activity of layered MnO2 for gaseous formaldehyde oxidation, Applied Catalysis B: Environmental, 239 (2018) 77-85.
[281] A. Massa, S. Hernández, A. Lamberti, C. Galletti, N. Russo, D. Fino, Electro-oxidation of phenol over electrodeposited MnOx nanostructures and the role of a TiO2 nanotubes interlayer, Applied Catalysis B: Environmental, 203 (2017) 270-281.
[282] Y.-q. Wang, B. Gu, W.-l. Xu, Electro-catalytic degradation of phenol on several metal-oxide anodes, Journal of Hazardous Materials, 162 (2009) 1159-1164.
[283] M. Nakayama, M. Shamoto, A. Kamimura, Surfactant-Induced Electrodeposition of Layered Manganese Oxide with Large Interlayer Space for Catalytic Oxidation of Phenol, Chemistry of Materials, 22 (2010) 5887-5894.

[284] W.-c. Peng, S.-b. Wang, X.-y. Li, Shape-controlled synthesis of one-dimensional α-MnO2 nanocrystals for organic detection and pollutant degradation, Separation and Purification Technology, 163 (2016) 15-22.
[285] L. Ukrainczyk, M. McBride, Oxidation and dechlorination of chlorophenols in dilute aqueous suspensions of manganese oxides: Reaction products, Environmental Toxicology and Chemistry, 12 (1993) 2015-2022.
[286] J. Qin, Q. Zhang, K.T. Chuang, Catalytic wet oxidation of p-chlorophenol over supported noble metal catalysts, Applied Catalysis B: Environmental, 29 (2001) 115-123.
[287] Y. Wang, A. Stone, The citric acid-MnIII,IVO2(birnessite) reaction. Electron transfer, complex formation, and autocatalytic feedback, Geochimica et Cosmochimica Acta, 70 (2006) 4463-4476.
[288] Y. Wang, A. Stone, Reaction of MnIII,IV (hydr)oxides with oxalic acid, glyoxylic acid, phosphonoformic acid, and structurally-related organic compounds, Geochimica et Cosmochimica Acta, 70 (2006) 4477-4490.
[289] V.P. Santos, M.F.R. Pereira, J.J.M. Órfão, J.L. Figueiredo, The role of lattice oxygen on the activity of manganese oxides towards the oxidation of volatile organic compounds, Applied Catalysis B: Environmental, 99 (2010) 353-363.
[290] S.S.T. Bastos, J.J.M. Órfão, M.M.A. Freitas, M.F.R. Pereira, J.L. Figueiredo, Manganese oxide catalysts synthesized by exotemplating for the total oxidation of ethanol, Applied Catalysis B: Environmental, 93 (2009) 30-37.
[291] W. Yao, F.J. Millero, The rate of sulfide oxidation by δMnO2 in seawater, Geochimica et Cosmochimica Acta, 57 (1993) 3359-3365.
[292] W. Yao, F.J. Millero, Oxidation of hydrogen sulfide by hydrous Fe(III) oxides in seawater, Marine Chemistry, 52 (1996) 1-16.
[293] J. Herszage, M. dos Santos Afonso, Mechanism of Hydrogen Sulfide Oxidation by Manganese(IV) Oxide in Aqueous Solutions, Langmuir, 19 (2003) 9684-9692.
[294] Y. Luo, S. Li, W. Tan, G. Qiu, Oxidation and Catalytic Oxidation of Dissolved Sulfide by Manganite in Aqueous Systems, Clays and Clay Minerals, 65 (2017) 299-309.
[295] E. Goldnik, T. Turek, Removal of hydrogen sulfide by permanganate based sorbents: Experimental investigation and reactor modeling, Chemical Engineering Science, 151 (2016) 51-63.
[296] W.-q. Ye, Y.-j. Li, L. Kong, M.-m. Ren, Q. Han, Feasibility of flue-gas desulfurization by manganese oxides, Transactions of Nonferrous Metals Society of China, 23 (2013) 3089–3094.
[297] I. Konkol, J. Cebula, A. Cenian, Oxidization of hydrogen sulfide in biogas by manganese (IV) oxide particles, Environmental Engineering Research, 26 (2020).
[298] K. Wlodarchak, D. Skutt, G. Deshinsky, A. Chan, E. Pedersen, Odor Reduction in a Wastewater Treatment Plant Using Potassium Permanganate, Proceedings of the Water Environment Federation, 2002 (2002) 72-81.
[299] F. Cadena, R.W. Peters, Evaluation of Chemical Oxidizers for Hydrogen Sulfide Control, Journal (Water Pollution Control Federation), 60 (1988) 1259-1263.
[300] S. Asaoka, H. Okamura, Y. Akita, K. Nakano, K. Nakamoto, K. Hino, T. Saito, S. Hayakawa, M. Katayama, Y. Inada, Regeneration of manganese oxide as adsorption sites for hydrogen sulfide on granulated coal ash, Chemical Engineering Journal, 254 (2014) 531-537.
[301] D. Patil, S. Chavan, J. U. Kennedy Oubagaranadin, A review of technologies for manganese removal from wastewaters, Journal of Environmental Chemical Engineering, 4 (2015).

[302] B. Keller-Lehmann, S. Corrie, R. Ravn, Z. Yuan, J. Keller, Preservation and simultaneous analysis of relevant soluble sulfur species in sewage samples, Proceedings of the Second International IWA Conference on Sewer Operation and Maintenance, Citeseer, 2006, pp. 28.
[303] P. K. Dutta, R. A. Rozendal, Z. Yuan, K. Rabaey, J. Keller, Electrochemical regeneration of sulfur loaded electrodes, 2009.
[304] A. Kamyshny, I. Ekeltchik, J. Gun, O. Lev, Method for the Determination of Inorganic Polysulfide Distribution in Aquatic Systems, Analytical Chemistry, 78 (2006) 2631-2639.
[305] W.E. Kleinjan, A.d. Keizer, A.J.H. Janssen, Kinetics of the chemical oxidation of polysulfide anions in aqueous solution, Water Research, 39 (2005) 4093-4100.
[306] J.R. Bolton, K.G. Bircher, W. Tumas, C.A. Tolman, Figures-of-merit for the technical development and application of advanced oxidation technologies for both electric-and solar-driven systems (IUPAC Technical Report), Pure Appl. Chem., 73 (2001) 627-637.
[307] K. Cho, Y. Qu, D. Kwon, H. Zhang, C.m.A. Cid, A. Aryanfar, M.R. Hoffmann, Effects of anodic potential and chloride ion on overall reactivity in electrochemical reactors designed for solar-powered wastewater treatment, Environ. Sci. Technol., 48 (2014) 2377-2384.
[308] F. Arjmand, A. Adriaens, Effect of cathodic polarisation on the corrosion behaviour of 316L stainless steel under static and dynamic conditions, CORROSION REVIEWS, 33 (2015).
[309] VanLondon, Conductivity Guide, 2018.
[310] L. Wang, P. Lu, C. Liu, Electro-oxidation of Sulfide on Ti/RuO2 Electrode in an Aqueous Alkaline Solution, 2015.
[311] F. M Al Kharafi, A. Y Saad, B. G Ateya, I. Ghayad, Electrochemical oxidation of sulfide ions on platinum electrodes, 2010.
[312] M. Thompson, C. Prado, l. Jiang, Amperometric Detection of Sulfide at a Boron Doped Diamond Electrode: The Electrocatalytic Reaction of Sulfide with Ferricyanide in Aqueous Solution, 2002.
[313] P. Giannozzi, R. Car, G. Scoles, Oxygen adsorption on graphite and nanotubes, The Journal of Chemical Physics, 118 (2003) 1003-1006.
[314] L. Qie, W. Chen, X. Xiong, C. Hu, F. Zou, P. Hu, Y. Huang, Sulfur-Doped Carbon with Enlarged Interlayer Distance as a High-Performance Anode Material for Sodium-Ion Batteries, Advanced Science, 2 (2015) n/a-n/a.
[315] C.-H. Chen, A. Halford, M. Walker, C. Brennan, S.C.S. Lai, D.J. Fermin, P.R. Unwin, P. Rodriguez, Electrochemical characterization and regeneration of sulfur poisoned Pt catalysts in aqueous media, Journal of Electroanalytical Chemistry, 816 (2018) 138-148.
[316] K. Rankin, D. Bejan, N.J. Bunce, Electrochemical Oxidation of the Sulfide Ion in Synthetic Geothermal Brines in Batch Cells Using Coke Electrodes, Industrial & Engineering Chemistry Research, 49 (2010) 6261-6266.
[317] J. Hastie, D. Bejan, N.J. Bunce, Oxidation of sulfide ion in synthetic geothermal brines at carbon-based anodes, The Canadian Journal of Chemical Engineering, 89 (2011) 948-957.
[318] T. Hunger, F. Lapicque, A. Storck, Electrochemical oxidation of sulphite ions at graphite electrodes, Journal of Applied Electrochemistry, 21 (1991) 588-596.
[319] E. Ayranci, B.E. Conway, Adsorption and electrosorption at high-area carbon-felt electrodes for waste-water purification: Systems evaluation with inorganic, S-containing anions, Journal of Applied Electrochemistry, 31 (2001) 257-266.
[320] T.J. Bandosz, On the Adsorption/Oxidation of Hydrogen Sulfide on Activated Carbons at Ambient Temperatures, Journal of Colloid and Interface Science, 246 (2002) 1-20.

[321] L.M. Le Leuch, A. Subrenat, P. Le Cloirec, Hydrogen Sulfide Adsorption and Oxidation onto Activated Carbon Cloths: Applications to Odorous Gaseous Emission Treatments, Langmuir, 19 (2003) 10869-10877.
[322] A. Ban, A. Schafer, H. Wendt, Fundamentals of electrosorption on activated carbon for wastewater treatment of industrial effluents, Journal of Applied Electrochemistry, 28 (1998) 227-236.
[323] A. Bagreev, F. Adib, T. Bandosz, pH of activated carbon surface as an indication of its suitability for H 2S removal from moist air streams, 2001.
[324] F. Adib, A. Bagreev, T.J. Bandosz, Effect of Surface Characteristics of Wood-Based Activated Carbons on Adsorption of Hydrogen Sulfide, Journal of Colloid and Interface Science, 214 (1999) 407-415.
[325] M. Gineys, R. Benoit, N. Cohaut, F. Béguin, S. Delpeux-Ouldriane, Behavior of activated carbon cloths used as electrode in electrochemical processes, Chemical Engineering Journal, 310 (2017) 1-12.
[326] M.L. Hami, M.A. Al-Hashimi, M.M. Al-Doori, Effect of activated carbon on BOD and COD removal in a dissolved air flotation unit treating refinery wastewater, Desalination, 216 (2007) 116-122.
[327] A. Bagreev, H. Rahman, T. Bandosz, Study of regeneration of activated carbons used as H 2 S adsorbents in water treatment plants, 2002.
[328] A.Q. Contractor, H. Lal, Two forms of chemisorbed sulfur on platinum and related studies, Journal of Electroanalytical Chemistry and Interfacial Electrochemistry, 96 (1979) 175-181.
[329] A.Q. Contractor, H. Lal, The nature of species adsorbed on platinum from SO2 solutions, Journal of Electroanalytical Chemistry and Interfacial Electrochemistry, 93 (1978) 99-107.
[330] A.V. Dribinskii, M.R. Tarasevich, V.E. Kazarinov, Electrocatalysis on carbon materials, Materials Chemistry and Physics, 22 (1989) 377-400.
[331] M.P. Cal, B.W. Strickler, A.A. Lizzio, S.K. Gangwal, High temperature hydrogen sulfide adsorption on activated carbon: II. Effects of gas temperature, gas pressure and sorbent regeneration, Carbon, 38 (2000) 1767-1774.
[332] C. Quijada, F.J. Huerta, E. Morallón, J.L. Vázquez, L.E.A. Berlouis, Electrochemical behaviour of aqueous SO2 at polycrystalline gold electrodes in acidic media: a voltammetric and in situ vibrational study: Part 1. Reduction of SO2: deposition of monomeric and polymeric sulphur, Electrochimica Acta, 45 (2000) 1847-1862.
[333] J. L. Zubimendi, R. Salvarezza, L. Vázquez, A. Arvia, Scanning Tunneling Microscopy Observation of Sulfur Electrodeposits on Graphite Single Crystals†, 1996.
[334] C. Quijada, J.L. Vázquez, Electrochemical reactivity of aqueous SO2 on glassy carbon electrodes in acidic media, 2005.
[335] M. Behm, D. Simonsson, Electrochemical production of polysulfides and sodium hydroxide from white liquor: Part I: Experiments with rotating disc and ring-disc electrodes, Journal of Applied Electrochemistry, 27 (1997) 507-518.
[336] Y. Xiao, S. Wang, D. Wu, Q. Yuan, Catalytic Oxidation of Hydrogen Sulfide Over Unmodified and Impregnated Activated Carbon, 2008.
[337] W. Feng, S. Kwon, E. Borguet, R. Vidic, Adsorption of Hydrogen Sulfide onto Activated Carbon Fibers: Effect of Pore Structure and Surface Chemistry, 2006.
[338] J. Xi, W. Zhang, Z. Li, H.p. Zhou, L. Liu, Z. Wu, X. Qiu, Effect of Electro-Oxidation Current Density on Performance of Graphite Felt Electrode for Vanadium Redox Flow Battery, 2013.

[339] X.-g. Li, K.-l. Huang, S.-q. Liu, N. Tan, L.-q. Chen, Characteristics of graphite felt electrode electrochemically oxidized for vanadium redox battery application, Transactions of Nonferrous Metals Society of China, 17 (2007) 195-199.
[340] W. Zhang, J. Xi, Z. Li, H. Zhou, L. Liu, Z. Wu, X. Qiu, Electrochemical activation of graphite felt electrode for VO2+/VO2+ redox couple application, Electrochimica Acta, 89 (2013) 429-435.
[341] C. Hu, F. Liu, H. Lan, H. Liu, J. Qu, Preparation of a manganese dioxide/carbon fiber electrode for electrosorptive removal of copper ions from water, J Colloid Interface Sci, 446 (2015) 359-365.
[342] P. Hosseini-Benhangi, C.H. Kung, A. Alfantazi, E. Gyenge, Controlling the Interfacial Environment in the Electrosynthesis of MnOx Nanostructures for High Performance Oxygen Reduction/Evolution Electrocatalysis, ACS Applied Materials & Interfaces, 9 (2017).
[343] M.I. Zaki, M.A. Hasan, L. Pasupulety, K. Kumari, Thermochemistry of manganese oxides in reactive gas atmospheres: Probing redox compositions in the decomposition course MnO2 → MnO, Thermochimica Acta, 303 (1997) 171-181.
[344] M. Chigane, M. Ishikawa, Manganese Oxide Thin Film Preparation by Potentiostatic Electrolyses and Electrochromism, Journal of The Electrochemical Society - J ELECTROCHEM SOC, 147 (2000).
[345] L. Zhong Zhao, V. Young, XPS studies of carbon supported films formed by the resistive deposition of manganese, Journal of Electron Spectroscopy and Related Phenomena, 34 (1984) 45-54.
[346] B. Babakhani, D.G. Ivey, Effect of electrodeposition conditions on the electrochemical capacitive behavior of synthesized manganese oxide electrodes, Journal of Power Sources, 196 (2011) 10762-10774.
[347] Z.B. Jildeh, J. Oberländer, P. Kirchner, P.H. Wagner, M.J. Schöning, Thermocatalytic Behavior of Manganese (IV) Oxide as Nanoporous Material on the Dissociation of a Gas Mixture Containing Hydrogen Peroxide, Nanomaterials (Basel), 8 (2018) 262.
[348] M. Dupont, S. Donne, Nucleation and Growth of Electrodeposited Manganese Dioxide for Electrochemical Capacitors, 2014.
[349] J. Herszage, M. Dos Santos Afonso, Mechanism of Hydrogen Sulfide Oxidation by Manganese(IV) Oxide in Aqueous Solutions, Langmuir, 19 (2003).
[350] J.E. Kostka, G.W. Luther, K.H. Nealson, Chemical and biological reduction of Mn (III)-pyrophosphate complexes: Potential importance of dissolved Mn (III) as an environmental oxidant, Geochimica et Cosmochimica Acta, 59 (1995) 885-894.
[351] N. Sergienko, E. Irtem, O. Gutierrez, J. Radjenovic, Electrochemical removal of sulfide on porous carbon-based flow-through electrodes, Journal of Hazardous Materials, 375 (2019) 19-25.
[352] B. G. Ateya, F.M. AlKharafi, A.S. Alazab, A. Abdullah, Kinetics of the Electrochemical Deposition of Sulfur from Sulfide Polluted Brines, 2007.
[353] P. Roy, S. Berger, P. Schmuki, TiO2 Nanotubes: Synthesis and Applications, Angewandte Chemie International Edition, 50 (2011) 2904-2939.
[354] C. Holder, R. Schaak, Tutorial on Powder X-ray Diffraction for Characterizing Nanoscale Materials, ACS Nano, 13 (2019) 7359-7365.
[355] M.N. Shaker, S.A. Bonke, J. Xiao, M.A. Khan, R.K. Hocking, M.F. Tesch, Insight into pH-Dependent Formation of Manganese Oxide Phases in Electrodeposited Catalytic Films Probed by Soft X-Ray Absorption Spectroscopy, ChemPlusChem, 83 (2018) 721-727.

[356] E.B. Godunov, A.D. Izotov, I.G. Gorichev, Dissolution of Manganese Oxides of Various Compositions in Sulfuric Acid Solutions Studied by Kinetic Methods, Inorganic Materials, 54 (2018) 66-71.
[357] N. Sergienko, J. Radjenovic, Manganese oxide-based porous electrodes for rapid and selective (electro)catalytic removal and recovery of sulfide from wastewater, Applied Catalysis B: Environmental, 267 (2020) 118608.
[358] M.R. Hoffmann, Kinetics and mechanism of oxidation of hydrogen sulfide by hydrogen peroxide in acidic solution, Environmental Science & Technology, 11 (1977) 61-66.
[359] V.I. Kravtsov, Outer and inner sphere mechanims of electrochemical steps of the metal complexes electrode reactions, Journal of Electroanalytical Chemistry and Interfacial Electrochemistry, 69 (1976) 125-131.
[360] J. Melder, P. Bogdanoff, I. Zaharieva, S. Fiechter, H. Dau, P. Kurz, Water-Oxidation Electrocatalysis by Manganese Oxides: Syntheses, Electrode Preparations, Electrolytes and Two Fundamental Questions, Zeitschrift für Physikalische Chemie, 234 (2020) 925-978.
[361] H. Tamura, T. Oda, M. Nagayama, R. Furuichi, Acid-Base Dissociation of Surface Hydroxyl Groups on Manganese Dioxide in Aqueous Solutions, Journal of The Electrochemical Society, 136 (1989) 2782-2786.
[362] X.H. Feng, L.M. Zhai, W.F. Tan, W. Zhao, F. Liu, J.Z. He, The controlling effect of pH on oxidation of Cr(III) by manganese oxide minerals, Journal of Colloid and Interface Science, 298 (2006) 258-266.
[363] W. Yao, F.J. Millero, Adsorption of Phosphate on Manganese Dioxide in Seawater, Environmental Science & Technology, 30 (1996) 536-541.
[364] A.T. Stone, Reductive Dissolution of Manganese(III/Iv) Oxides by Substituted Phenols, Environmental Science & Technology, 21 (1987) 979-988.
[365] A.T. Stone, J.J. Morgan, Reduction and dissolution of manganese(III) and manganese(IV) oxides by organics: 2. Survey of the reactivity of organics, Environmental Science & Technology, 18 (1984) 617-624.
[366] P.K. Dutta, K. Rabaey, Z. Yuan, J. Keller, Spontaneous electrochemical removal of aqueous sulfide, Water Research, 42 (2008) 4965-4975.
[367] E. Vaiopoulou, P. Melidis, A. Aivasidis, Sulfide removal in wastewater from petrochemical industries by autotrophic denitrification, Water Research, 39 (2005) 4101-4109.
[368] A. Bagreev, T. Bandosz, Thermal Regeneration of a Spent Activated Carbon Previously Used as Hydrogen Sulfide Adsorbent, Carbon, 39 (2001) 1319-1326.
[369] E. O. Vilar, F. de, L. de, S. de, Study of the electrical conductivity of graphite felt employed as a porous electrode, Brazilian Journal of Chemical Engineering, 15 (1998).
[370] S. Zhang, G. Chen, Manganese oxide based materials for supercapacitors, Energy Materials: Materials Science and Engineering for Energy Systems, 3 (2008) 186-200.
[371] J. Huang, Z. Wang, M. Hou, X. Dong, Y. Liu, Y. Wang, Y. Xia, Polyaniline-intercalated manganese dioxide nanolayers as a high-performance cathode material for an aqueous zinc-ion battery, Nature Communications, 9 (2018) 2906.
[372] B. Liao, H. Li, X. Wang, M. Xu, L. Xing, Y. Liao, X. Liu, W. Li, Significantly improved cyclability of lithium manganese oxide, simultaneously inhibiting electrochemical and thermal decomposition of the electrolyte by the use of an additive, RSC Adv., 7 (2017) 46594-46603.
[373] A. Kumar, S.R. Samadder, Performance evaluation of anaerobic digestion technology for energy recovery from organic fraction of municipal solid waste: A review, Energy, 197 (2020) 117253.

[374] R. Lupitskyy, D. Alvarez-Fonseca, Z.D. Herde, J. Satyavolu, In-situ prevention of hydrogen sulfide formation during anaerobic digestion using zinc oxide nanowires, Journal of Environmental Chemical Engineering, 6 (2018) 110-118.
[375] H. Lin, N. Williams, A. King, B. Hu, Electrochemical sulfide removal by low-cost electrode materials in anaerobic digestion, Chemical Engineering Journal, 297 (2016) 180-192.
[376] A.J.H. Janssen, P.N.L. Lens, A.J.M. Stams, C.M. Plugge, D.Y. Sorokin, G. Muyzer, H. Dijkman, E. Van Zessen, P. Luimes, C.J.N. Buisman, Application of bacteria involved in the biological sulfur cycle for paper mill effluent purification, Science of The Total Environment, 407 (2009) 1333-1343.
[377] E. Ryckebosch, M. Drouillon, H. Vervaeren, Techniques for transformation of biogas to biomethane, Biomass and Bioenergy, 35 (2011) 1633-1645.
[378] A. Gupta, S. Ibrahim, A. Shoaibi, Advances in Sulfur Chemistry for Treatment of Acid Gases, Progress in Energy and Combustion Science, 54 (2016) 65-92.
[379] R. Kettner, N. Liermann, New Claus tail-gas process proved in German operation, (1988).
[380] D.A. Bell, B.F. Towler, M. Fan, Chapter 6 - Sulfur Recovery, in: D.A. Bell, B.F. Towler, M. Fan (Eds.) Coal Gasification and Its Applications, William Andrew Publishing, Boston, 2011, pp. 113-136.
[381] J.S. Eow, Recovery of sulfur from sour acid gas: A review of the technology, Environmental Progress, 21 (2002) 143-162.
[382] O. Okoro, Z. Sun, Desulphurisation of Biogas: A Systematic Qualitative and Economic-Based Quantitative Review of Alternative Strategies, 3 (2019) 76.
[383] O.W. Awe, Y. Zhao, A. Nzihou, D.P. Minh, N. Lyczko, A Review of Biogas Utilisation, Purification and Upgrading Technologies, Waste and Biomass Valorization, 8 (2017) 267-283.
[384] J.B.M. Klok, M. de Graaff, P.L.F. van den Bosch, N.C. Boelee, K.J. Keesman, A.J.H. Janssen, A physiologically based kinetic model for bacterial sulfide oxidation, Water Research, 47 (2013) 483-492.
[385] C. Cline, A. Hoksberg, R. Abry, A. Janssen, Biological Process for H~ 2S Removal from Gas Streams: The Shell-Paques/THIOPAQ™ Gas Desulfurization Process, (2003).
[386] L.C.C. Koe, F. Yang, Evaluation of a Pilot-Scale Bioscrubber for the Removal of Hydrogen Sulphide, Water and Environment Journal, 14 (2000) 432-435.